UNIVERSITY OF SOUTHAMPTON
FACULTY OF ENGINEERING AND APPLIED SCIENCE
School of Electronics and Computer Science

Optimality and Iterative Learning Control: Duality and Input Prediction

by

Muhammad Ali Alsubaie

Thesis for the degree of Doctor of Philosophy

March 2011

UNIVERSITY OF SOUTHAMPTON

ABSTRACT

FACULTY OF ENGINEERING AND APPLIED SCIENCE
SCHOOL OF ELECTRONICS AND COMPUTER SCIENCE

Doctor of Philosophy

OPTIMALITY AND ITERATIVE LEARNING CONTROL: DUALITY AND INPUT PREDICTION

by Muhammad Ali Alsubaie

This thesis considers the use of optimal techniques within iterative learning control (ILC) applied to linear systems. Two different aspects are addressed: the first is the duality relationship existing between iterative learning control and repetitive control which allows the synthesis of controllers developed in one domain to be applied in the other. Significant extensions to existing duality framework are made by eliminating an explicit current-error feedback loop and providing the facility of both current error feedback, and previous error feedforward within the control structure. This, in turn, with the case when either state-feedback or output-feedback is used to solve the ILC control paradigm extends the range of underlying plants to which the framework can be applied. In this context optimal control is used to solve the stabilisation problem which yields solutions for both RC and ILC cases in terms of state-feedback, and for ILC in terms of output-injection. These significantly extend the range of underlying plants to which the framework can be applied. The second aspect addressed is the selection of a suitable first input. Whilst ILC algorithms have been shown to offer a high level of performance both theoretically and in practical applications, resulting error convergence is generally highly dependent on the initial choice of input applied. Optimal techniques are therefore applied to generate the most appropriate initial input to speed up the learning process over subsequent trials. Two approaches are developed to tackle the problem, both involving optimal solutions. The first is frequency domain bases, and involves a description of system uncertainty. An input is constructed which maximises convergence in the presence of uncertainty and noise, making use of the Fast Fourier Transform (FFT). The second approach is time domain based and an initial input is constructed using a library of previous references and their associated converged inputs. The assumption of system linearity is used to find the choice of previous inputs which maximises robust convergence. It is then shown how the frequency and time domain schemes may be combined. Both the duality and initial input techniques developed in this thesis have been evaluated experimentally on a gantry robot testbed, and the results obtained confirm the success of these additions to the ILC/RC framework.

Contents

Nomenclature viii

Declaration of Authorship ix

Acknowledgements xi

1 Introduction 1
- 1.1 Thesis Outline . . . 2

2 Literature Review and Background to Iterative Learning and Repetitive Control 5
- 2.1 ILC Literature . . . 5
- 2.2 ILC Development . . . 8
  - 2.2.1 Optimisation Based ILC . . . 10
    - 2.2.1.1 The Inverse Algorithm . . . 14
    - 2.2.1.2 The Adjoint Algorithm . . . 14
  - 2.2.2 ILC Experimental Applications . . . 16
- 2.3 Repetitive Control . . . 21
  - 2.3.1 Survey of the Repetitive Control Applications Literature . . . 23

3 Experimental Test Facility: The Multi-Axis Gantry Robot 27
- 3.1 Gantry Robot Structure and Specifications . . . 27
- 3.2 Modelling the Gantry . . . 29
  - 3.2.1 Test Parameters . . . 32
  - 3.2.2 Previous Use of the Gantry Robot in ILC/RC Experimental Studies 35

4 Iterative Learning Control and Repetitive Control Design via Duality 38
- 4.1 Introduction . . . 38
- 4.2 Internal Model Principle Framework . . . 38
  - 4.2.1 Dual ILC and RC Framework . . . 41
- 4.3 Controller Design in the Duality Framework . . . 45
  - 4.3.1 ILC Approach Development in the Duality Framework . . . 46
  - 4.3.2 Dual RC Controller Design . . . 51
  - 4.3.3 Stability Conditions for the developed ILC and Dual RC schemes 55
  - 4.3.4 Experimental verification . . . 56
    - 4.3.4.1 Experimental Verification — ILC . . . 56
    - 4.3.4.2 Experimental Verification for the Dual RC approach . . 60

4.4 Iterative Learning Control and Repetitive Control Duality Framework with Output Injection . . . 66
4.4.1 ILC Scheme with output Injection . . . 68
4.4.2 Stability Conditions for ILC/RC with Output Injection Scheme . . 72
4.5 Summary of Dual Control Structure . . . 72
4.6 Comparing the Performance of the Duality Based ILC with Selected Optimisation based ILC Designs . . . 74
4.7 Iterative Learning Control and Repetitive Control Duality Framework with Explicit Current-error Feedback . . . 75
4.7.1 Repetitive Control Scheme with Explicit Current-error Feedback . 77
4.7.2 Iterative Learning Control Scheme with Explicit Current-error Feedback . . . 80
4.7.3 Stability Conditions for the Duality framework between RC and ILC with Explicit Current-error feedback . . . 84
4.7.4 Experimental Verification of the Duality Framework with Explicit Current-error Feedback . . . 85
4.7.4.1 Experimental Verification for the RC Framework with Explicit Current-error Feedback . . . 85
4.7.4.2 Experimental Verification for the ILC Framework with Explicit Current-error Feedback . . . 89
4.8 Conclusions . . . 89

5 Model and Experience-Based Initial Input Construction for Iterative Learning Control 92
5.1 Introduction to Initial Input Construction Idea . . . 92
5.1.1 Discrete Fourier Transform . . . 94
5.2 Model-based Initial Input Construction . . . 95
5.2.1 Experimental Verification for Model-Based Initial Input Construction in ILC . . . 102
5.3 Time-domain Experience-based Input Construction . . . 103
5.3.1 Shifted Previous Reference Trajectories . . . 106
5.3.2 Experimental Verification for the Time domain Initial Input Construction Approach . . . 108
5.3.2.1 Experimental Verification for the Time-Domain Shifted Previous Reference Trajectories Initial Input Construction 110
5.4 Hybrid Model and Experience-based Approach . . . 111
5.4.1 Experimental Verification for the Hybrid Model Experienced-Based Approach . . . 113
5.5 Frequency-domain Experience-based Input Construction . . . 114
5.5.1 Experimental Verification for the Frequency-Domain Experience-Based Input Construction . . . 115
5.6 Summary of Chapter . . . 117

6 Conclusions and Future Work 119

References 122

List of Figures

1.1 The general idea of iterative learning control 2
1.2 Flow chart of the thesis structure. 4

2.1 Iterative learning control update structure from Bristow et al. (2006). . . 6
2.2 Arimoto D-type ILC Algorithm. 7
2.3 A frontal view of a patient using the robotic workstation Hughes et al. (2010). 17
2.4 A schematic diagram showing the initial and final position of the shoulder, elbow and arm in tracking a trajectory while supported with a robot Hughes et al. (2009). 18

3.1 Gantry robot test facility with the axes marked. 28
3.2 X-axis frequency-response 30
3.3 Y-axis frequency-response 31
3.4 Z-axis frequency-response 32
3.5 X-axis reference in pick and place task. 33
3.6 3D reference trajectories prototype. 33
3.7 Hybrid ILC and PID controller - series arrangement. 34

4.1 Periodic signal w generated by an autonomous system with appropriate initial conditions w_{w0}. 39
4.2 Past error feedforward block. 40
4.3 Repetitive control feedback representation. 42
4.4 Iterative learning control feedback representation. 43
4.5 Representation of $\phi(z)$ for a) past-error feedforward and b) for current-error feedback. 43
4.6 Synthesized iterative learning control scheme. 48
4.7 Internal model-based iterative learning control scheme. 49
4.8 Internal model-based iterative learning control scheme a) past-error case and b) current-error feedback. 50
4.9 Synthesized repetitive control scheme. 52
4.10 Internal model-based repetitive control scheme. 53
4.11 Internal model-based repetitive control scheme. 53
4.12 Mean squared error for the selection of five different weighting parameters for 200 trials in new ILC design, $D_w = 0$. 57
4.13 3D plot for the output signal of the gantry X-axis for the first 20 trials, $D_w = 0$. 57

4.14 3D plot for the input signal of the gantry X-axis for the first 20 trials, $D_w = 0$. 58
4.15 3D plot for the error signal of the gantry X-axis for the first 20 trials, $D_w = 0$. 58
4.16 Mean squared error for the selection of six different weighting parameters for 200 trials in new ILC design, $D_w = 1$. 60
4.17 3D plot for the output signal of the gantry X-axis for the first 50 trials, $D_w = 1$. 60
4.18 3D plot for the input signal of the gantry X-axis for the first 50 trials, $D_w = 1$. 61
4.19 3D plot for the error signal of the gantry X-axis for the first 50 trials, $D_w = 1$. 61
4.20 The mean squared error for different sets of weighting parameters for the new RC design, $D_w = 0$. 62
4.21 The output of the gantry X-axis for the first 15 trials in new RC design, $D_w = 0$. 63
4.22 3D plot of the output signal for the new RC design, $D_w = 0$. 63
4.23 3D plot of the input signal for the new RC design, $D_w = 0$. 64
4.24 3D plot of the error signal for the new RC design, $D_w = 0$. 64
4.25 The mean squared error for different sets in the new RC framework in current-error case, $D_w = 1$. 65
4.26 The output of the gantry X-axis for the first 15 trials in new RC design, $D_w = 1$. 66
4.27 3D plot of the output signal for the new RC design, $D_w = 1$. 66
4.28 3D plot of the input signal for the new RC design, $D_w = 1$. 67
4.29 3D plot of the error signal for the new RC design, $D_w = 1$. 67
4.30 Synthesized iterative learning control scheme. 68
4.31 Internal model-based iterative learning control scheme for a) past-error feedforward and b) current-error feedback. 69
4.32 Comparison between the new RC/ILC designs in both state-output feedback and the growth in plants considered. 73
4.33 Comparison against the Adjoint algorithm 75
4.34 Comparison against the inverse algorithm 76
4.35 Comparison against norm optimal 76
4.36 Repetitive control with existing feedback controller $C(z)$. 77
4.37 Repetitive control with current-error feedback. 78
4.38 Internal model-based repetitive control scheme. 79
4.39 Iterative learning control set-up 80
4.40 Iterative learning control added to existing feedback controller $C(z)$. . . . 82
4.41 Internal model-based iterative learning scheme. 82
4.42 Mean squared error for six different sets of weighting parameters in RC framework with explicit current-error. 86
4.43 Reference tracking progress in the reported repetitive framework for 15 trials. 86
4.44 3D plot for the output signal for explicit current feedback RC design for the first 20 trials. 87

4.45 3D plot for the input signal for explicit current feedback RC design for the first 20 trials. 88
4.46 3D plot for the error signal for explicit current feedback RC design for the first 20 trials. 88
4.47 Mean squared error for different weighting parameter sets with explicit current feedback ILC design for 200 trials. 90
4.48 3D plot for the output signal for explicit current feedback ILC design. . . 90
4.49 3D plot for the input signal for explicit current feedback ILC design. . . . 91
4.50 3D plot for the error signal for explicit current feedback ILC design. . . . 91

5.1 Two separate paths for the initial input construction idea. 94
5.2 Effect of model-based initial input selection on X-axis a) input, b) output, and c) error during second trial. 104
5.3 X-axis error evolution using model-based initial input selection. 104
5.4 Set of three stored references for experience-based input selection. 108
5.5 Effect of experience-based initial input selection on X-axis a) input, b) output, and c) error during second trial. 109
5.6 X-axis error evolution using experience-based initial input selection. . . . 109
5.7 X-axis error evolution using shifted previous references (shift = $20/100 = 0.02$s). 110
5.8 Effect of shifted experience-based initial input selection on X-axis a) input, b) output, and c) error during second trial. 111
5.9 Hybrid approach mean squared error with $Q = 1, 3$ for a) $M = 1$, b) $M = 2$, and c) $M = 3$. 114
5.10 Composite frequency-domain approach with $Q = 1, 2, 3$ and $M = 3, 5$. . . 116
5.11 Composite frequency-domain approach with $Q = 1, 2, 3$ and $M = 3, 5$. . . 117

List of Tables

4.1 Parameter sets for designing K and L in new ILC scheme for PE case. . . 57
4.2 Parameter sets for designing K and L in new ILC scheme for CE case. . . 59
4.3 Parameter sets for designing K and L in new RC scheme for PE case. . . 62
4.4 Parameter sets for designing K and L in new RC scheme for CE case. . . 65
4.5 State-feedback and output-feedback representations for the duality framework structure. 73
4.6 Parameter sets for designing $[K_r \ K]$ and L in RC scheme with explicit current-error. 86
4.7 Parameter sets for designing K and $\begin{bmatrix} L_l^T & L^T \end{bmatrix}$ in ILC scheme with explicit current-error. 89

Nomenclature

A, B, C, D	state space system matrices
$G(z)$	plant model in discrete time
L	learning gain
t	time
$y_d(t)$	reference signal
k	trial index
$e_k(t)$	tracking error at trial k
$u_k(t)$	input function at trial k
$y_k(t)$	measured output at trial k
$x(t)$	system state in time domain
$x_k(t)$	system state at trial k in discrete-time
x_0	state-space description initial condition
z^{-1}	delay operator in discrete-time
M^T	the transpose of the matrix M
M^{-1}	the inverse of the matrix M
$\mathrm{Re}\{m_i\}$	the real part the i^{th} element of m
$\mathrm{Im}\{m_i\}$	the imaginary part the i^{th} element of m
$\|.\|$	norm
$\mathbb{R}$	the field of real numbers
$\mathbb{C}$	the field of complex numbers

Declaration of Authorship

I, *Muhammad Ali Alsubaie*

declare that the thesis entitled

"Optimality and Iterative Learning Control: Duality and Input Prediction"

and the work presented in it are my own. I confirm that:

- this work was done wholly or mainly while in candidature for a research degree at this University;
- where any part of this thesis has previously been submitted for a degree or any other qualification at this University or any other institution, this has been clearly stated;
- where I have consulted the published work of others, this is always clearly attributed;
- where I have quoted from the work of others, the source is always given. With the exception of such quotations, this thesis is entirely my own work;
- I have acknowledged all main sources of help;
- where the thesis is based on work done by myself jointly with others, I have made clear exactly what was done by others and what I have contributed myself;
- parts of this work have been published as:
  - Freeman, C., Alsubaie, M., Cai, Z., Lewin, P., and Rogers, E. (2010). Initial Input Selection for Iterative Learning Control. *ASME Journal of Dynamic Systems, Measurement and Control.* (In Press)

- Alsubaie, M., Freeman, C., Cai, Z., Rogers, E. and Lewin, P. (2010). Iterative Learning and Repetitive Controller Design Via Duality with Experimental Verification. In: 49*th IEEE Conference on Decision and Control*, December 15-17, 2010, Atlanta, Georgia, USA. (In Press)
- Freeman, C., Alsubaie, M., Cai, Z., Rogers, E. and Lewin, P. (2010) Model and Experienced-based Initial Input Construction for Iterative Learning Control. *International Journal of Adaptive Control and Signal Processing.* (In Press)
- Alsubaie, M., Cai, Z., Freeman, C., Rogers, E. and Lewin, P. (2010) Selecting the Initial Input for Iterative Learning Control: Algorithms with Experimental Verification. In: *UKACC International Conference on CONTROL 2010*, 7-10 of September. 2010, Coventry, UK. pp 61-66.
- Alsubaie, M., Freeman, C., Cai, Z., Lewin, P. and Rogers, E. (2009) ILC Initial Input Selection with Experimental Verification. In: *Symposium on Learning Control at IEEE CDC 2009*, December 14-15, 2009, Shanghai, China.
- Alsubaie, M., Cai, Z., Freeman, C., Lewin, P. and Rogers, E. (2008) Repetitive and Iterative Learning Controllers Designed by Duality with Experimental Verification. In: *The 17th IFAC World Congress*, July 6-11, 2008, Seoul, Korea. pp 3562-3567.

Signed:

Date: 17/03/2011

Acknowledgements

Thanks to Dr. Christopher Freeman and Professor Eric Rogers and Professor Paul Lewin for their support and being there when ever I needed help. Your effort is appreciated and I wish you all the best. As well I would like to give a special thanks to Dr. Zhonglun Cai; Jack, for his continuous help.

Thank you all

I dedicate the work presented in this thesis to my wife for being supportive and patient all the time, my beautiful kids Abdalrahman, Ali and lovely Mariam. I wish you all the best and I hope that you are all proud of me.

Muhammad Ali Alsubaie

Chapter 1

Introduction

Many systems in the process industries and elsewhere execute the same finite duration task over and over again. The exact sequence of operations is that the task is completed and then the process is reset to its original location ready for the start of the next execution or trial. Iterative Learning Control (ILC) is a methodology which has been specifically developed for such systems where the novel feature is the use of information from previous trials to update the control signal to be used on the current trial. Often the computations involved can be completed in the time taken for the resetting. Also in some cases there is an additional time lapse between the completion of the resetting and the start of the next trial to, for example, allow for unwanted transients to decay. The most basic control problem is to design the control input such that the system learns, by iteration from trial-to-trial to produce the required output or reference signal whilst ensuring that the control signal does not exceed the limits imposed by the actuators used. Most often, the reference signal is assumed to be supplied before ILC design begins and remains fixed during the design and, if appropriate, implementation phases.

Figure 1.1 shows a schematic diagram of an ILC scheme where the memory part stores the control input and system output generated on the previous trial. This is the simplest case but it is also possible to consider ILC laws where information from a finite number, greater than one, previous trials is used to compute the current trial input. The use of previous trial information is a form of feedforward control, i.e., from trial-to-trial, but it is also possible to combine trial-to-trial updating with current trial feedback where the latter can be used to regulate along the trial dynamics.

Given a desired reference trajectory, an ILC algorithm is successful for a dynamic system provided it constructs a sequence of inputs which, when applied to the system, produces an output sequence with the properties that as the trial number increases the trial outputs converge to the reference trajectory and the sequence of control inputs applied also converges, where convergence is measured by appropriate signal space norms. These two properties are sometimes referred to as convergent learning.

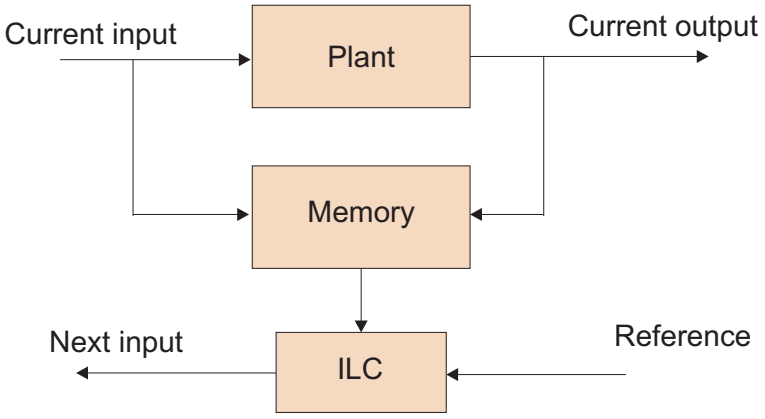

FIGURE 1.1: The general idea of iterative learning control

Repetitive Control (RC) is especially targeted at the tracking and/or rejection of arbitrary periodic signals with a fixed period. Tracking/disturbance rejection of periodic signals has many applications, such as hard disk drives and in electric power supply devices. Given a periodic reference signal, the idea is to force the system to learn the desired input by storing the error signal for one period, and then using this signal to update the controller, and so on.

There has been a large volume of work undertaken on ILC and RC since they were originally proposed and in each case there is clear evidence of experimental verification both in the laboratory and actual application settings but there still remain areas which require further investigation in order to maximise the benefits obtained by adopting either strategy for a given application. In this thesis two of these are addressed as described next.

1.1 Thesis Outline

The thesis consists of six chapters where the main body of original work is given in Chapters 4 and 5. In Chapter 2 a literature review of ILC and RC is given. The problem statement and mathematical formulation of the ILC and RC designs are considered and the distinctions with other forms of control, especially those classed as learning, explained. Properties of ILC are illustrated with a numerical example. The advantages of ILC compared to other conventional controllers are explained. The main optimisation techniques employed to improve performance are discussed, together with solutions based on optimisation formulation such as the adjoint and inverse algorithms.

Chapter 3 gives a description of the gantry robot testbed used in the experimental work reported in this thesis. This testbed has been extensively used to benchmark both ILC and RC algorithms. After a brief physical description, the chapter moves on to describe

the construction of the mathematical models for the three axes, including justification of the assumptions invoked.

In Chapter 4 a previously reported duality between classes of linear model-based ILC and RC algorithms is first introduced. This is followed by a description of the deficiencies of the current results, which motivates the new results developed in this chapter.

In the main part of this chapter new ILC/RC design methodologies are developed based on the existing framework where the new ILC/RC duality problem is considered in the case of the availability of either current-error or past-error feedforward signals. The derivation of these new algorithms uses Linear Quadratic Regulator (LQR) theory, and a comparison of the two settings for design is given in terms of the availability of state-feedback or the presence of a disturbance observer. The final part of the chapter gives the results of experimental application to the gantry robot.

Chapter 5 introduces the concept of initial input selection for speeding up the learning process from two different points of view; the first where model availability is considered and the second where no plant model is used and instead past response data form the basis for design. The construction is based in either the frequency-domain or time-domain depending on the structure of the problem and the information given for each case.

A hybrid model combining both frequency-domain and time-domain approaches is developed to overcome missing data when employing the past response data approach. Comparison with a zero initial input in terms of performance incurred over subsequent trials is undertaken to verify effectiveness in speeding up the learning process. The analysis is also extended to reference signals of different durations. Again, the new algorithms are experimentally tested on the gantry robot.

Chapter 6 concludes the thesis with a critical overview of the progress made and topics for future work are discussed. The following figure summarises the thesis structure.

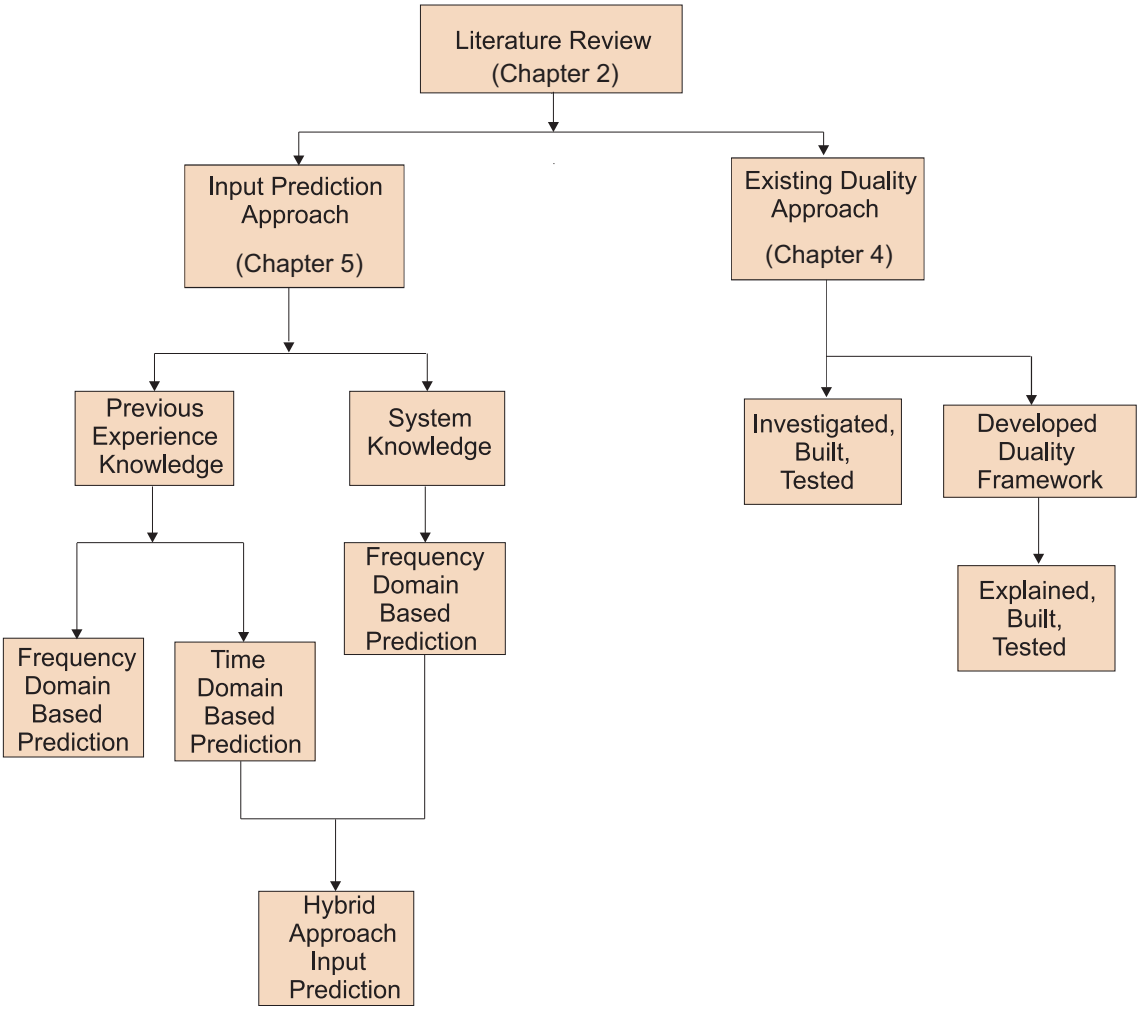

FIGURE 1.2: Flow chart of the thesis structure.

Chapter 2

Literature Review and Background to Iterative Learning and Repetitive Control

In Chapter 1 a general level introduction to Iterative Learning Control (ILC) and Repetitive Control (RC) was given together with some discussion of the classes of systems to which they are applicable. This chapter surveys the literature in both areas, including the influence of optimisation based approaches which are used in this thesis.

2.1 ILC Literature

Several publications Moore and Chen (2003.); Norrlof and Gunnarsson (2002a); Ahn et al. (2007) credit the original work on ILC to an American patent in 1967. Others refer the originality of ILC to a Japanese scientist Uchiyama (1978) who published his work at that time in Japanese, e.g. Hara et al. (1988); Moore and Chen (2002); Norrlof and Gunnarsson (2002b), but the first introduction of ILC in the control and robotics communities is credited to Arimoto et al. (1984b). In general, ILC mimics the human mechanism of learning a task, such as learning to play tennis, which is repeated with the result or output of one attempt used to correct or adjust the effort applied on next one. In particular, the basic aim is to improve performance while executing the same task over a finite duration by learning from past executions, known as trials, conducted over a finite trial duration. This concept applies to many industrial applications such as robotics, chemical batch processes, food processing and automated manufacturing plants. There is no single, universal definition of iterative learning control, but one definition of

ILC is given in Amann et al. (1996a): "*iterative learning control considers systems that repetitively perform the same task with a view to sequentially improving accuracy*".

ILC uses information provided from previous executions of the task to sequentially improve tracking of the reference signal. This is done by updating the control input between trials. The input is highly dependent on the trial error, the difference between trial output and reference signal, see Figure 2.1. A resetting time is required between trials for the system states to reset to its initial states which in this thesis is assumed to be the same for all trials and, if suitable, to do all the required computations to update the control signal for the next trial.

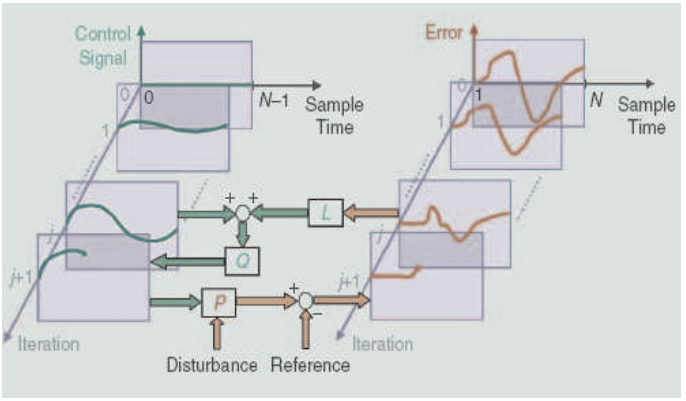

FIGURE 2.1: Iterative learning control update structure from Bristow et al. (2006).

In this section an overview of the ILC literature is given, starting with algorithm development and proceeding through to applications reported in the literature. The starting point is the continuous-time case where the plant dynamics are assumed to be modelled, at least for initial studies, by a linear time invariant state-space model written in ILC notation as

$$\begin{aligned} \dot{x}_k(t) &= Ax_k(t) + Bu_k(t), \quad x(t_0) = x_0 \\ y_k(t) &= Cx_k(t) + Du_k(t) \end{aligned} \tag{2.1}$$

where the integer-valued subscript $k \geq 0$ denotes the trial, also termed as iteration or pass in some literature, and $x_k(t) \in \mathbb{R}^n$, $u_k(t) \in \mathbb{R}$, $y_k(t) \in \mathbb{R}$ are the state, input and output vectors respectively on trial k. The control task is to force the output y_k to track the desired output, or reference signal, y_d over a finite and fixed trial interval, or duration T, i.e., $t \in [0, T]$ as k increases. In the vast majority of the literature, the following are assumed to hold.

- Every trial is of the same duration T.
- The initial state vector on each trial is the same, i.e., $x_k(0) = d$, $k \geq 1$, where the

entries in the vector d have known constant value.

- The plant dynamics are time invariant.
- The plant dynamics and the output $y_k(t)$, $t \in [0, T]$ are deterministic.

Some of the assumptions can be relaxed, including the time invariant assumption, and these will also be discussed in the literature review that follows.

The novel idea in ILC is to use information from the previous trial, or a finite number of them, to update the input used on the next trial and thereby sequentially improve performance, where the basic requirement is to force the trial to-trial error $e_k(t)$ to zero where $e_k(t) = y_d(t) - y_k(t)$, as $k \to \infty$ under some suitable signal norm.

Suppose that the plant (2.1) has relative degree one or zero. Then an Arimoto type Arimoto et al. (1984b,a) ILC scheme given by

$$u_{k+1}(t) = u_k(t) + \Gamma \dot{e}_k(t) \tag{2.2}$$

where Γ is a diagonal learning gain matrix, will ensure that

$$\lim_{k\to\infty} e_k(t) = \lim_{k\to\infty} (y_d(t) - y_k(t)) \to 0 \tag{2.3}$$

for all $t \in [0, T]$, and hence $\lim_{k\to\infty} y_k(t) \to y_d(t)$, if

$$||I - CB\Gamma||_i < 1 \tag{2.4}$$

where $||\cdot||_i$ is an operator norm and $i \in \{1, 2, \ldots, \infty\}$.

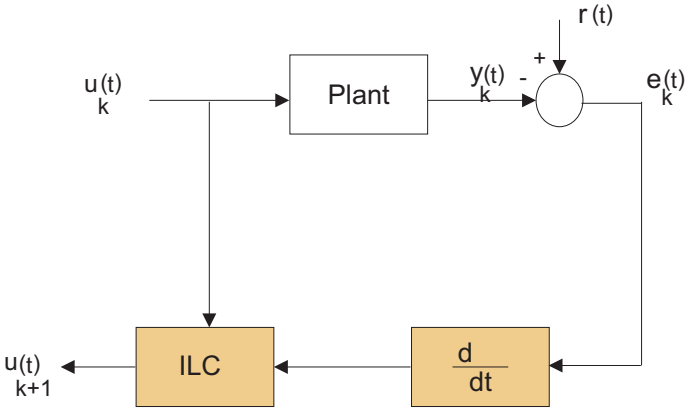

FIGURE 2.2: Arimoto D-type ILC Algorithm.

Note that the basic formula for selecting the learning gain matrix (2.4) does not require information about the system matrix A and, in particular, that the plant is stable, i.e., all eigenvalues of this matrix have strictly negative real parts. This implies that ILC can

be effective for model-uncertain systems though some knowledge of the system structure, such as its relative degree, is needed. This is a key characteristic of ILC but it also the case that for an unstable plant the along the trial performance could be unacceptable. This problem is discussed again when the discrete-time plant model ILC literature is reviewed.

2.2 ILC Development

Starting from the Arimoto-type ILC algorithm of the form (2.2) a number of more general ILC laws can be introduced. For example, a Proportional plus Integral plus Derivative (PID) update law is Moore et al. (1993)

$$u_{k+1}(t) = u_k(t) + \Phi e_k(t) + \Psi \int e_k(\tau)d\tau + \Gamma \dot{e}_k(t) \tag{2.5}$$

where Φ, Ψ and Γ are learning gain matrices. A higher-order ILC, i.e. information from a finite number of previous trials is used, has the form Chen and Wen (1999)

$$u_{k+1}(t) = \Lambda_0 u_k(t) + \sum_{k=1}^{N}(I - \Lambda)P_k u_k(t) + \sum_{k=1}^{N}(\Phi_k e_{i-k+1}(t) + \Psi_k \int e_{i-k+1}(\tau)d\tau + \Gamma_k \dot{e}_{i-k+1}(t)) \tag{2.6}$$

If $\sum_{i=1}^{N} P_k = I$, then by appropriate selection of the learning gain matrices $e_k(t)$ converges to zero asymptotically as $k \to \infty$.

A time-varying, P-type (no integral and derivative terms) ILC algorithm is

$$u_{k+1}(t) = u_k(t) + \Gamma_k(t)e_k(t) \tag{2.7}$$

where the proportional learning gain matrix $\Gamma_k(t)$ is now time-varying.

In this first-order ILC algorithm, by properly choosing the learning gain matrix $\Gamma_k(t)$, the ILC scheme will converge to zero steady-state error for systems of relative degree zero. Similar results can be developed for systems of relative degree one or higher. In this simple ILC algorithm, the key feature is to make use of information from the most recent past trial for the current update. One of the possible time-varying higher-order ILC algorithm is

$$u_{k+1}(t) = u_k(t) + \sum_{i=k}^{k-l} \Gamma_i(t)(y_d(t) - y_i(t)) \tag{2.8}$$

which uses information from the previous $l > 1$ trials in computing the current trial input. These algorithms highlight the perspective that ILC is a control algorithm that uses all available past information for the performance improvement of a periodic system.

For applications where discrete domain implementation is to be used, the choices are to either design the control law in continuous-time and then emulate or sample the plant model. The discrete counterpart of (2.1) is

$$\begin{aligned} x_k(t+1) &= Ax_k(t) + Bu_k(t) \quad x_k(0) = x_0 \\ y_k(t) &= Cx_k(t) + Du_k(t) \end{aligned} \tag{2.9}$$

A large class of discrete ILC algorithms have been proposed based on lifting applied to (2.9) to obtain a standard linear system model. Introduce the supervectors

$$\begin{aligned} U_k &= [u_k(0), u_k(1), \cdots, u_k(N-1)]^T \\ Y_k &= [y_k(m), y_k(m+1), \cdots, y_k(N-1+m)]^T \\ Y_d &= [y_d(m), y_d(m+1), \cdots, y_d(N-1+m)]^T \\ E_k &= [Y_d - Y_k] = (e_k(m), e_k(m+1), \cdots, e_k(m+N-1)]^T \end{aligned}$$

where N denotes the sample number given by $N = \frac{T}{t_s}$, t_s is the sampling time obtained from $t_s = \frac{1}{f_s}$, and m denotes the system relative degree. The system dynamics can now be written as

$$y_k = G_p u_k \tag{2.10}$$

where

$$G_p = \begin{bmatrix} D & 0 & 0 & \cdots & 0 \\ CB & D & 0 & \cdots & 0 \\ CAB & CB & D & \cdots & 0 \\ \vdots & \vdots & \vdots & \ddots & \vdots \\ CA^{N-2}B & CA^{N-3}B & CA^{N-4}B & \cdots & D \end{bmatrix} \tag{2.11}$$

A very large volume of literature on the design of discrete-time ILC algorithms uses the lifted setting for analysis. Examples of algorithm development include Amann et al.

(1996a); Owens et al. (2006); Moore et al. (1993); Lee et al. (2000); Frueh and Phan (2000); Moore et al. (2005).

One problem with the lifted approach to ILC design is that it can only be used to study trial-to-trial error convergence. Also, due to the finite trial length, trial-to-trial error convergence can be achieved for an unstable plant. If the plant is unstable or the performance along the trial is unacceptable then one option is first to design a control law for the plant to achieve stability and/or give acceptable transient performance and then apply ILC to the resulting controlled system. This is a two step design procedure.
An alternative route is to make use of a 2D system settings for analysis. Signals in these systems are functions of two independent variables and the control related analysis of them is based on the Roesser (1975); Fornasini and Marchesini (1978) state-space models.

Repetitive processes are another class of 2D systems Rogers et al. (2007) where the direction of information propagation in one direction only occurs over a finite duration and hence match with ILC. Recently, Hladowski et al. (2010) have shown how these settings can be used to design ILC laws for trial-to-trial error convergence and performance. The design in this case can be completed using Linear Matrix Inequalities and experimental verification on the gantry robot also used in this thesis has been undertaken.

The property of trial-to-trial error convergence is fundamental to ILC and has seen a huge volume of work for both linear and nonlinear systems in either the continuous or discrete time settings. One source for the literature are the survey papers Bristow et al. (2006); Ahn et al. (2007). In this thesis, the setting for analysis is the discrete-time domain.

One issue which has received relatively little attention in the literature is the direct dependence of the error on trial k with that of the first trial through

$$e_{k+1} = (I - G_p L)e_k = (I - G_p L)(I - G_p L)e_{k-1} = (I - G_p L)^{k+1} e_0 \tag{2.12}$$

Designing the learning gain to reduce the trial-to-trial error is a key ILC design objective and Ahn et al. (2007); Bristow et al. (2006) again provide a starting point for many design algorithms. An alternative to speed up the learning rate is to focus on the initial error, that is, for $k = 1$. This, in turn, means focusing on the choices of the initial input. Chapter 5 of this thesis gives substantial new results in this area.

2.2.1 Optimisation Based ILC

Optimal techniques are widely used in ILC either to design the learning gain, or to consider the effects of parameters on error convergence. Optimisation is the process of

finding the best solution, to either maximise or minimise a cost function. A very widely considered class of ILC algorithms under this heading are termed Norm Optimal, Amann et al. (1996a,b, 1998), and are based in an abstract Hilbert space setting. One major advantage of the general problem setting is that it allows the simultaneous description of linear and nonlinear dynamics, either continuous or discrete plant with either time-invariant or time-varying dynamics. This abstract model setting is introduced next with subsequent specialisation to a linear quadratic cost function for linear models that is used in this thesis.

Let the space of output signals $\mathcal{Y}$ be a real Hilbert space and also $\mathcal{U}$ be a real, and possibly distinct, Hilbert space of input signals. The respective inner products, denoted by $\langle ., . \rangle$, and for example, $\|x\|_{\mathcal{Y}}$ denotes the norm of $x \in \mathcal{Y}$.

The Hilbert space setting includes both continuous and discrete-time systems as special cases with the system dynamics described in operator terms as

$$y = G_p u + z_0 \tag{2.13}$$

where $G_p : \mathcal{U} \to \mathcal{Y}$ is a linear operator mapping from the input space to the output space and z_0 denotes the initial conditions. If y_d is the reference trajectory, then the tracking error is

$$e = y_d - y = y_d - z_0 - G_p u \tag{2.14}$$

and without loss of generality, y_d can be replaced by $y_d - z_0$ and hence zero state initial conditions can be assumed without loss of generality.

The ILC procedure, if convergent, solves the problem $y_d = G_p u_\infty$ for u_∞. If G_p in (2.10) is invertible, the solution to this problem is

$$u_\infty^* = G_p^{-1} y_d \tag{2.15}$$

A basic assumption in ILC is that a direct inversion of G_p is not acceptable since it would require an exact knowledge of the plant model and involves derivatives of reference trajectory. This solution is highly sensitive to noise and other disturbances due to the high-frequency gain characteristic. Also the inversion of the whole plant G_p is unnecessary as the solution only requires finding the pre-image of the reference trajectory y_d under G_p.

The ILC optimisation problems considered here is equivalent to finding the minimizing input u_∞ for the optimisation problem

$$u_\infty = \min_u \{\|e_k\|_{\mathcal{Y}}^2 : e = y_d - y, \quad y = G_p u\} \tag{2.16}$$

There are many iterative procedures to solve the above equation and the steepest-descent is one case which, as detailed first in Furuta and Yamakita (1987), has particular attractions for the design of learning control systems. In the case of norm optimal ILC these are as follows.

The norm optimal ILC algorithm has these advantages over alternatives:

- Automatic selection of the step size.
- Potential for improved robustness through the use of causal feedback of current trial data and feedforward of data from previous trials.

This is achieved by computing at the end of trial k the control input on trial $k+1$ as the solution to the minimum norm optimisation problem

$$\min_{u_{k+1}} \{J_{k+1}(u_{k+1}) : e_{k+1} = y_d - y_{k+1},\ y_{k+1} = G_p u_{k+1}\} \tag{2.17}$$

where the performance index used is given by

$$J_{k+1}(u_{k+1}) := \|e_{k+1}\|_{\mathcal{Y}}^2 + \|u_{k+1} - u_k\|_{\mathcal{U}}^2 \tag{2.18}$$

The choice of the initial control input can be arbitrary but, it will be a good first guess at the solution problem in practice. Chapter 5 of this thesis gives substantial new results on this choice with experimental verification.

The solution to this ILC minimum norm optimisation problem can be interpreted as the determination of control input for trial $k+1$ with the following properties: 1) the error term in (2.18) reflects the design requirement of reducing the tracking error in an optimal way. 2) the control input applied does not rapidly change from one trial to the next.

The benefits of this approach follow from the simple interlacing result

$$\|e_{k+1}\|_{\mathcal{Y}}^2 \leq J_{k+1}(u_{k+1}) \leq \|e_k\|_{\mathcal{Y}}^2, \forall k \geq 0 \tag{2.19}$$

which is a consequence of optimality and the fact that the non-optimal choice of $u_{k+1} = u_k$ would lead to the relation $J_{k+1}(u_k) = \|e_k\|_{\mathcal{Y}}^2$.

The steps in obtaining the norm optimal algorithm are given in Amann et al. (1998, 1996a), and consist of finding the derivative of (2.18) with respect to u_{k+1} to obtain the stationary points and substitution from (2.13) and (2.14) to obtain the update law of the form

$$u_{k+1} = u_k + G_p^* e_{k+1} \tag{2.20}$$

where G_p^* is the adjoint operator of G_p. This equation represents the formal update relation for the class of norm optimal ILC algorithms. The error can now be written as

$$(I + G_p G_p^*) e_{k+1} = e_k \tag{2.21}$$

which leads to

$$e_{k+1} = (I + G_p G_p^*)^{-1} e_k \tag{2.22}$$

and the recursive relation for the input evolution

$$u_{k+1} = (I + G_p^* G_p)^{-1}(u_k + G_p^* y_d), \quad \forall k \geq 0$$

This has a number of useful properties, for example,by monotonicity the following limits exists

$$\lim_{k\to\infty} \|e_k\|^2 = \lim_{k\to\infty} J_k(u_k) =: J_\infty \geq 0 \tag{2.23}$$

Consider a system described by the state-space model (2.1) and in the Hilbert space setting define the input and output function spaces as

$$\mathcal{U} = L_2^r\,[0,T], \;\; \mathcal{Y} = L_2^m\,[0,T]$$

The inner products on $\mathcal{Y}$ and $\mathcal{U}$ are defined as

$$\begin{aligned} \langle y_1(t), y_2(t)\rangle &:= \frac{1}{2}\int_{t=0}^{T} y_1^T(t) Q y_2(t) dt \\ \langle u_1(t), u_2(t)\rangle &:= \frac{1}{2}\int_{t=0}^{T} u_1^T(t) R u_2(t) dt \end{aligned}$$

where Q and R are symmetric positive-definite matrices. The initial conditions are taken to be homogeneous without loss of generality because the plant response due to non-zero initial conditions can be absorbed into $y_d(t)$. One special case of this problem formulation

is a cost function of the LQR form

$$J_{k+1}(u_{k+1}) = \frac{1}{2}\int_0^T \{e_{k+1}^T(t)Qe_{k+1}(t) + (u_{k+1}(t) - u_k(t))^T R(u_{k+1}(t) - u_k(t))\}dt \quad (2.24)$$

This is an optimal tracking and disturbance accommodation problem (regarding $u_k(t)$ as a known disturbance on trial $k+1$). In this particular case, the solution for computing the current trial input is the adjoint solution given by (2.20). The solution obtained is non-causal and can not be implemented in this form. The non-causal representation can transformed into a causal algorithm using state-feedback representation (Rogers et al. (2007) gives a detailed description of the solution). The causal ILC developed in this context requires the availability of the state-feedback.

Ratcliffe et al. (2006b) gave a detailed analysis for the particular choices of $Q = qI$ and $R = rI$, also q and r are nonnegative real scalars and in each case I is the identity matrix with compatible dimensions. This concluded that the ration $\frac{q}{r}$ is a critical factor in determining trial-to-trial error convergence.

2.2.1.1 The Inverse Algorithm

The inverse algorithm is a one step solution to (2.15) where the plant model must be invertible or else can be appropriately pre-conditioned to have this property. The control law is

$$u_{k+1} = u_k + \epsilon_{k+1} G_p^{-1} e_k \quad (2.25)$$

where ϵ_{k+1} is a scalar whose effects and selection has received considerable attention in the literature, for example in Ratcliffe et al. (2006b).

The inverse approach is known to be sensitive to noise and disturbances. In Harte et al. (2005) the stability, monotonicity and robustness of the inverse was examined where the plant uncertainty has to satisfy a matrix positivity requirement for the inverse solution to be applicable. Low-pass filtering is one way of improving the inverse algorithm sensitivity to noise and disturbances. This is treated by, for example, Lee et al. (1994) using the time domain for analysis and Freeman et al. (2009b) in the frequency domain. Further analysis of the inverse ILC algorithm for both minimum and non-minimum phase linear systems can be found in, for example, Kinosita et al. (2002).

2.2.1.2 The Adjoint Algorithm

The adjoint algorithm (known also as the gradient-based algorithm) is another form of updating law where the learning gain is designed in an optimal setting. This approach is treated in, for example, Hatonen et al. (2009, 2004). The update law is of the form in (2.20) and is a steepest-descent method.

In order to regulate trial-to-trial error convergence, Furuta and Yamakita (1987) designed a steepest-descent approach to set a limit to β on the step length, in (2.26) in the absence of model uncertainty, resulting in a control law of the form

$$u_{k+1} = u_k + \beta_{k+1} G_p^* e_k \tag{2.26}$$

A modified steepest-descent approach has also been developed which considers the presence of multiplicative model uncertainty in the selection of the step length, β. This produced better results (Hatonen et al. (2003)) than the algorithm of Furuta and Yamakita (1987) when both were experimentally applied to the gantry robot also used in the work reported in this thesis.

There is a very large volume of literature on optimisation based ILC and the review above has only focused on the algorithms used in this thesis. The survey papers Ahn et al. (2007); Bristow et al. (2006) are good starting points for the literature on alternatives.

A large volume of the currently available literature on ILC for nonlinear plant dynamics focuses on trial-to-trial error convergence proofs. The survey papers Ahn et al. (2007); Bristow et al. (2006) again provide a starting point for the literature on this topic. One nonlinear ILC algorithm that has seen applications in, for example, stroke rehabilitation, is the Newton method. By setting up links between nonlinear ILC problems and nonlinear multivariable equations, the Newton method is introduced into the ILC framework. In application this algorithm decomposes a nonlinear ILC problem into a sequence of linear time-varying ILC problems. Simulations on a discrete non-linear system and a manipulator model display its advantages.

The original work Lin et al. (2006) on the Newton method ILC used a known determinate system model with the same initial conditions on each trial and reference signals, and no disturbances. In case when system model is partly or totally unknown, either the control should be robust and/or system identification could be applied to acquire numerical system models. Disturbances and uncertainties on the system, the initial condition, and the reference signal. This is one of the areas in Newton method based ILC for which further work is required.

Another area of nonlinear model ILC that has seen much research is to consider the ILC problem from an adaptive control viewpoint. It is shown in French and Rogers (2000) that some standard Lyapunov adaptive designs can be modified in a straightforward manner to give a solution to either the feedback or feedforward ILC problem. Some of the common assumptions of nonlinear ILC are relaxed, for example, the common linear growth assumption on the nonlinearities and can be applied by systems of arbitrary relative degree. This initial work also showed that, in general, a linear rate of convergence of the mean squared error can be achieved, and a simple robustness analysis was also given given.

Finally for linear plants it was shown that a linear rate of mean squared error convergence can be achieved for non-minimum phase plants. Work building on this initial analysis includes Xu et al. (2008); Chien and Tayebi (2008); Sun et al. (2006). There is also much work to be done on stochastic ILC building, for example, on the initial work in Saab (2002).

2.2.2 ILC Experimental Applications

In terms of applications, ILC arose initially from consideration of robotic control problems and it is perhaps not surprising that this area has always been a strong topic for published work. This includes general robotic applications including rigid manipulators and flexible manipulators, see, for example, Hamamoto and Sugie (2002); Shin et al. (2003); Tayebi (2004); Yao et al. (2004), mechatronics design Wood et al. (2000), robots with adaptive learning Sun and Mills (1998), with the Kalman filter Norrlof (2002), underwater robotics Sakagami et al. (2003); Sakagami and Kawamura (2004), mobile robots Norrlof (2004) and arc welding processes Holm et al. (2002). Current trends in ILC research for robots include the use of a gantry robot for benchmarking designs where this robotic system is also used in this thesis Hatonen et al. (2003); Ratcliffe et al. (2004); Rogers (2008); Hladowski et al. (2010); Ratcliffe et al. (2006b) and also as a practical motivation for observer-based ILC as discussed next.

Traditionally ILC has been applied to systems where the controlled variable is the measured variable. In industrial robot applications this is typically not the case since in a standard industrial robot the motor angles are measured, but the control objective is to follow a desired tool path. Hence there is a problems if the controlled variables cannot be measured, and this is confirmed by ILC experiments performed on a robot, Wallen et al. (2008). This motivates the need to use an estimate of the controlled variable in the ILC algorithm to be able to improve the performance. The aim is to present a framework for the situation when an ILC algorithm is combined with a procedure for generating an estimate of the controlled variable. One dealing with this issue Gunnarsson et al.

(2007), where the ILC algorithm uses an estimate of the arm angle from measurements of motor angle and arm-angular acceleration of a flexible one-link robot arm. The paper Wallen et al. (2009) also discusses these issues, based on simulations of a realistic robot model. In Schollig and D'Andrea (2009) the model error of a state-space model linearised along the desired trajectory is estimated using a Kalman filter in the trial-domain. The control signal for the next trial is given by minimising the deviation of the states from the desired trajectory. Another example is Tayebi and Xu (2003), where the estimated states for a class of time-varying nonlinear systems are used in an ILC algorithm and asymptotic behaviour of the system is treated.

The focus in the work research cited above is on specific estimation and/or ILC algorithm techniques, whilst Wallen et al. (2009) develops a framework for analysis of properties of the ILC algorithm when an estimate of the controlled variable is used in the ILC algorithm, and an expression for asymptotic error of controlled variable when an ILC algorithm based on an estimate of the controlled variable has converged.

Another major applications area for ILC is rotary systems where the motion of such systems is often disturbed by position-dependent or time-periodic external disturbances. Applications in this general area include vibration suppression in rotating machinery Li et al. (2004), switched reluctance motors Sahoo et al. (2004) and an ac servo motor Shi (2002). Process control is another area where the application of ILC is a long-standing topic. Work here includes laser cutting Tsai and Chen (2004), chemical processes Xu et al. (1999) and injection moulding Tan et al. (2003).

Bio-engineering/bio-medical applications of ILC is another topic which has some previous work Huang et al. (2003b,a); Wu et al. (2000). More recently there has been a major ongoing programme of research on ILC for robotic assisted stroke rehabilitation which has followed through to successful clinical trials.

Practising by repetition and using feedback from previous attempts to enhance the upcoming repetition performance enables a patient to have a re-learn skills after having a stroke. Since practice is limited due to impaired movement following stroke, no feedback is received. For FES applied to remedy this problem, a suitable strategy is used where after the completion of an attempt, the performance is measured, and the resulting data is used to adjust the level of stimulation applied for the next attempt. The ILC strategy is that, as the number of attempts increases, the error between the required reference and the measured output decreases under an appropriate measure. The aim is that the stroke patient re-learns how to do the required movement without the stimulation.

In stroke rehabilitation, a 3D complex functional task is needed to follow but there are vast number of 2D tasks where rehabilitation would also significantly improve mobility. One side of the body of a stroke patient may exhibit partial paralysis and they may have little or no ability to reach out in the 2D plane with the affected arm.
In a robotic-assisted system Freeman et al. (2009c,d,a); Hughes et al. (2009, 2010); Le et al. (2010) stroke patients are seated with the affected arm supported by a robot with elliptical reaching trajectories displayed onto a target above their hand. Figure 2.3 shows a frontal view of a patient using the robot.

FIGURE 2.3: A frontal view of a patient using the robotic workstation Hughes et al. (2010).

Functional Electrical Stimulator (FES) is applied to the stroke patient's triceps muscle for tracking assistance along the reference trajectory. After completing one attempt, the arm is returned to the same starting position in preparation for the next. In this reset time the ILC controller computes the next stimulation applied on the next trial. Again, as the number of trials increase the error decreases with the overall aim that the patient's hand moves along the required trajectory. Figure 2.4 shows a plan view of the patient arm position in tracking the reference trajectory while the arm is supported with a robot.

There is a considerable volume of ongoing work on the applications of ILC in semiconductor manufacturing problems. For example, in high-speed motion systems such as the reticle and the wafer stages of a wafer scanner Van de Wal et al. (2002) learning can significantly improve upon performance. This is because of the repetitive nature of its scanning motion Dijkstra and Bosgra (2002); Rotariu et al. (2003, 2004). Variation in the scanning motion, however, avoids the application of the resulting commands learned at a specific motion to be effective in achieving performance when applied during a different motion. As one example of this area, in Heertjes and Van de Molengraft (2009)

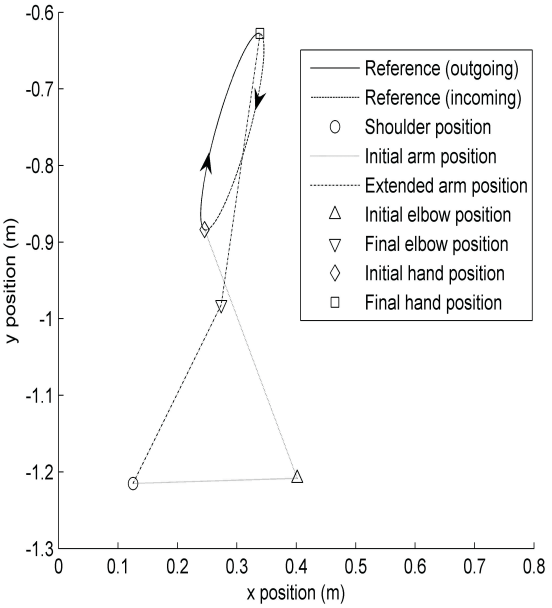

FIGURE 2.4: A schematic diagram showing the initial and final position of the shoulder, elbow and arm in tracking a trajectory while supported with a robot Hughes et al. (2009).

the forces learned for a representative acceleration set-point are mapped onto a finite impulse response (FIR) model. In the wafer scanning example, this is done prior to the process of wafer illumination whereas during this process the learned forces are replaced by generalized learned forces being the result of the finite impulse response model and the acceleration set-points at hand; this is different from a run-to-run control approach such as for example considered by Bode et al. (2004) which lacks in situ performance measurement (the wafer needs to be further processed) and in which all set-points are known. In a general multi-input multi-output feed-forward setting, the advantages are twofold. On one hand, learning during the process of wafer scanning is avoided. This maintains the high standard of performance in terms of wafer throughput. On the other hand, learning is based on a small sub-set of a generally large variation of wafer set-points. This constitutes the efficiency of the method.

Many applications involve a flexible structure that has to be repositioned in order to perform an operation. In turn, the corresponding point-to-point motion can, however, introduce vibrations into the structure, thereby increasing settling time or degrading the accuracy with which the operation can be performed. In literature, many input shaping strategies have been presented to suppress residual vibrations in flexible structures performing point-to-point motions. A comparison of different input shapers is given in Singer et al. (1999); Singh and Singhose (2002). Basically, these input shapers focus on actuation of the system during the point-to-point motion, in an attempt to suppress

residual vibrations during observation of the system after completion of the motion.

There is a body of literature which uses ILC for this application area where the command signal is updated using measured data from previous trials, i.e., by learning from previous experience. The fact that the adapted ILC strategy iteratively improves the command signal using measured data means that it is an interesting extension to current model based input shapers.

ILC has also found application in the control of manufacturing systems. For example, cross-coupled control has been applied to multi-axis systems in which there is a primary objective that defines manufacturing process performance. Less emphasis is placed on individual axis performance in favour of a coupled axis, appropriately defined to measure the primary performance objective Koren (1980); George and Tomizuka (2001). A long standing example of the CCC approach is a computer numerically controlled (CNC) robot where the primary objective is the dimensional accuracy of a manufactured part, not individual axis objectives. Performance is defined by a coupled axis, termed the contour error, which is the normal distance from the prescribed trajectory and is a metric of the primary objective, i.e. dimensional accuracy.

The redefinition of performance objectives developed in cross-coupled control has been integrated into the ILC to form cross-coupled iterative learning control Barton and Alleyne (2008) to form cross-coupled ILC with experimental verification. By directly considering the primary objective and exploiting trial repetition, this new form of ILC has been shown to achieve superior performance in comparison to alternatives for contoured trajectory tracking problems Barton and Alleyne (2008); Barton et al. (2008).

Cross-coupled control and cross-coupled ILC have been traditionally applied to planar manufacturing robots in which the x- and y-axes have similar yet individual dynamics and are actuated and sensed by identical hardware. Cross-coupled ILC is a special form of a multi-input multi-output (MIMO) approach in which two single-input single-output (SISO) systems are coupled together through the output. In Barton et al. (2010) cross-coupled ILC has been applied to a general set of systems, where the individual dynamics, as well as the actuation and sensing hardware, need not be common among the different systems. Note also that MIMO ILC is a relatively unexplored area.

The area of robustness of ILC control is one where much work remains to be done, and it is not the case that this can be addressed by directly copying over existing tools from, for example, H_∞/H_2-based robust control theory for standard linear systems. The special issue of the International Journal of Robust and Nonlinear Control Owens and Rogers (2008) explains the problems involved in developing a robust control theory for linear

model-based ILC and associated algorithms and to provide experimental-based evidence of expected performance. It consists of six papers, which cover major areas of activity where progress has been made and most of them also include the results of experimentally testing the resulting control schemes.
In the first of these papers, give new results on robust control based on the H_∞ approach for examples where there is uncertainty associated with the plant model and also trial-to-trial domain input-output disturbances (where the latter have no counterparts in non-ILC problems). The second paper by French gives substantial results on the use of the gap-metric in ILC, which results in provable robustness properties and also some insights into how a general solution to the so-called 'long-term' stability problem could be achieved by this route. This problem, again unique to ILC, has been observed in both simulation studies and experimental results. It results in divergence of the trial-to-trial error sequence after a large number of trials despite a period of trials where apparent convergence has occurred. In the literature to date, this has been attributed to a number of causes but a theory to explain why it arises is still missing (and hence design algorithms, that can counter this effect).
The next paper by van de Wijdeven and Bosgra gives results on the application of ILC to the long-standing and well-researched area of residual vibration suppression. The analysis and experimental results given in this paper demonstrate that ILC can bring benefits not available in other approaches. In the next paper, Merry et al. address the fact that in practical applications, the tracking errors on successive trials contain repetitive and non-repetitive parts. ILC only controls the repetitive part and the entry of the non-repetitive part into the learning system has a negative impact on the performance. This paper gives an analysis of this situation and develops and illustrates experimentally, a wavelet-based method of removing the detrimental non-repetitive disturbances.
In the penultimate paper, Zhang et al. address issues related to multi-rate ILC with algorithm development and experimental verification. The final paper by Ratcliffe et al. considers the steepest descent algorithm, which has played a central ongoing role in ILC from the very early work. This contribution develops a new version of this algorithm for application to plants where the uncertainty associated with the plant model is assumed to be multiplicative and gives the results of experimental verification on a gantry robot.

In robustness analysis and design for discrete linear model based ILC based on the lifted approach, the uncertainty model matrices can appear in products of lifted model description and this complicates analysis. Moreover, the along the trial dynamics are subsumed within in the lifted model, essentially 2D dynamics are lifted to the 1D domain. An alternative is to use a 2D systems setting for analysis where recent research has seen robust ILC algorithms designed in this system experimentally tested on the gantry robot used in this thesis.

2.3 Repetitive Control

Many signals in engineering are periodic or can be approximated by a periodic signal over a large enough time interval (i.e. $y_d(t) = y_d(t+T)$) where T denotes the period of the reference signal. Such signals arise, for example, in engines, electric motors, and hard-disc drives.

An important control problem is to track a periodic signal with the output of the plant or to reject a periodic disturbance acting on a control system. In the former, T will be known a priori by the nature of the task performed. In the latter it can be identified using established methods.
To solve this problem, a relatively new research area termed repetitive control (RC) has emerged. The idea is to use information from previous cycles, periods or trials to modify the control signal so that the overall system learns to track perfectly a given T-periodic reference signal. The first known RC algorithm which uses this approach is often credited to Inoue et al. (1981) where the RC used to obtain a desired proton acceleration pattern in a proton synchotron magnatic power supply.
Since then, RC has been applied to several practical applications, for example in robotics Kaneko and Horowitz (1997); Elci et al. (2002), motors Yasuhide et al. (1999), the servo system of an optical disk drive Moon et al. (2002) and in a peristaltic pump Hillerstrom and Sternby (1993). Most currently reported RC algorithms are designed for continuous-time, and they either do not give perfect tracking or require that the original process is positive-real, see, for example, Freeman et al. (2008b), where the P-type update law was considered.

An optimality-based RC algorithm Freeman et al. (2008b) was developed to overcome these limitations for discrete linear time-invariant systems. This algorithm results in exponential convergence under mild controllability and observability conditions.

As a starting point for continuous-time RC setting, consider a SISO system with the following state-space model, where the state vector is assumed to be of dimension n

$$\begin{aligned} \dot{x}(t) &= Ax(t) + Bu(t), \quad x(0) = x_0 \\ y(t) &= Cx(t) + Du(t) \end{aligned} \tag{2.27}$$

A reference signal y_d is given, and it is known that $y_d(t) = y_d(t+T)$, for a given T. The control design objective is to find a feedback controller that makes the system in

(2.27) track the reference signal as accurately as possible (i.e. $\lim_{t\to\infty} e(t) = 0,\ e(t) := y_d(t) - y(t)$), under the assumption that the reference signal $y_d(t)$ is T-periodic.

Consider the problem of control design for T-periodic disturbance/reference accommodation. Then by the Internal Model Principle (IMP) a model for the T-periodic signal involved has to be included in the stabilising feedback loop, i.e., introduced by the controller. Suppose therefore that the controller is of the form

$$[Mu](t) = [Ne](t) \tag{2.28}$$

where M and N are suitable operators. Then a model of the disturbance/reference signal must be included in M and since the reference signal is T-periodic it follows that its model is given by the operator $(1-\sigma_T)$, where $[(1-\sigma_T)v](t) = v(t) - v(t-T)$ for an arbitrary $v : \mathbb{R} \to \mathbb{R}$, where $\mathbb{R}$ denotes the field of real numbers. In Yamamoto (1993b) the following RC algorithm for the case considered here was studied

$$u(t) = u(t-T) + e(t) \tag{2.29}$$

which is the result of simply setting $M = (1-\sigma_T)$ and $[Nv](t) = v(t)$ for an arbitrary $v : \mathbb{R} \to \mathbb{R}$. This choice of operators satisfies the necessary condition for asymptotic convergence given in Francis and Wonham (1975).
The algorithm (2.29) has been analysed by several authors, for example, Yamamoto (1993a); Owens et al. (2001). It turns out that, if the system (2.27) is positive-real, then $e(.) \in L_2[0,\infty)$ (this does not imply that $\lim_{t\to\infty} e(t) = 0$).

Suppose that a relaxation parameter $\alpha \in (0,1)$ is introduced into (2.29) to give

$$u(t) = \alpha u(t-T) + Ke(t) \tag{2.30}$$

and suppose that $K \in \mathbb{R},\ K > 0$. Then a sufficient condition for closed-loop stability is

$$\sup_{w\geq 0} \left|\frac{\alpha}{1+G(jw)K(jw)}\right| < 1 \tag{2.31}$$

where $G(s) = C(SI_n - A)^{-1}B + D$ is the transfer function of (2.27). The result is a direct application of the small gain theorem Deoser and Vidyasagar (1975).
Equation (2.31) implies that the control law given in (2.30) converges to a T-periodic solution and the output $y(t)$ converges to a T-periodic solution where

$$Y(s) = \frac{\frac{K}{1-\alpha}G(s)}{1+\frac{K}{1-\alpha}}r(s) \tag{2.32}$$

It is clear that if $\alpha \to 1$, then an infinite feedback gain is required. This issue has also been addressed in Freeman et al. (2008b) where a new algorithm for discrete-time implementation is developed since it is impossible to implement a delay block using analogue components. This algorithm combines polynomial system and optimal approaches.

The definitions and principles behind ILC and RC, suggest that they are very similar in structure. This matter was investigated in De Roover and Bosgra (1997); De Roover et al. (2000) where it was shown that they are related by a duality. The duality is a consequence of the location of the internal model inside the feedback loop where this reference in explicity showed that if the internal model was located in the input side, this is an ILC controller, and an RC controller if it is located in the system output.

Under this duality, an ILC controller design also gives an RC controller and vice versa. The existing analysis is, however, applicable to a limited range of plants due to the requirement that an explicit current-error loop is present. In Chapter 4, substantial new analysis is given which removes this limitation and experimental verification on the gantry robot is also given.

2.3.1 Survey of the Repetitive Control Applications Literature

Repetitive control has been extensively used in many control areas such as compact disk and hard disk arm actuators Chew and Tomizuka (1990), Onuki and Ishioka (2001), robotics Ye and Wang (2006), Kim and Tsao (2000) in electro-hydraulics, torque vibration suppression in motor control Hattori et al. (2000) and power electronics applications, for example, unity power factor rectifiers Zhou and Wang (2003) and pulsewidth-modulated inverters Zhou and Wang (2002); Tzou et al. (2002a). In power electronic systems, Normally the reference and disturbance signals appearing in control loops (in this case, source and load currents, respectively) are, in steady state, periodic signals with only odd harmonics in their Fourier series expansion. Then if the usual repetitive control methodology is used in these systems, the open-loop transfer function will include a high gain in all the harmonic frequencies Grino et al. (2003). However, it is not necessary to include a high gain at even-harmonic frequencies; it only means a waste of control effort and a reduction of system robustness without improving system performance Griñó et al. (2007). Besides, the introduction of a high gain at even-harmonic frequencies generally implies that the open-loop transfer function includes an integral term that corresponds to zero frequency harmonic. So, together with the inclusion of sensors that use transformers in the loop, gives closed loops that are not internally stable. Hence, traditional repetitive controllers must be precluded in systems with pure derivative terms in order to obtain internally stable closed-loop systems. This is an example of how repetitive control can solve stability and performance problems with periodic references/disturbances.

Another major application area for repetitive control is in electrical drives/power electronics. In recent years, closed-loop regulated pulse-width modulated (PWM) inverters have enjoyed extensive application in many types of ac power conditioning systems such as uninterruptible power supply (UPS), automatic voltage regulator (AVR), and programmable ac source (PACS). In these applications, the PWM inverters must maintain a sinusoidal output waveform under various types of loads, and this is achievable only by employing feedback control techniques Tzou et al. (2002b).

Extensive research has been directed to the closed-loop regulation of PWM inverters employing various feedback control schemes to achieve excellent dynamic response and low harmonic distortion Kawamura and Hoft (1984); Cha et al. (1990). However, most research was concentrated on improving the transient response through using instantaneous feedback control either by analog or microprocessor-based digital control techniques. In the deadbeat control approach Hua and Hoft (1992), the control signal depends on a precise PWM inverter load model, and the performance of the system is sensitive to parameter and load variations. Another drawback of the deadbeat control scheme is that it requires a larger actuating signal to achieve the deadbeat effect. Sliding mode control (SMC) with feedforward nonlinear compensation has been developed for the closed-loop regulation of a PWM inverter citejung2002discrete. Although the SMC-controlled PWM inverter can achieve fast dynamic response and is insensitive to parameter and load variations, locating a satisfactory sliding surface is extremely difficult. Also, its performance degrades under a limited sampling rate.

In most ac power conditioning systems, phase-controlled nonlinear loads are major sources of waveform distortion. Due to the periodic characteristics in voltage regulation, this type of nonlinear load results in periodic distortion in its output waveform. Hence this area is ac prime candidate for the application of repetitive control. A number of modified repetitive control schemes have been developed for use in various industrial applications Inoue et al. (1981); Chew and Tomizuka (1990). Repetitive control theory has also been applied to a PWM inverter employed in UPS systems to generate high-quality sinusoidal output voltage Haneyoshi et al. (1986).

Electrical power quality has been, in recent years, an important and growing problem because of the proliferation of nonlinear loads such as power electronic converters in typical power distribution systems. Particularly, voltage harmonics and power distribution equipment problems result from current harmonics produced by nonlinear loads. This fact has led to the proposal of more stringent requirements regarding power quality like those specifically collected in the standards IEC-61000-3-2,4 and IEEE-519. Much work has been done in the area of active filter control Akagi (2002); Buso et al. (2002); Jin-

takosonwit et al. (2002). Nevertheless, it seems that, as a conclusion, the main point is the need for high-gain current control loops Buso et al. (2002); Fukuda and Imamura (2005). Perhaps, the easiest way to obtain them is to use some kind of hysteresis controller (or relay controller) Singh et al. (2002). However, this controller has the disadvantage of a varying switching frequency, which produces a continuous harmonic spectrum. This problem is not present in fixed-frequency pulsewidth modulated schemes that have their high-frequency content around switching frequency harmonics. Therefore, it would be interesting to develop digital controllers with pulsewidth modulators (PWMs) for the active filter system.

Fulfilling these requirements, there is a technique, called repetitive control, that allows control loops to be designed with a high gain at the harmonic frequencies of a fundamental one. This methodology arose from the Internal Model Principle (IMP) Fukuda and Imamura (2005); Francis and Wonham (1976) in control theory and is particularly suitable for periodic-signal tracking problems and periodic-signal disturbance rejection problems. Therefore, the necessary high-gain requirements of current control loops in active filters can be met with this approach. Particularly, this paper uses the repetitive control technique to design high-gain digital controllers for the current loops of the three-phase four-wire active filter.

The control of energy systems is currently a very active topic in the control community and here too there are areas where repetitive control can be used to significant effect. During the past two decades, a wide range of control schemes have been tested at a distributed solar collector field, with the aim of controlling the field output temperature Camacho et al. (2007a,b). One of the main difficulties in the control of this system is the excitement of its intrinsic resonance dynamics when a high performance is required to the controller Berenguel and Camacho (1996); Camacho et al. (1997); Johansen et al. (2000). With a grey-box model of the system, which is developed from an energy balance of the system Cohen and Johnson (1956); Meaburn and Hughes (1993), it has been established that these resonance/antiresonance modes are related to residence time of the fluid inside the collector. The residence time of the fluid is, also, related to the only control variable of this type of system in the form of the fluid velocity. Consequently when the fluid velocity is used to control the output temperature of the distributed solar collector field the frequencies where the resonance/antiresonance modes can be located change. This fact makes difficult to counteract the resonance dynamics by means of a control system.

One solution, which has demonstrated good performance to cancel the effects caused by the resonance/antiresonance dynamics is to treat these resonance dynamics as internal periodic disturbances and to add a repetitive controller to the control system. The

repetitive controller acts as a secondary controller and its main aim is to compensate for the resonance/antiresonance dynamics while another controller, such as proportional-integral-derivative (PID) plus a feedforward controller, is the main controller and its function is to maintain the output temperature as close to the setpoint as possible Alvarez et al. (2007). This is an example of so-called plug-in control.

Most often, the repetitive controller is used to reject/track external periodic disturbances/references which have a fixed frequency or their frequency is well known. In other cases, the frequency of the signal to be rejected or tracked changes in a closed range and hence an adaptive repetitive controller which changes its sampling time according to the frequencies of the resonance system dynamics can be used in these situations Hillerstrom (1996); Cao and Ledwich (2002). However, in this case the resonance modes frequency range is wider and, as has been pointed out previously Álvarez et al. (2010).

Position-based periodic motion have appeared in vast industrial processes such as cam-followers. The output motion driven by the cam period varies in the time-domain but is fixed in the angular position-domain and this is called time-varying periodic motion Cao and Ledwich (2002); Zhenwei and Ledwich (2001); Wang and Tsao (2004). A plug-in type repetitive control scheme for reducing tracking errors via position-based periodic reference signals and/or disturbances is developed in Hsu et al. (2008). Two kinds of control strategies, namely disturbance feedforward and disturbance rejection control, are proposed to investigate control performance with time-varying periodic disturbances. The implementation technique utilized in this position-based repetitive controller is discussed in detail, and an anti-vibration control system with position-base load disturbances generated by a cam is realized.

Chapter 3

Experimental Test Facility: The Multi-Axis Gantry Robot

In this chapter a description of the gantry robot facility used to obtain the experimental results reported in this thesis is given. The robot can be configured to operate in both ILC and RC modes. Focusing on the former area, the robot system replicates a commonly encountered industrial application to which ILC is applicable. In particular, the sequence of operations performed is to collect an object from a fixed location, transfer it over a finite duration, place it on a moving conveyor under synchronization, and finally return to the original location to collect the next object, and so on. This facility has already been extensively used to benchmark a range of linear model-based ILC and RC algorithms and the results in this thesis will also extend and supplement the experimental data already available in the ILC and RC literature. The material in this chapter begins with a brief outline of the physical structure and then proceeds to explain the development of the mathematical models for each axis and the assumptions invoked.

3.1 Gantry Robot Structure and Specifications

Figure 3.1 shows a photograph of the system with the axes marked. The gantry robot is a commercially available system found in several industrial applications. The robot is located above one end of a plastic chain conveyor, and is tasked with collecting payloads from a dispenser and placing them onto the moving conveyor beneath. The robot must synchronize both speed and position with the conveyor to achieve accurate placement of the payload.

The gantry robot can be treated as three separate SISO systems, one for each axis, which can operate simultaneously to locate the end-effector anywhere within a cuboid

work envelope. The lowest X-axis moves in the horizontal plane, parallel to the conveyor beneath. The Y-axis is mounted on the X-axis and moves in the horizontal plane, but perpendicular to the conveyor. The Z-axis is the shorter vertical axis mounted on the Y-axis. The X- and Y-axes consist of linear brushless dc motors, while the Z-axis is a linear ball-screw stage powered by a rotary brushless dc motor. All motors are energized by performance-matched dc amplifiers. Axis position is measured by means of linear or rotary optical incremental encoders as appropriate. The input to each axis is a demand voltage (V), and the output is its position (mm). The control algorithm is implemented on a Pentium 4 PC running under the Linux operating system which is suitable for real-time control applications. Control software is written in the C++ language, comprising a highly modular approach in which the core program, control algorithms, data saving, axes homing, and user menus are written in separate files to increase program reliability and stability. Since no changes were required in the structure of the software, implementation of the algorithms described in this thesis only required additional control algorithm code to be written. This is called every sample to generate the new control input.

FIGURE 3.1: Gantry robot test facility with the axes marked.

3.2 Modelling the Gantry

Modelling of each robot axis was performed following completion of its construction in 2003, and involved open-loop frequency-response tests. These are detailed in Ratcliffe (2005), and the procedures employed and results obtained are now summarised.

A sine-wave of known frequency and magnitude is first sent to the plant. The resulting output consists of a sine-wave of shifted phase and different magnitude. The phase shift is recorded in degrees and the magnitude difference as gain in decibels (dB). Sweeping through frequencies of interest, the resulting data can be used to generate a Bode plot which encapsulates the dynamics of the plant. Using the Bode plotting rules it is then possible to identify key features of the Bode plot such as poles, zeros and resonant frequencies, from which an approximate transfer-function can be generated. When deriving the transfer-functions for the gantry robot, a least-mean-square algorithm was implemented to further increase the accuracy of the transfer-function models.

For the X-axis, the frequency range for the model construction tests, each termed an experiment, was from 0.1 to 80 Hz, 0.1 to 130 Hz for the Y-axis and 0.1 to 125 Hz for the Z-axis. The frequency-response of each axis was plotted on a Bode diagram and an approximation of the transfer-function for the corresponding dynamics obtained. Figures 3.2, 3.3 and 3.4 are taken from Ratcliffe (2005) and show the Bode plots obtained for two experiments and the final selected model for the X, Y, and Z-axes respectively.

The resulting X-axis transfer-function which was given in Ratcliffe (2005) and will be used in this thesis is

$$\begin{aligned} G_X(s) &= \frac{13077183.4436\ (s+113.4)}{s\ \ (s^2+61.57s+1.125\times10^4)} \\ &\times \frac{(s^2+30.28s+2.13\times10^4)}{(s^2+227.9s+5.647\times10^4)\ (s^2+466.1s+6.142\times10^5)} \end{aligned} \tag{3.1}$$

Similarly, the Y-axis transfer-function is

$$G_Y(s) = \frac{23.7356\ \ (s+661.2)}{s\ \ (s+213.35+359.00j)(s+213.35-359.00j)} \tag{3.2}$$

and for the Z-axis

$$G_Z(s) = \frac{15.8869\ \ (s+850.3)}{s\ \ (s+353.81+461.03j)(s+353.81-461.03j)} \tag{3.3}$$

For digital control systems design and implementation, a zero-order hold with a sampling frequency of 100 Hz is used for all tests described in this thesis. The corresponding X-axis state-space model matrices (state, input, output and direct feedthrough respectively) are given below for all three axes.

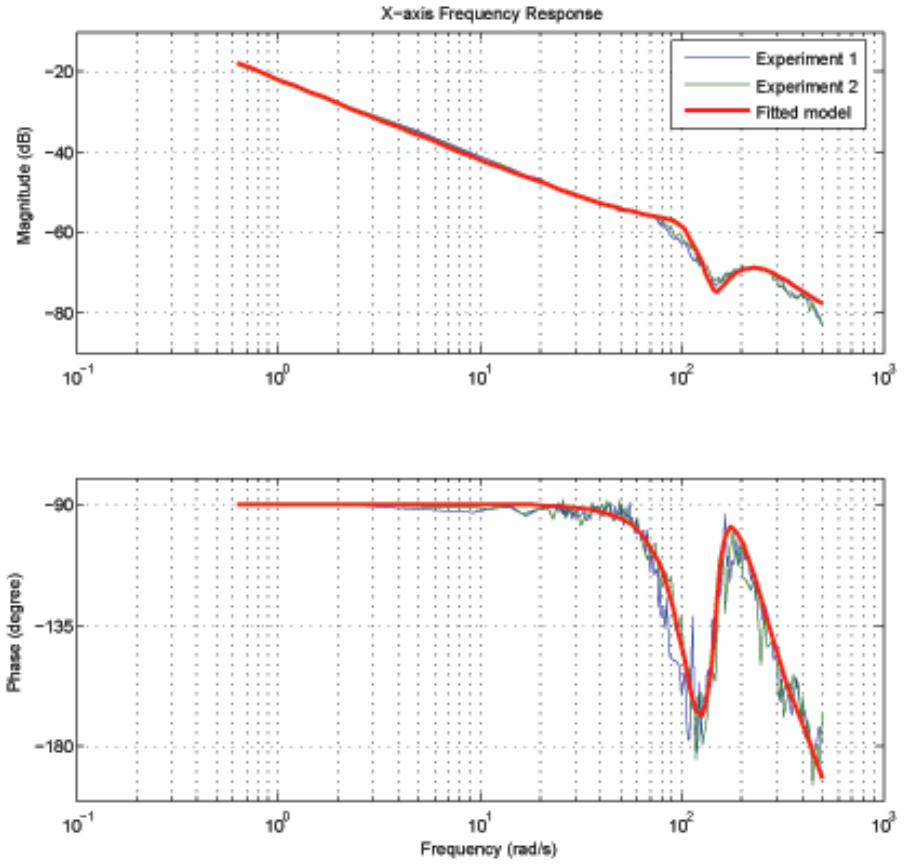

FIGURE 3.2: X-axis frequency-response

- The X-axis state-space matrices are

$$A = \begin{bmatrix} 2.4100 & -0.8559 & 0.8487 & -0.5894 & 0.3019 & -0.1943 & 0.3150 \\ 4 & 0 & 0 & 0 & 0 & 0 & 0 \\ 0 & 1 & 0 & 0 & 0 & 0 & 0 \\ 0 & 0 & 1 & 0 & 0 & 0 & 0 \\ 0 & 0 & 0 & 1 & 0 & 0 & 0 \\ 0 & 0 & 0 & 0 & 0.5 & 0 & 0 \\ 0 & 0 & 0 & 0 & 0 & 0.5 & 0 \end{bmatrix}$$

$$B = \begin{bmatrix} 0.0313 \\ 0 \\ 0 \\ 0 \\ 0 \\ 0 \\ 0 \end{bmatrix}$$

$$C = \begin{bmatrix} 0.0095 & -0.0023 & 0.0048 & -0.0027 & 0.0029 & -0.0011 & 0.0029 \end{bmatrix}$$

$$D = 0$$

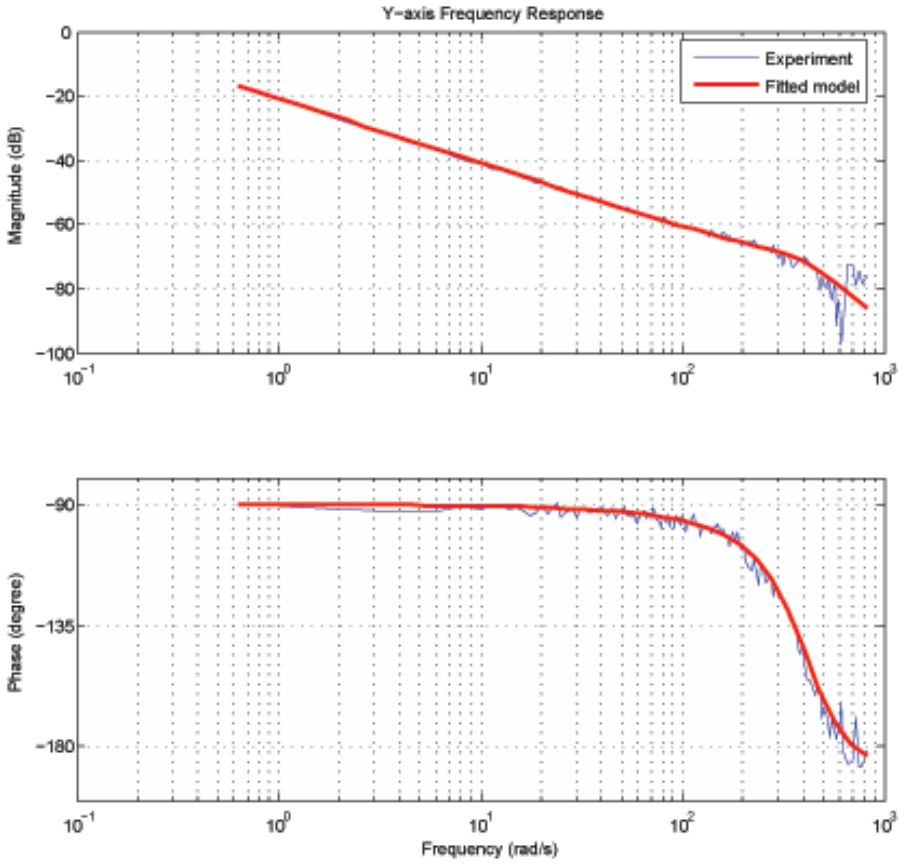

FIGURE 3.3: Y-axis frequency-response

- The Y-axis state-space matrices are

$$
\begin{aligned}
A &= \begin{bmatrix} -0.1067 & 1 & 0 \\ -0.0026 & -0.1067 & 0.3149 \\ 0 & 0 & 1 \end{bmatrix} \\
B &= \begin{bmatrix} 0 \\ 0 \\ 0.0313 \end{bmatrix} \\
C &= \begin{bmatrix} 0.0013 & 0.0081 & 0.0261 \end{bmatrix} \\
D &= 0
\end{aligned}
$$

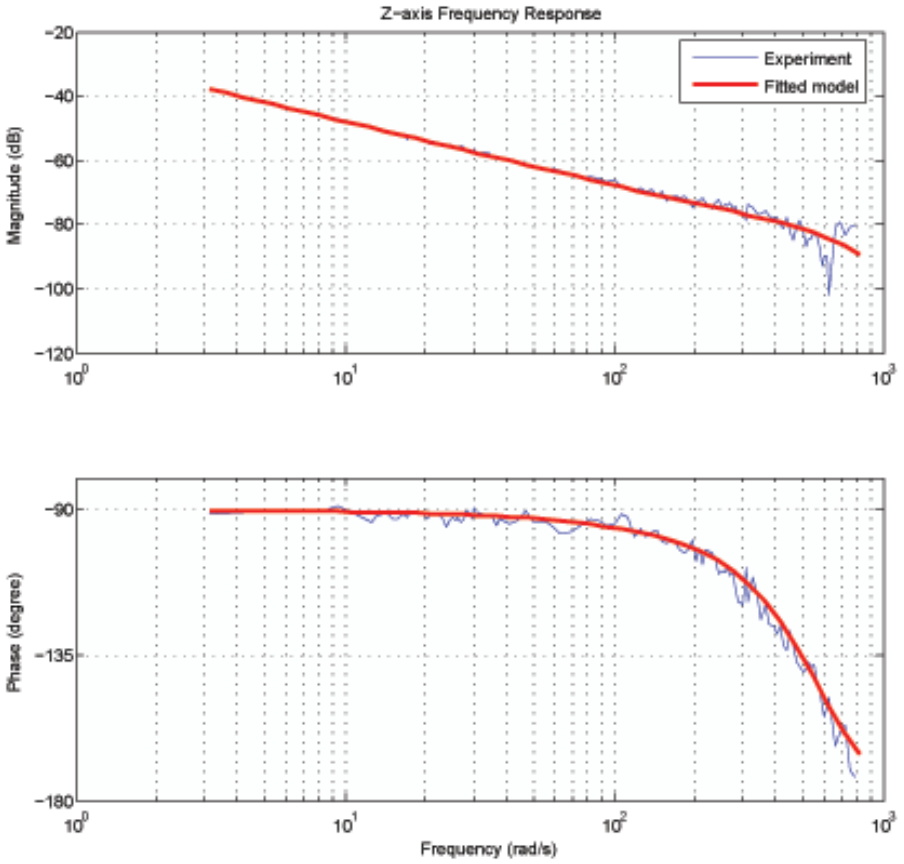

FIGURE 3.4: Z-axis frequency-response

- The Z-axis state-space matrices are

$$
\begin{aligned}
A &= \begin{bmatrix} -0.0030 & 1 & 0 \\ -0.0008 & -0.0030 & 0.3035 \\ 0 & 0 & 1 \end{bmatrix} \\
B &= \begin{bmatrix} 0 \\ 0 \\ 0.0156 \end{bmatrix} \\
C &= \begin{bmatrix} 0.0004 & 0.0071 & 0.0233 \end{bmatrix} \\
D &= 0
\end{aligned}
$$

3.2.1 Test Parameters

With all axes operating simultaneously, the reference trajectories for the axes produce a three-dimensional synchronizing pick and place action. The reference for the X-axis, shown in Figure 3.5, accelerates the robot to match velocity with the conveyor which is running beneath, then returns the axis to its start position ready for the next operation. The trajectory produces a work rate of 30 units per minute which is equivalent to a trial

time period of 2 s. Using a sampling frequency of 100 Hz, this generates 200 samples per trial. Figure 3.6 shows the 3D reference trajectory.

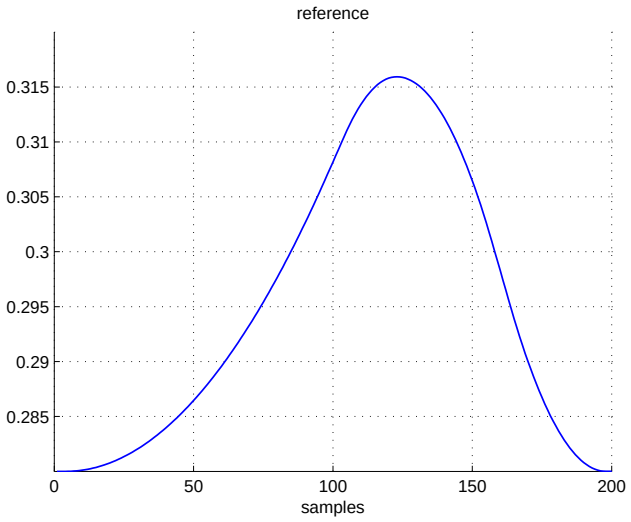

FIGURE 3.5: X-axis reference in pick and place task.

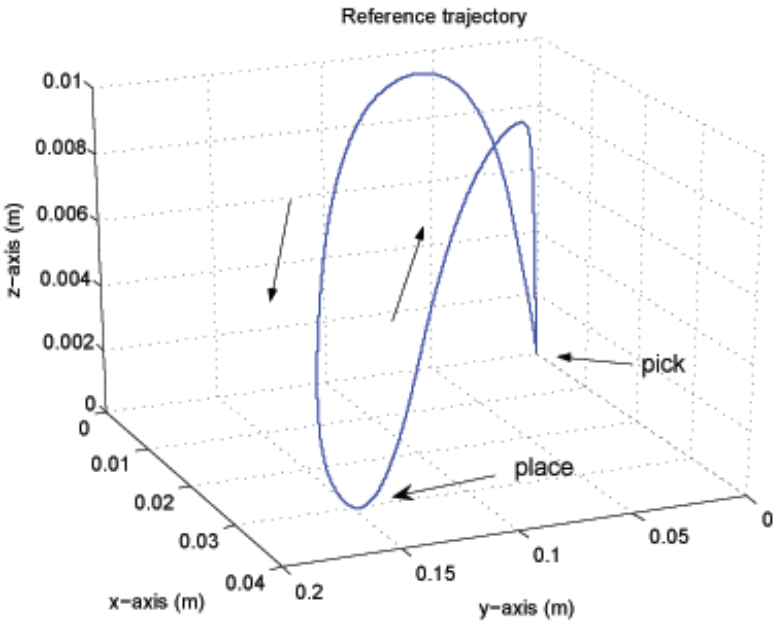

FIGURE 3.6: 3D reference trajectories prototype.

In ILC mode of operation, a 2 s stoppage time exists between each trial, during which the next input to the plant is calculated. The stoppage time also allows vibrations induced in the previous trial to die away and prevents vibrations from being propagated between trials. Before each trial, the axes are reset to within ± 30 mm of a known starting location to minimize the effects of initial state error. As well as recording input voltage and axis position during trials $10, 20, \cdots$, beginning with trial 1, the control software also calculates the Mean-Square-Error (MSE) for position over each trial. This is useful

for analysing overall performance of the system and highlights whether the tracking is generally improving or deteriorating. For trial k it is calculated using

$$MSE_k = \frac{1}{N}\sum_{i=0}^{N-1} e_k^2(i) \tag{3.4}$$

where N is the number of samples in each trial.

In RC mode of operation, there is no stoppage time between trials and so all calculations must be completed in the inter-sample period. After an initial resetting of axes position, the test runs continuously, with each reference trajectory 'looped' such that $y_d(i+N) = y_d(i)$ where N is the number of samples per trial and y_d is the reference. The plant input and output are given by u, y respectively, and the error is $e = y_d - y$. For ease of comparison with ILC, each consecutive N sample 'slice' is termed a trial, hence allowing signals to be represented analogously to those of ILC. In particular, for trial k the MSE is calculated as

$$MSE_k = \frac{1}{N}\sum_{i=0}^{N-1} e^2(i + (k-1)N) \tag{3.5}$$

As noted in the previous chapter, ILC and RC can either be directly applied to the system or process under consideration or after a pre-stabilising control loop has been applied. Figure 3.7 shows one possible arrangement in the latter case where a pre-stabilizing Proportional plus Integral plus Derivative (PID) feedback control loop has been applied.

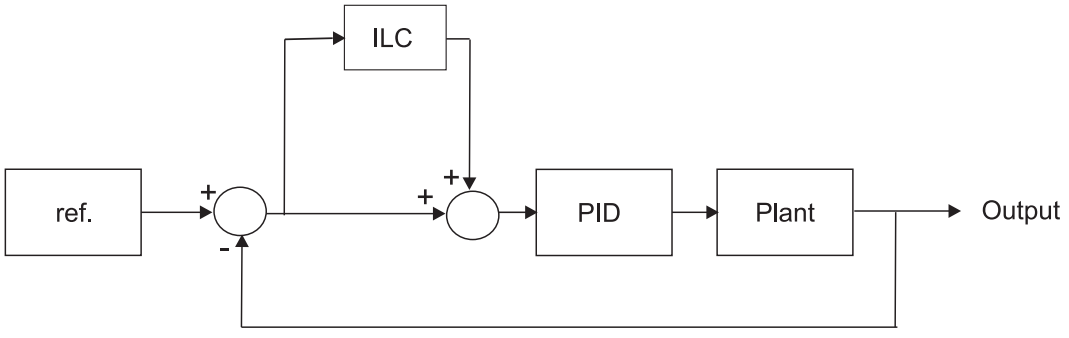

FIGURE 3.7: Hybrid ILC and PID controller - series arrangement.

This is termed a series arrangement of ILC and PID. When using such an arrangement, the system is simply taken as the closed-loop PID and plant loop, and the subsequent ILC/RC design applied to this system. Another common arrangement exists in which the output of the ILC/RC block instead is added to the output of the PID controller. This is termed a parallel configuration, and in practice, yields very similar results to the series arrangement Ratcliffe (2005).

3.2.2 Previous Use of the Gantry Robot in ILC/RC Experimental Studies

The gantry robot has already been used to experimentally test, and compare the performance of, many ILC and RC algorithms. Examples can be found in Hladowski et al. (2010, 2009), Freeman et al. (2009b), Ratcliffe et al. (2006b); Chu et al. (2010 (CD ROM), Cai et al. (2008a), Freeman et al. (2008a), Rogers (2008), Ratcliffe et al. (2007).
The majority of previous experimental tests using the gantry, including all those described in Ratcliffe (2005), do not use a pre-stabiliser, applying the control input directly to each axis in the absence of a PID controller. To facilitate straightforward comparison, therefore, all experiments in Chapter 4 of this thesis also do not use any form of pre-stabilising controller.

The experiments in Chapter 5 however, which are not intended for benchmarking, have a pre-stabilising PID controller configured as in Figure 3.7. This has been selected to more closely represent a typical situation that may be encountered in industry, where the ILC update is 'plugged-in' in to an existing feedback controller. It hence is intended to increase the generality of the initial input construction techniques described in Chapter 5, in which full details of the PID gains employed are supplied.

In both ILC and RC, it is often observed in practice that high frequencies gradually start to grow in amplitude as the trials or repetitions progress. This is caused by the presence of signal noise and modelling uncertainty which destabilises the system. Frequency domain analysis can be used to obtain frequency-wise stability bounds for standard ILC and RC approaches Freeman et al. (2009b, 2008c). Since the plant modelling uncertainty typically increases as the frequency increases, in practice there exists a frequency above which these bounds cannot be satisfied, and hence above which frequencies may start to build. This problem has been much reported in both control methodologies, but can be tackled by applying a low-pass filter to the control signal, u. In the case of ILC, the filter is applied to u_k between each trial, often taking the form of a low-pass zero-phase filter which modifies the amplitude of each frequency and not its phase. In practice, such a filter causes unwanted transient effects near each end of the signal, which can be tackled by appending a mirrored copy of the signal to each end, and then filtering the composite signal. Having done this, only the middle copy is used as the next control input Longman (2000). The addition of a filter $F(z)$ applied to the control input changes the plant model from $P(z)$ to $P(z)F(z)$ and hence the controller should ideally be designed for this new composite model. There are two reasons why this usually is not done in practice:

1. In the frequency-domain, steady-state interpretation, the controller is designed for each frequency component individually. The filter is used to remove frequencies for which the uncertain plant description cannot satisfy a known stability criterion. A zero-phase filter with sharp cut-off has little interaction with frequencies below the

cut-off, and hence redesign of the ILC scheme is usually unnecessary.

2. In practice, it is far easier to keep the ILC scheme the same and simply to add a filter. This avoids the possibility of a far higher order controller, and also the prospect of an iterative design loop where the filter and controller are redesigned many times. It of course relies on the assumption that the filter does not negatively impact on the system performance over frequencies intended to be learnt, but this is often found to be justified in practice, especially when using a zero-phase filter Longman (2000).

Perhaps the simplest way to implement a zero-phase filter is to design a low-pass filter in Finite Impulse Response (FIR) or Infinite Impulse Response (IIR) form. At the conclusion of each trial, the next control input is calculated and, as described above, then 'sandwiched' between two additional mirrored copies in order to remove the effect of transients. This composite signal is then filtered in both forward and reverse time (in Matlab this is achieved using the `filtfilt` command). Having done this, the middle section of the filtered signal is taken and used as the next control input.

In RC it is not possible to implement a zero-phase filter on the control input due to their inherent non-causal characteristic. Such a filter may be designed, for example in FIR form, and then shifted the required number of samples backwards in time needed for causality. However, this clearly compromises the zero-phase quality by adding a non-zero phase-shift, especially significant as the filter order is likely to be large. Another issue is the high computational cost, since the filtering operation must be conducted within each sample instant. Such complications mean that in RC a filter cannot simply be added to an existing repetitive controller, as described in the ILC case. Instead a filter must be designed beforehand, and RC designed for the connected system. For uniformity of underlying system model, therefore, a filter is not used in any of the RC experiments described in this thesis. A filter *is* used for all the ILC experiments described in this thesis, for two reasons

1. The majority of previous ILC experimental results using the gantry robot, including those in Ratcliffe (2005); Cai (2009), used a filter, and a similar one is used here to aid fair comparison.

2. The growth of high frequencies is generally greater in ILC due to the transients injected at the beginning of each trial, and hence a filter is usually necessary.

This filter is a 4^{th} order low-pass Chebychev filter with a 5 Hz passband edge and 1 decibel peak-to-peak ripple in the passband, given by

$$\frac{10^{-3} \times (0.1298 + 0.5194z^{-1} + 0.7791z^{-2} + 0.5194z^{-3} + 0.1298z^{-4})}{1 - 3.6079z^{-1} + 4.9795z^{-2} + -3.1108z^{-3} + 0.7415z^{-4}} \tag{3.6}$$

Between each trial of ILC it is applied in the manner described above to filter the new control input, both in forward and reverse time, to result in a zero-phase characteristic. For the reasons expounded above, all RC schemes implemented in this thesis will not include a filter.

Chapter 4

Iterative Learning Control and Repetitive Control Design via Duality

4.1 Introduction

In this chapter optimisation techniques are applied to develop a framework where iterative learning and repetitive controllers are linked by a duality relationship, which provides a mechanism for synthesis of controllers between domains. A duality framework linking the two approaches was reported in De Roover et al. (2000) but lacked a procedure through which it could be applied for controller design, thereby limiting the potential for exploitation. In this chapter techniques from optimal control are applied to derive controllers suitable for implementation. Then the framework is expanded to yield new controller structures which are linked by duality. Furthermore, experimental verification is conducted using the gantry robot to evaluate the results in De Roover et al. (2000) together with those of the new controllers shown to belong to the duality framework.

4.2 Internal Model Principle Framework

Both ILC and RC are concerned with tracking or rejecting periodic signals. It is known that any periodic signal can be generated by an autonomous system operating in a positive feedback loop where the plant model is a pure delay operator as in Figure 4.1, Inoue et al. (1981). By the internal model principle Francis and Wonham (1975) it

is known that accommodation of these periodic signals can be made through duplication of the periodic model inside the feedback control loop. This has directly led to the RC approach, but is also applicable to ILC by duality. The system shown in Figure 4.1 can be realized by the state-space system given in (4.1), where z^{-N} denotes a delay of N samples.

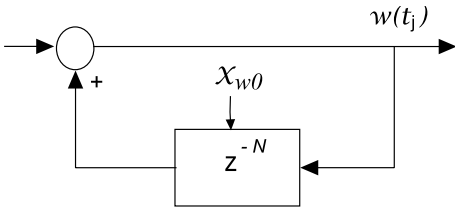

FIGURE 4.1: Periodic signal w generated by an autonomous system with appropriate initial conditions w_{w0}.

$$\begin{aligned} x_w(t_{k+1}) &= A_w x_w(t_k) + B_w v(t_k), \quad x_w(t_0) = x_{w0} \\ w(t_k) &= C_w x_w(t_k) + D_w v(t_k) \end{aligned} \tag{4.1}$$

where A_w is an $N \times N$ matrix, B_w is an $N \times 1$ vector, C_w is a $1 \times N$ row vector and D_w is a scalar direct feedthrough between the input and output with the structure given in (4.2) to (4.5), respectively. All eigenvalues of the matrix A_w lie on the unit circle in the complex plane.

$$A_w = \begin{bmatrix} 0 & 1 & 0 & \cdots & 0 \\ 0 & 0 & 1 & \cdots & 0 \\ \vdots & \vdots & \vdots & \ddots & \vdots \\ 0 & 0 & 0 & \cdots & 1 \\ 1 & 0 & 0 & \cdots & 0 \end{bmatrix} \tag{4.2}$$

$$B_w = \begin{bmatrix} 0 & \cdots & 0 & 0 & 1 \end{bmatrix}^T \tag{4.3}$$

$$C_w = \begin{bmatrix} 1 & 0 & 0 & \cdots & 0 \end{bmatrix} \tag{4.4}$$

and

$$D_w = \begin{cases} 1 & \text{current-error feedback} \\ 0 & \text{past-error feedforward} \end{cases} \tag{4.5}$$

The two cases of D_w correspond to alternative block structures of the delay operator inside the feedback loop; if $D_w = 1$ this corresponds to the structure in Figure 4.1 and if $D_w = 0$ it corresponds to the structure shown in Figure 4.2.

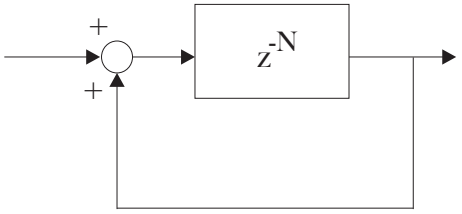

FIGURE 4.2: Past error feedforward block.

The ILC and RC approaches differ in the way the periodic compensation is applied but they are not equivalent. It has, however, been shown in De Roover and Bosgra (1997) that they are related by duality as a consequence of the difference in location of the internal model inside the controller. In fact, RC has the structure of a servo compensator as a result of the location of the internal model at the system output whereas the ILC has the structure of a disturbance observer due to the location of the internal model at the system input. These results have led to a general framework for the design of multiple-input multiple-output (MIMO) ILC and RC controllers where a number of existing schemes in both cases appear as special cases on making suitable modifications to the internal model (see De Roover and Bosgra (1997); De Roover et al. (2000)). The ability to treat RC and ILC in the same framework is highly appealing since controllers found to operate well in one arena can, in principle, be synthesised for application to the other. In De Roover et al. (2000) this structure was used to derive dual ILC and RC schemes which incorporate separate past-error and current-error feedback control loops.

In this chapter, a novel ILC/RC approach is formulated using both current-error (CE) feedback and past-error (PE) feedforward in which state-feedback is used to solve the stabilisation (and hence tracking) problem, then a dual RC/ILC scheme which uses output feedback is developed. These controllers complete a set of ILC/RC controllers that extend the set of underlying plants which may be controlled under the duality framework using both state and output feedback. Controllers reported using the duality approach in De Roover et al. (2000) are explained and experimental results for the X-axis of the gantry robot are given.

4.2.1 Dual ILC and RC Framework

Let the MIMO plant to be controlled be defined as

$$\begin{aligned} x(t+1) &= Ax(t) + Bu(t), \quad x(0) = x_0 \\ y(t) &= Cx(t) + Du(t) \end{aligned}$$

with corresponding transfer-function matrix $G(s) = C(sI_{n_x} - A)^{-1}B + D$. Here $y(t) \in \mathbb{R}^{n_y}$, $u(t) \in \mathbb{R}^{n_u}$ and $x(t) \in \mathbb{R}^{n_x}$ represent the output, input and the states respectively. I_{n_x} denotes the $n_x \times n_x$ identity matrix, and a sample time of unity is assumed for notational simplicity. In the case of ILC, this is run over a finite trial interval of N samples, with resetting of the initial plant states between trials. In RC the reference signal, denoted by $r(t)$ in this chapter, is periodic with period N (i.e. $r(t+N) = r(t)$) and the control update process occurs on-line, with no resetting between periods.
The robust periodic control problem can be stated as follows:

Find a feedback controller $K(z)$ such that the resulting closed-loop system has the following properties.

1. *Asymptotic stability.*
2. *The tracking error tends to zero exponentially for all periodic reference vectors r and periodic input signal satisfying (4.1).*
3. *The two properties listed above are robust to perturbations in the model plant dynamics.*

The solution to this robust periodic control problem is given by the internal model principle Francis and Wonham (1975). In particular, suppose that the controller $K(z)$ contains in each channel a realisation of the disturbance generating system driven by the error $E(z)$. Also let $K(z)$ be such that the feedback connection of $K(z)$ and $G(z)$ is internally stable. Then $K(z)$ solves the robust periodic control problem.

Both ILC and RC attempt to solve the robust periodic control problem and hence it follows that the internal model principle provides a solution for these cases. Also this principle can be formulated as a servo compensator where the disturbance model is realized in each channel of the output space (or vector) or, dually, in each channel of the input space (or vector). In De Roover et al. (2000) the first case here corresponds to implementation of an RC controller and the second uses the structure of a disturbance

observer and corresponds to an ILC controller.

Considering the general class of RC past-error algorithms, the update law can be written in general form as

$$u(t+N) = u(t) + R(z)e(t) \tag{4.6}$$

where $R(z)e(t)$ is shorthand notation for $\mathcal{Z}^{-1}\{R(z)\} * e(t)$ and $R(z)$ is a discrete-time transfer-function. The output equation can be written as

$$\begin{aligned} y(t+N) &= y(t) + P(z)R(z)e(t) \\ y(t+N) - y(t) &= P(z)R(z)e(t) \\ (z^N I_{n_y} - I_{n_y})y(z) &= P(z)R(z)e(z) \\ y(z) &= \phi(z)P(z)R(z)e(z) \\ y(z) &= P(z)R(z)\phi(z)e(z) \end{aligned} \tag{4.7}$$

where $P(z)$ represents the plant and $\phi(z)$ represents the delay transfer-function $(z^N I_{n_y} - I_{n_y})^{-1}$. Commutation of $\phi(z)$ in the last relation of (4.7) is due to the $n_y \times n_y$ diagonal structure of $\phi(z)$ with identical diagonal elements. This leads to the block diagram structure of Figure 4.3.

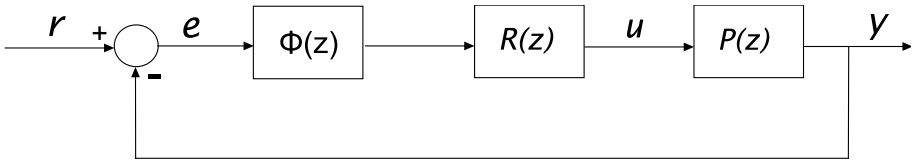

FIGURE 4.3: Repetitive control feedback representation.

In the case of ILC, on trial k the past-error update law is written as

$$u_{k+1}(t) = u_k(t) + L(z)e_k(t) \tag{4.8}$$

where $L(z)$ is a discrete-time transfer-function matrix. A similar analysis to (4.7), and neglecting the effects of the initial conditions, gives the following expression for the system output

$$y(z) = P(z)\phi(z)L(z)e(z) \tag{4.9}$$

where $\phi(z)$ again represents the delay transfer-function matrix $(z^N I_{n_u} - I_{n_u})^{-1}$. Figure 4.4 shows the ILC configuration in terms of a feedback representation.

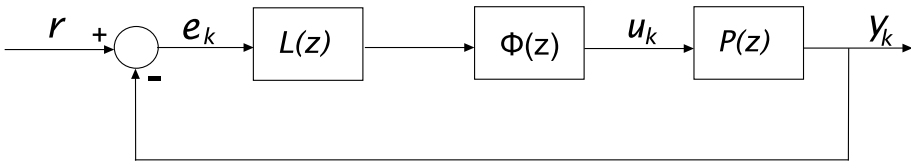

FIGURE 4.4: Iterative learning control feedback representation.

Note that Figures 4.3 and 4.4 use the delay transfer-function which has an internal representation given in Figure 4.5a (past-error), where $(z^{-N}I)$ represents a delay of one period with N samples. If $\phi(z)$ is a causal dynamic system, it has N states in each channel.

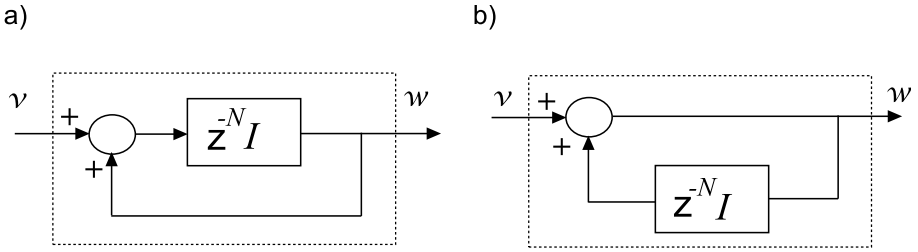

FIGURE 4.5: Representation of $\phi(z)$ for a) past-error feedforward and b) for current-error feedback.

In RC there are n_y channels as $\phi(z)$ operates in the output space, whereas in ILC $\phi(z)$ has n_u channels as it operates in the input space.

The first step in stability analysis De Roover et al. (2000) for the RC feedback system is to isolate the delay chain of the internal model to obtain the equivalent system representation shown in Figure 4.5 Hara et al. (1988). The delay chain has unity gain and hence by the small gain theorem Deoser and Vidyasagar (1975) a sufficient condition for stability is

$$\|I_{n_y} - P(z)R(z)\|_i < 1 \tag{4.10}$$

for some induced i norm. Repeating the analysis given above for the RC case, leads to the following sufficient condition for stability of the ILC scheme

$$\|I_{n_u} - L(z)P(z)\|_i < 1 \tag{4.11}$$

This framework extends to incorporate the current-error feedback structure which corresponds to the internal model shown in Figure 4.5b. This leads to high gain solutions Owens (1992); Chen et al. (1996). Here (4.6) is replaced in the RC case by

$$u(t+N) = u(t) + R(z)e(t+N) \tag{4.12}$$

with internal model ϕ defined as $(I_{n_y} - I_{n_y}z^{-N})^{-1}$, and repeating the analysis given above leads to the following sufficient condition for stability of this latest version of RC

$$\|(I_{n_y} + P(z)R(z))^{-1}\|_i < 1 \tag{4.13}$$

In ILC case, (4.8) is replaced by

$$u_{k+1}(t) = u_k(t) + L(z)e_{k+1}(t) \tag{4.14}$$

with $\phi(z)$ defined as $(I_{n_u} - I_{n_u}z^{-N})^{-1}$, and the associated stability condition is

$$\|(I_{n_u} + L(z)P(z))^{-1}\|_i < 1 \tag{4.15}$$

Dual ILC and RC controllers are now developed which can incorporate PE feedforward and CE feedback. These will demonstrate the power of the duality framework, and present a set of state and output feedback RC and ILC designs. It will also be shown that these extend the range of plants for which tracking is possible in this setting. A solution to the output feedback design problem is also developed.

4.3 Controller Design in the Duality Framework

The approach taken in this thesis is to stabilise the series connection of the plant and the internal model structure using controllers which encompass both error structures (CE and PE). The resulting controllers complement those developed in De Roover et al. (2000) and extend the set of control structures operating within the same duality framework. To begin analysis, it is first necessary to extend the internal model description (4.1) to include the MIMO case. To achieve this, define the matrices

$$A_r = \begin{bmatrix} A_w & 0 & \cdots & 0 \\ 0 & A_w & \cdots & 0 \\ \vdots & \vdots & \ddots & \vdots \\ 0 & 0 & \cdots & A_w \end{bmatrix} \tag{4.16}$$

$$B_r = \begin{bmatrix} B_w & 0 & \cdots & 0 \\ 0 & B_w & \cdots & 0 \\ \vdots & \vdots & \ddots & \vdots \\ 0 & 0 & \cdots & B_w \end{bmatrix} \tag{4.17}$$

$$C_r = \begin{bmatrix} C_w & 0 & \cdots & 0 \\ 0 & C_w & \cdots & 0 \\ \vdots & \vdots & \ddots & \vdots \\ 0 & 0 & \cdots & C_w \end{bmatrix} \tag{4.18}$$

and

$$D_r = \begin{bmatrix} D_w & 0 & \cdots & 0 \\ 0 & D_w & \cdots & 0 \\ \vdots & \vdots & \ddots & \vdots \\ 0 & 0 & \cdots & D_w \end{bmatrix} \tag{4.19}$$

where each diagonal block is repeated n_y times for the RC case. In a similar way define $\{A_l, B_l, C_l, D_l\}$ where each diagonal block is repeated n_u times for the ILC case,

$$\begin{aligned} A_l &= \texttt{diag}\{A_w, A_w, \cdots, A_w\} \\ B_l &= \texttt{diag}\{B_w, B_w, \cdots, B_w\} \\ C_l &= \texttt{diag}\{C_w, C_w, \cdots, C_w\} \\ D_l &= \texttt{diag}\{D_w, D_w, \cdots, D_w\} \end{aligned} \tag{4.20}$$

Then the internal model $\phi(z)$ is given for the two considered error cases (PE and CE) by the following transfer-function

$$C_r(zI_{N_y} - A_r)^{-1}B_r + D_r = \begin{cases} (z^N I_{n_y} - I_{n_y})^{-1} & \text{if} \quad D_w = 0 \\ (I_{n_y} - z^{-N} I_{n_y})^{-1} & \text{if} \quad D_w = 1 \end{cases} \tag{4.21}$$

and

$$C_l(zI_{N_u} - A_l)^{-1}B_l + D_l = \begin{cases} (z^N I_{n_u} - I_{n_u})^{-1} & \text{if} \quad D_w = 0 \\ (I_{n_u} - z^{-N} I_{n_u})^{-1} & \text{if} \quad D_w = 1 \end{cases} \tag{4.22}$$

for RC and ILC, respectively.

4.3.1 ILC Approach Development in the Duality Framework

The position of the internal model for ILC is shown in Figure 4.4. In the duality framework previously considered, this was shown to correspond to a disturbance observer/-compensator, leading to the designs in De Roover et al. (2000). In this section the control structure developed effectively contains two realisations of the internal model, allowing it to use a servomechanism arrangement to fulfil the periodic tracking task whilst still corresponding to the ILC structure.

First the ILC system shown in Figure 4.4 is considered. Here for PE feedforward $\phi(z) = (z^N I_{n_u} - I_{n_u})^{-1}$, and the relationship between the output of the internal model and the input is governed by the following equation, where $u_k(t)$ represents the output and $v_k(t)$ represents the input signal

$$\frac{u_k(t_k)}{v_k(t_k)} = \phi(z) = (z^N I_{n_u} - I_{n_u})^{-1} \tag{4.23}$$

Hence the internal model input $v_k(t_k) = u_k(t_{k+N}) - u_k(t_k)$ is the input difference from trial-to-trial, $\tilde{u}(t_k)$. For the CE case the input/output relationship is governed by $v_k(t_{k+N}) = u_k(t_{k+N}) - u_k(t_k)$. Now define the series connection between $\phi(z)$ and $P(z)$ using the internal model in (4.1) in a state-space representation as

System

$$\begin{aligned} x_{k+1} &= Ax_k + Bu_k & (4.24)\\ y_{k+1} &= Cx_k + Du_k & (4.25) \end{aligned}$$

with error

$$e_k = r - Cx_k - Du_k \tag{4.26}$$

Internal Model

$$\begin{aligned} x_{l,k+1} &= A_l x_{l,k} + B_l \tilde{u}_k & (4.27)\\ u_k &= C_l x_{l,k} + D_l \tilde{u}_k & (4.28) \end{aligned}$$

Coupled system

$$\begin{bmatrix} x_{l,k+1} \\ x_{k+1} \end{bmatrix} = \begin{bmatrix} A_l & 0 \\ BC_l & A \end{bmatrix} \begin{bmatrix} x_{l,k} \\ x_k \end{bmatrix} + \begin{bmatrix} B_l \\ BD_l \end{bmatrix} \tilde{u}_k \tag{4.29}$$

and the error is given by

$$e_k = r - \begin{bmatrix} DC_l & C \end{bmatrix} \begin{bmatrix} x_{l,k} \\ x_k \end{bmatrix} - DD_l \tilde{u}_k \tag{4.30}$$

The key observation here is that regulation of this system solves the tracking problem, since its input is the trial to trial difference, $\tilde{u}(t_k)$ and its output is the error. This can be accomplished using techniques from adaptive control or robust control, but here optimal

control via state-feedback is considered, leading to a control input and an observer of the following form

Control Input

$$\tilde{u}_k = -K \begin{bmatrix} \hat{x}_{l,k} \\ \hat{x}_k \end{bmatrix} \tag{4.31}$$

and

Observer

$$\begin{aligned} \begin{bmatrix} \hat{x}_{l,k+1} \\ \hat{x}_{k+1} \end{bmatrix} &= \begin{bmatrix} A_l & 0 \\ BC_l & A \end{bmatrix} \begin{bmatrix} \hat{x}_{l,k} \\ \hat{x}_k \end{bmatrix} - \begin{bmatrix} B_l \\ BD_l \end{bmatrix} K \begin{bmatrix} \hat{x}_{l,k} \\ \hat{x}_k \end{bmatrix} \\ &+ L(e_k + \begin{bmatrix} DC_l & C \end{bmatrix} \begin{bmatrix} \hat{x}_{l,k} \\ \hat{x}_k \end{bmatrix}) + LDD_l\tilde{u}_k \\ &= \begin{bmatrix} A_l & 0 \\ BC_l & A \end{bmatrix} \begin{bmatrix} \hat{x}_{l,k} \\ \hat{x}_k \end{bmatrix} - \begin{bmatrix} B_l \\ BD_l \end{bmatrix} K \begin{bmatrix} \hat{x}_{l,k} \\ \hat{x}_k \end{bmatrix} \\ &+ L\left(\begin{bmatrix} DC_l & C \end{bmatrix}\right)(\begin{bmatrix} \hat{x}_{l,k} \\ \hat{x}_k \end{bmatrix} - \begin{bmatrix} x_{l,k} \\ x_k \end{bmatrix}) + Lr \end{aligned} \tag{4.32}$$

The overall scheme is shown in Figure 4.6, where the observer introduced is activated by the error and the observer state-feedback.

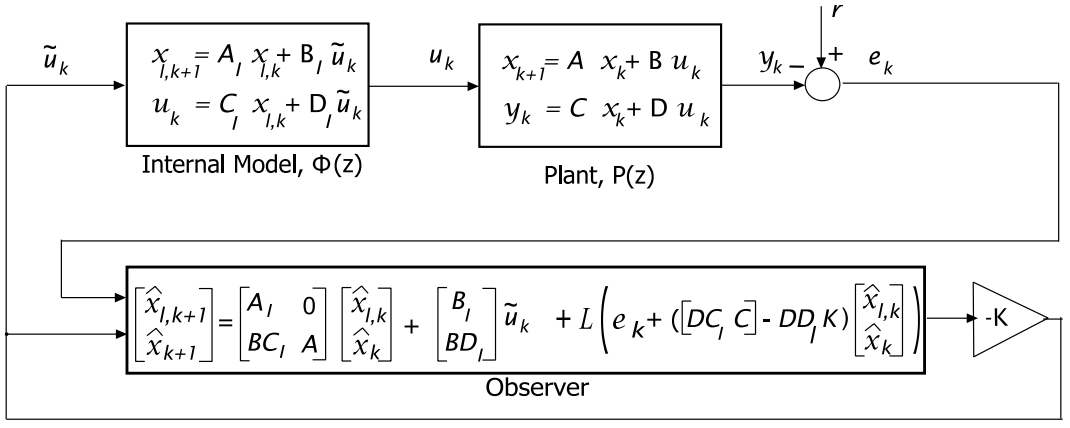

FIGURE 4.6: Synthesized iterative learning control scheme.

The feedback loop, or path, including $z^{-N} I_{N_u}$, must be stabilized before proceeding further with the analysis. This is defined by the path between the vector signals `in` and

`out` respectively in the equivalent system shown in Figure 4.7. The small gain theorem can again be used to give a sufficient condition for stability.

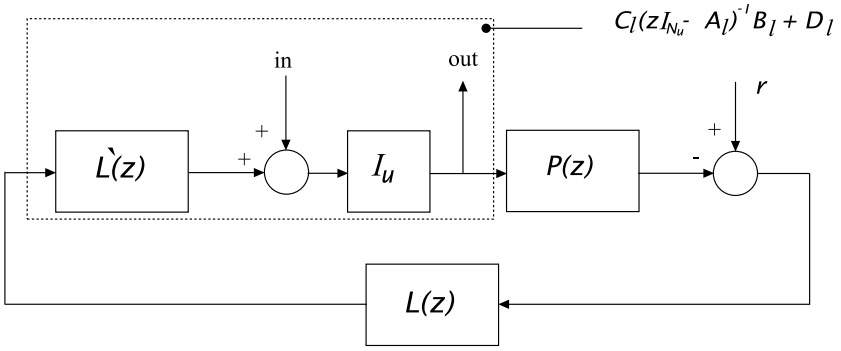

FIGURE 4.7: Internal model-based iterative learning control scheme.

Figures 4.6 and 4.7 are equivalent when $L(z)$ in Figure 4.7 is chosen as

$$L(z) := -K\left(zI - \begin{bmatrix} A_l & 0 \\ BC_l & A \end{bmatrix} + \begin{bmatrix} B_l \\ DB_l \end{bmatrix} K - L\left(\begin{bmatrix} DC_l & C \end{bmatrix} - DD_lK\right)\right)^{-1} L$$

where $L'(z)$ in Figure 4.7 is such that $C_l(zI_{N_u} - A_l)^{-1}B_l + D_l = (I_{n_u} - z^{-N}I_{n_u})^{-1}L'(z)$ and that $L'(z) = D_l + C_lB_lz^{-1} + C_lA_lB_lz^{-2} + \cdots + C_lA_l^{N-1}B_lz^{-N}$. Note that the presence of the term D_l in this equation means that either the current or past-error signal can be included in the design.

Figure 4.8 shows the two cases in terms of internal model-based ILC schemes where part a) gives the structure in the past-error feedforward case and part b) that for the current-error case. The regulation condition is formed by deriving the relationship between `out` and `in` for both cases. For the past-error case the equation is

$$\text{out}(z) = (G(z) + P(z))\, G(z)^{-1}\text{in}(z) \tag{4.33}$$

and for the current-error case the equation is

$$\text{out}(z) = G(z)\,(G(z) - P(z))^{-1}\,\text{in}(z) \tag{4.34}$$

where $G(z)$ in both cases is given by

$$G(z) = \begin{bmatrix} DC_l & C \end{bmatrix} \left(zI - \begin{bmatrix} A_l & 0 \\ BC_l & A \end{bmatrix} + \begin{bmatrix} B_l \\ DB_l \end{bmatrix} K \right)^{-1} \begin{bmatrix} B_l \\ DB_l \end{bmatrix} + DD_l$$

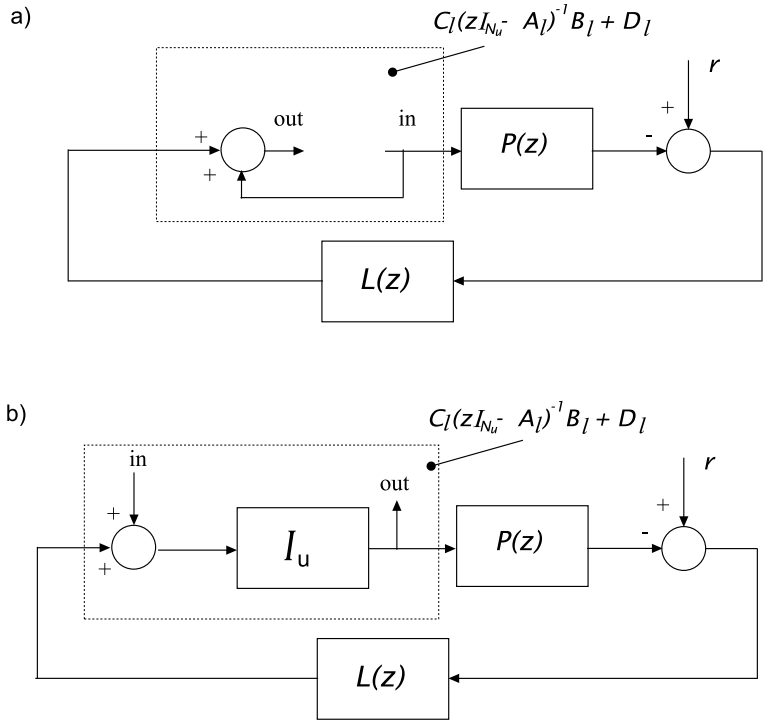

FIGURE 4.8: Internal model-based iterative learning control scheme *a*) past-error case and *b*) current-error feedback.

The equivalent system, which defines the feedback dynamics, is given by

$$\begin{bmatrix} \tilde{x}_{l,k+1} \\ \tilde{x}_{k+1} \end{bmatrix} = \underbrace{\begin{bmatrix} A_l & 0 \\ BC_l & A \end{bmatrix}}_{\text{system matrix}} \begin{bmatrix} \tilde{x}_{l,k} \\ \tilde{x}_k \end{bmatrix} - \underbrace{\begin{bmatrix} B_l \\ BD_l \end{bmatrix}}_{\text{input matrix}} \overbrace{K}^{\text{state-feedback}} \begin{bmatrix} \tilde{x}_{l,k} \\ \tilde{x}_k \end{bmatrix} \tag{4.35}$$

which must be stabilized to solve the tracking problem. This can also be seen by noting that the input to (4.29) is the trial-to-trial control difference and its output is the error. The LQR approach is selected to regulate the states and drive the error to zero. A suitable cost function is to minimise

$$\begin{aligned} \min \quad & \sum_{k=1}^{\infty} \eta_k^T Q \eta_k + \mu_k^T R \mu_k \\ \eta_{k+1} \quad &= \begin{bmatrix} A_l & 0 \\ BC_l & A \end{bmatrix} \eta_k - \begin{bmatrix} B_l \\ BD_l \end{bmatrix} \mu_k \\ \mu_k \quad &= K \eta_k \end{aligned} \tag{4.36}$$

which can be computed for K using the `dlqr` function in Matlab. The observer matrix L can be computed in the form of a standard Kalman estimator for the coupled system (4.29) using the `kalman` function in Matlab, with process covariance matrix $\hat{Q}$ and measurement covariance matrix $\hat{R}$.

Note that the separation principle permits separate design of K and L.

4.3.2 Dual RC Controller Design

The analysis above has implemented ILC as a servomechanism and hence the development of a RC dual is more straightforward than in De Roover and Bosgra (1996); De Roover et al. (2000) since no change in the stabilisation structure is required.

To produce an RC dual of the ILC control scheme developed above consider the repetitive system shown in Figure 4.3 which gives (for PE) $v(t_{k+N}) = v_k(t_k) + e_k(t_k)$, so that the internal model output $v_k(t_k)$ in Figure 4.9 comprises trial-to-trial error integration (for CE case it would be $v(t_{k+N}) = v_k(t_k) + e_k(t_{k+N})$) . The presence of this signal, together with the internal error signal, e_k, ensures that regulation of the coupled system yields tracking of the periodic reference $r(t)$. Consider the system given in (4.24) and the error given in (4.26), then the internal model which has the error signal as its input is given by

$$x_{r,k+1} = A_r x_{r,k} + B_r e_k \tag{4.37}$$

$$v_k = C_r x_{r,k} + D_r e_k \tag{4.38}$$

Coupling the two systems in series (plant and internal model) produces a system with the following structure

$$\begin{bmatrix} x_{r,k+1} \\ x_{k+1} \end{bmatrix} = \begin{bmatrix} A_r & -BC_r \\ 0 & A \end{bmatrix} \begin{bmatrix} x_{r,k} \\ x_k \end{bmatrix} + \begin{bmatrix} -B_r D \\ B \end{bmatrix} u_k + \begin{bmatrix} B_r \\ 0 \end{bmatrix} r \tag{4.39}$$

Again, LQR based state-feedback is used to regulate the system and hence drive the error to zero. Thus the control input is selected as

$$u_k = -K \begin{bmatrix} \hat{x}_{r,k} \\ \hat{x}_k \end{bmatrix} \tag{4.40}$$

The states are estimated using the observer

$$\begin{aligned} \begin{bmatrix} \hat{x}_{r,k+1} \\ \hat{x}_{k+1} \end{bmatrix} &= \begin{bmatrix} A_r & -B_r C \\ 0 & A \end{bmatrix} \begin{bmatrix} \hat{x}_{r,k} \\ \hat{x}_k \end{bmatrix} + \begin{bmatrix} -B_r D \\ B \end{bmatrix} u_k \\ &+ L \left(v_k - \left(\begin{bmatrix} C_r & -D_r C \end{bmatrix} + D_r DK \right) \begin{bmatrix} \hat{x}_{r,k} \\ \hat{x}_k \end{bmatrix} \right) \end{aligned} \tag{4.41}$$

The overall scheme is shown in Figure 4.9, where the observer introduced is fed by the state-feedback and the internal model output. Again, stabilisation of the feedback loop including $z^{-N} I_{N_y}$ is required, and this loop is defined by the path between the signals `in` and `out` appearing in the equivalent system shown in Figure 4.10.

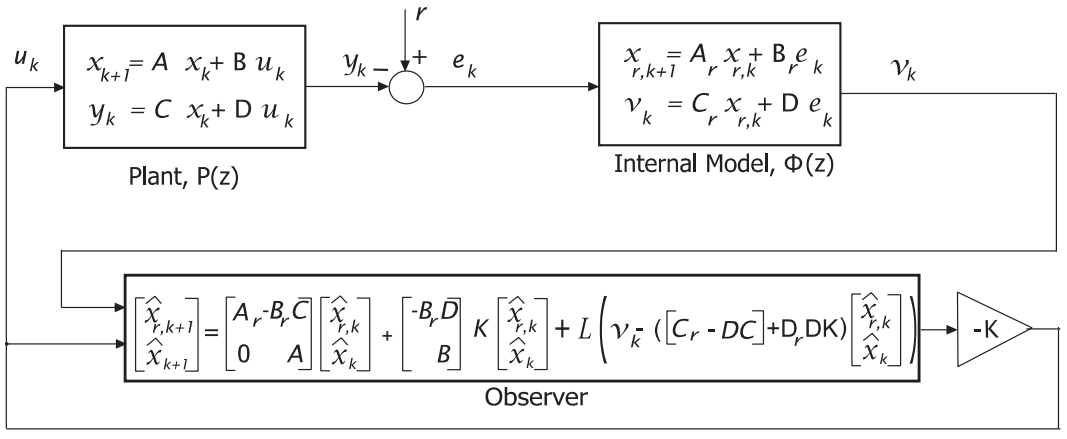

FIGURE 4.9: Synthesized repetitive control scheme.

Comparing Figures 4.9 and 4.10 it follows that $R(z)$ is defined as

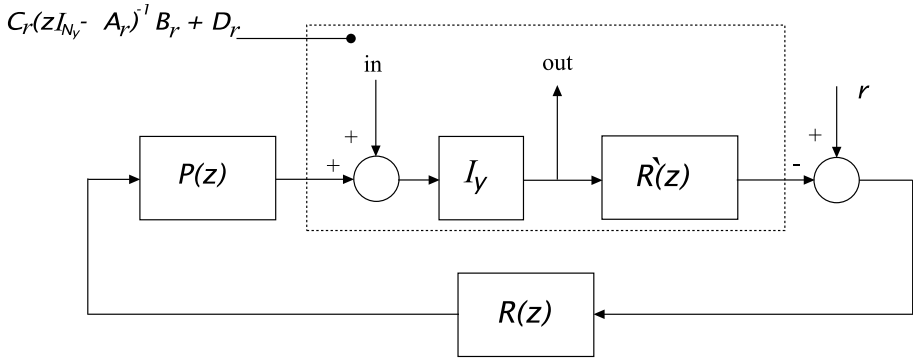

FIGURE 4.10: Internal model-based repetitive control scheme.

$$R(z) := -K\left(zI - \begin{bmatrix} A_r & -B_rC \\ 0 & A \end{bmatrix} + \begin{bmatrix} B_rD \\ -B \end{bmatrix} K + L\left(\begin{bmatrix} C_r & -D_rC \end{bmatrix} + D_rDK\right)\right)^{-1} L$$

and $R'(z)$ is such that $C_r(zI_{N_y} - A_r)^{-1}B_r + D_r = R'(z)(I_{n_y} - z^{-N}I_{n_y})^{-1}$. Hence $R'(z) = D_r + C_rB_rz^{-1} + C_rA_rB_rz^{-2} + \cdots + C_rA_r^{N-1}B_rz^{-N}$. Here the presence of the D_r term allows both the CE and PE cases to be addressed. In order to find the equation governing the two variables `in` and `out`, the structure is separated into two figures, Figure 4.11 *a*) and *b*).

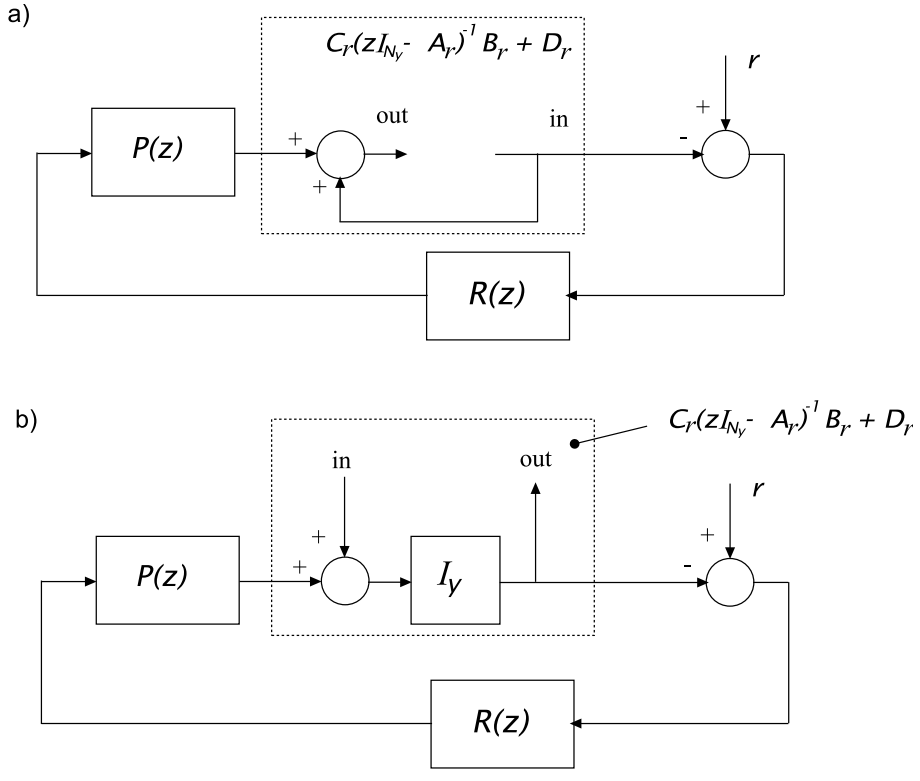

FIGURE 4.11: Internal model-based repetitive control scheme.

In both cases the relationship is the same as that of (4.33) and (4.34) respectively with $G(z)$ defined as

$$G(z) = \begin{bmatrix} C_r & -D_rC \end{bmatrix} \left(zI - \begin{bmatrix} A_r & -B_rC \\ 0 & A \end{bmatrix} + \begin{bmatrix} B_rD \\ -B \end{bmatrix} K \right)^{-1} \begin{bmatrix} B_rD \\ B \end{bmatrix} - D_rD$$

Hence

$$\begin{bmatrix} \tilde{x}_{r,k+1} \\ \tilde{x}_{k+1} \end{bmatrix} = \underbrace{\begin{bmatrix} A_r & -B_rC \\ 0 & A \end{bmatrix}}_{\text{system matrix}} \begin{bmatrix} \tilde{x}_{r,k} \\ \tilde{x}_k \end{bmatrix} - \underbrace{\begin{bmatrix} B_rD \\ -B \end{bmatrix}}_{\text{input matrix}} \underbrace{K}_{\text{state-feedback}} \begin{bmatrix} \tilde{x}_{r,k} \\ \tilde{x}_k \end{bmatrix} \tag{4.42}$$

and regulation of this system ensures tracking of the reference, which follows immediately on noting that the output of the series connection (4.39) is cycle-to-cycle error integration.

LQR is again be applied to calculate state-feedback matrix K where the separation principle permits K and L to be designed independently. The matrix K is computed as the solution of the LQR problem

$$\begin{aligned} \min \quad & \sum_{k=1}^{\infty} \eta_k^T Q \eta_k + \mu_k^T R \mu_k \\ \eta_{k+1} \quad &= \begin{bmatrix} A_r & -B_rC \\ 0 & A \end{bmatrix} \eta_k - \begin{bmatrix} B_rD \\ -B \end{bmatrix} \mu_k \\ \mu_k \quad &= K \eta_k \end{aligned} \tag{4.43}$$

which can be achieved using the `dlqr` function in Matlab. The observer matrix L can be computed in the form of a standard Kalman estimator for the coupled system (4.39) using the `kalman` function in Matlab, with process covariance matrix $\hat{Q}$ and measurement covariance matrix $\hat{R}$.

Note that, despite the differing structure compared with the RC scheme considered in De Roover et al. (2000), which incorporated an explicit current-error feedback loop, together with an observer for only the plant, $P(z)$, the same equivalent structure (4.42), results in both cases.

4.3.3 Stability Conditions for the developed ILC and Dual RC schemes

The design of the ILC scheme (4.31) and the RC scheme (4.40) involves the selection of the gain matrices $\{L, K\}$ in each case. The following results give necessary and sufficient conditions for their existence, and are special cases of the general servo compensator and disturbance observer problem, full proofs of which are given in De Roover and Bosgra (1996).

Theorem 4.1. *Consider the ILC law (4.31) and suppose that L is chosen such that* $\begin{bmatrix} A_l & 0 \\ BC_l & A \end{bmatrix} - L \begin{bmatrix} DC_l & C \end{bmatrix}$ *is asymptotically stable. Suppose also that K is chosen such that the linear system (4.35) is asymptotically stable. Then (4.31) solves the problem under consideration if, and only if,*

$$\operatorname{rank}\left(\begin{bmatrix} \lambda I - A & B \\ -C & D \end{bmatrix}\right) = n_x + n_y$$

for all λ in the spectrum of the matrix A_w, (consisting of N roots equally spaced on the unit disk).

Theorem 4.2. *Consider the RC law (4.40) and suppose that L is chosen such that* $\begin{bmatrix} A_r & -B_rC \\ 0 & A \end{bmatrix} - L \begin{bmatrix} C_r & -D_rC \end{bmatrix}$ *is asymptotically stable. Suppose also that K is chosen such that the linear system (4.42) is asymptotically stable. Then (4.40) solves the problem under consideration if, and only if,*

$$\operatorname{rank}\left(\begin{bmatrix} \lambda I - A & B \\ -C & D \end{bmatrix}\right) = n_x + n_y$$

for all λ in the spectrum of the matrix A_w.

Theorems 4.1 and 4.2 require that the plant transfer-function does not have transmission zeros which are also eigenvalues of the disturbance system and that it must have at least as many inputs as outputs.

Remark 4.1 *It is the duplication of the internal model in the controllers developed in this chapter which has allowed the ILC controller to take the form of a servomechanism, rather than the alternative disturbance observer/compensator structure previously considered in De Roover et al. (2000). It has therefore been shown that the same structure of controller is feasible for both ILC and RC cases, and they may therefore be considered duals of each other.*

In order to compare the use of output feedback and output injection, a disturbance observer/compensator implementation will be derived in Section 4.4 using the internal model structures shown in Figure 4.5.

4.3.4 Experimental verification

This section gives the results of an experimental programme where the algorithms developed so far in this chapter are applied to the X-axis of the gantry robot and discrete-time model of this axis detailed in Chapter 3. All experiments were undertaken using a sampling frequency of 100 Hz. All experiments in this Chapter use the X-axis reference shown in Figure 3.5.

4.3.4.1 Experimental Verification — ILC

The first set of experiments aims to establish if the use of current-error information provides advantages when compared to the previous-error feedforward approach. The matrices in the LQR cost function (4.36) have been selected following extensive investigation of many different forms, and are given by $Q = \begin{bmatrix} Q_1 I_{N_u} & 0 \\ 0 & Q_2 I_{n_x} \end{bmatrix}$ and $R = R_1 I_{n_u}$, and Table 4.1 gives the values of the scalars Q_1, Q_2 and R_1 used for the experiments. As previously described, the Matlab `dlqr` function is used to provide the solution. The process and measurement covariance matrices used in the calculation of the observer matrix L are given by $\hat{Q} = \begin{bmatrix} \hat{Q}_1 I_{N_u} & 0 \\ 0 & \hat{Q}_2 I_{n_x} \end{bmatrix}$ and $\hat{R} = \hat{R}_1 I_{n_y}$. As described previously, the Matlab `kalman` function is used to yield the solution. The controller shown in Figure 4.6 has been implemented using the software environment described in Chapter 3. In the ILC framework the plant is reset between each iteration, however the state matrices $\hat{x}_{l,k}$ and $\hat{x}_k$ appearing in the observer, and $x_{l,k}$ appearing in the internal model are not reset. The system therefore starts with the final state values from the previous trial. The filter (3.6) is used in all the ILC experiments described in this Chapter, and is applied to the input signal, u_k, during the reset period between trials, in the manner described in Chapter 3. However, the input signal u_k equates to the state matrix of the internal model, and hence it is the states $x_{l,k}$ which are filtered between iterations.

Figure 4.12 shows the measured mean square error produced by the controlled system in each case plotted against trial number. These results were obtained with $D_w = 0$. Of these results, Set 4 has the lowest error over the earlier trials and a similar level to the other sets for the rest of the 200 trials completed.

Figures 4.13, 4.14 and 4.15 show a 3D plot for the output, input and error signals for Set

	Designing K			Designing L		
Set	Q_1	Q_2	R_1	$\hat{Q}_1$	$\hat{Q}_2$	$\hat{R}_1$
1	10	0.1	1	10	0.1	1
2	100	0.1	1	100	0.1	1
3	100	0.1	1	10	1	1
4	10	1	1	10	0.1	1
5	100	1	1	10	1	1

TABLE 4.1: Parameter sets for designing K and L in new ILC scheme for PE case.

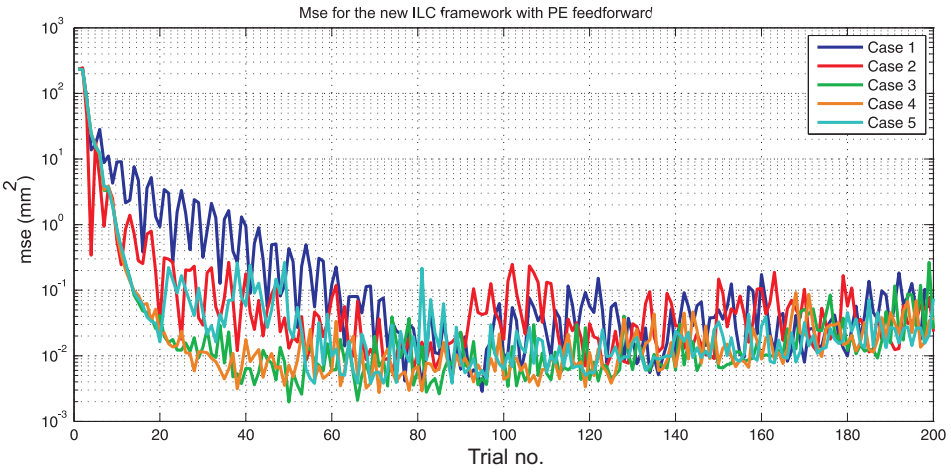

FIGURE 4.12: Mean squared error for the selection of five different weighting parameters for 200 trials in new ILC design, $D_w = 0$.

4. In these, and all other experimentally measured data in this thesis the zero-phase filter used in Cai et al. (2008a) for the gantry robot is employed. The reason for using this filter is that ILC algorithms can exhibit higher frequency noise build up as the number of trials increases and the tracking of the reference signal then begins to degrade.

In the input signal of Figure 4.14 some ripples remain at the beginning and the end of early trials. These ripples indicate that the implementation needs to be more effective by reducing the number of computations between trials. The tests in this part are also not sufficient to examine all possible gain parameters, so there may exist values of the weighting which lead to further performance improvement. A trade off between convergence rate and robustness is always required when selecting the weighting sets. Faster error convergence is not always the best solution for performance along trials (faster convergence can lead to higher input demand which damage the actuators.

For the case of current-error feedback where D_w is set to 1, different sets of weighting parameters were implemented and the sets producing the best experimental results are

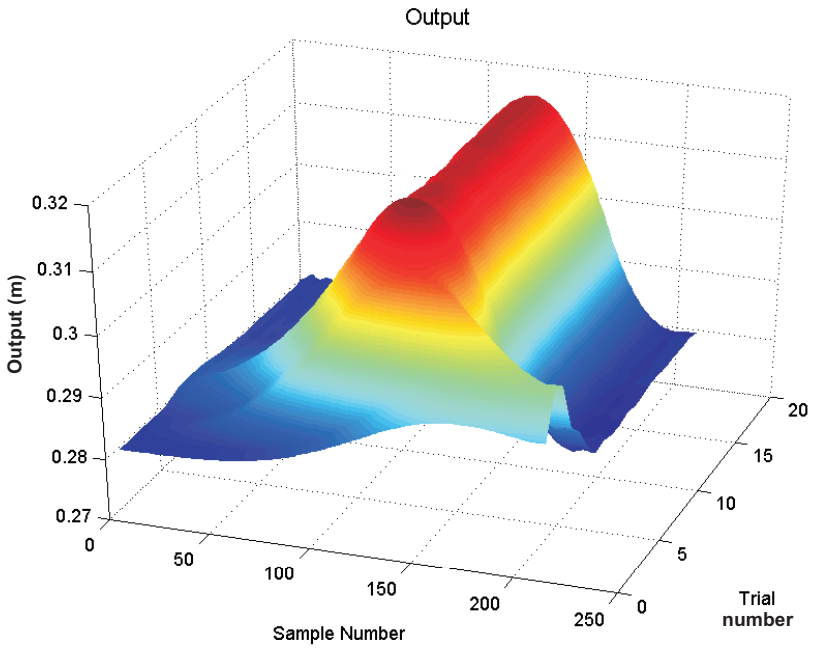

FIGURE 4.13: 3D plot for the output signal of the gantry X-axis for the first 20 trials, $D_w = 0$.

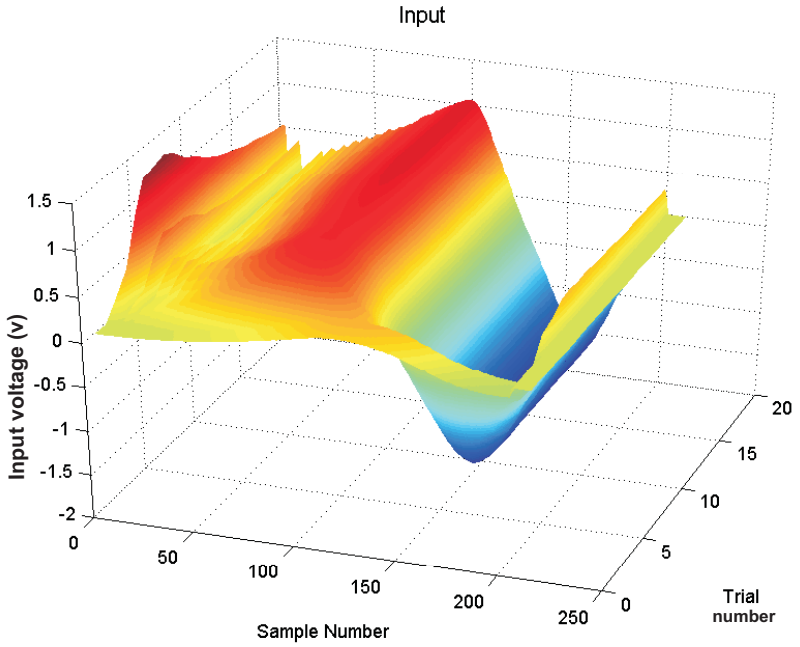

FIGURE 4.14: 3D plot for the input signal of the gantry X-axis for the first 20 trials, $D_w = 0$.

given. The matrices in the LQR cost function (4.36) are given by $Q = \begin{bmatrix} Q_1 I_{N_u} & 0 \\ 0 & Q_2 I_{n_x} \end{bmatrix}$ and $R = R_1 I_{n_u}$, with the Matlab `dlqr` function used to provide the solution. The process and measurement covariance matrices used in the calculation of the observer matrix L

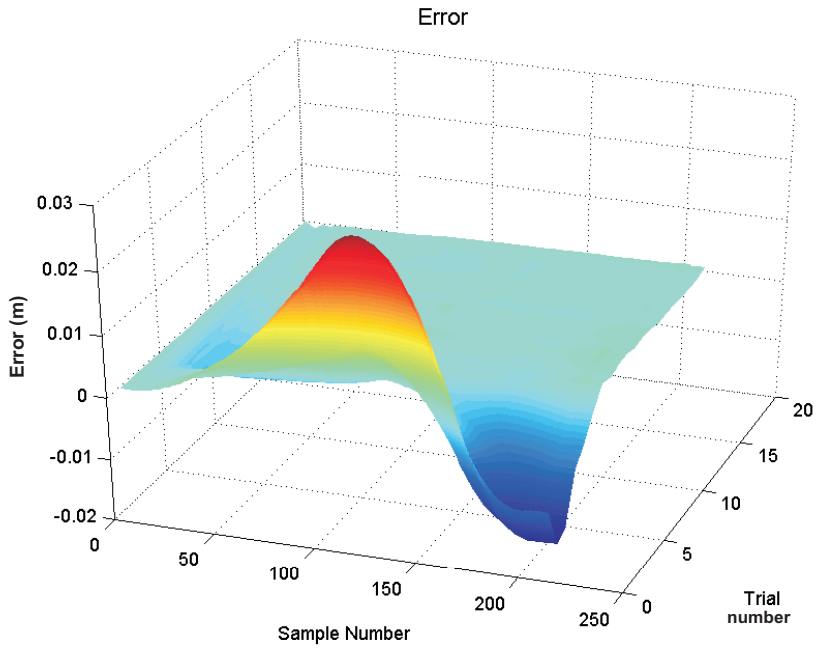

FIGURE 4.15: 3D plot for the error signal of the gantry X-axis for the first 20 trials, $D_w = 0$.

via the Matlab `kalman` function are given by $\hat{Q} = \begin{bmatrix} \hat{Q}_1 I_{N_u} & 0 \\ 0 & \hat{Q}_2 I_{n_x} \end{bmatrix}$ and $\hat{R} = \hat{R}_1 I_{n_y}$. Table 4.2 gives the sets of weighting parameters found to provide the best tracking performance and error norm reduction over 200 trials.

	Designing K			Designing L		
Set	Q_1	Q_2	R_1	$\hat{Q}_1$	$\hat{Q}_2$	$\hat{R}$
1	100	1	1	0.1	1	1
2	200	1	1	0.1	1	1
3	10	1	1	1	1	1
4	100	1	1	1	1	1
5	200	1	1	1	1	1
6	500	1	1	1	1	1

TABLE 4.2: Parameter sets for designing K and L in new ILC scheme for CE case.

The mean squared error versus trial number plots for the six sets is given in Figure 4.16, which show a very fast error convergence for all sets with a variety of learning speeds depending on the weighting parameters selected.

The experimental data for set 4 is shown below (Figures 4.17, 4.18 and 4.19) which has high quality reference tracking with very low norm of error after few trials. The reference tracking occurs within few trials and the error decays until it reaches very low values. The input has small ripples at the beginning which might indicate that padding the reference

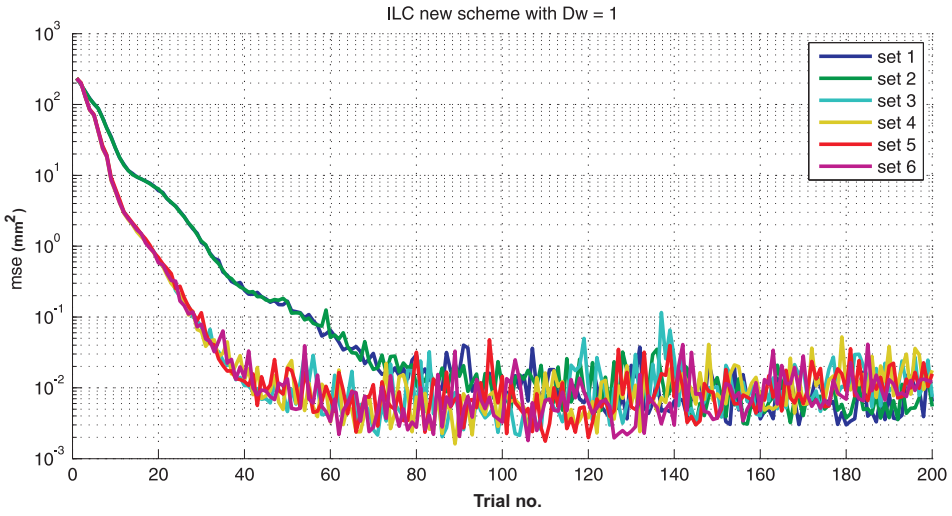

FIGURE 4.16: Mean squared error for the selection of six different weighting parameters for 200 trials in new ILC design, $D_w = 1$.

with zeros for the first few samples would remedy this behaviour. In completing the 200 trials, no noticeable divergence behaviour appears which reflects the robustness of the design as long as the overall system with the feedback gain K is stable.

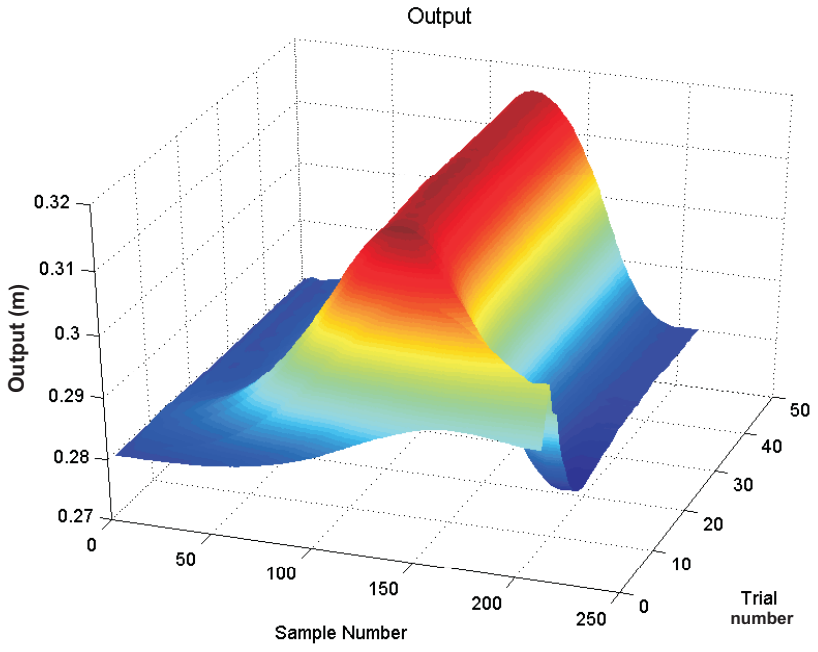

FIGURE 4.17: 3D plot for the output signal of the gantry X-axis for the first 50 trials, $D_w = 1$.

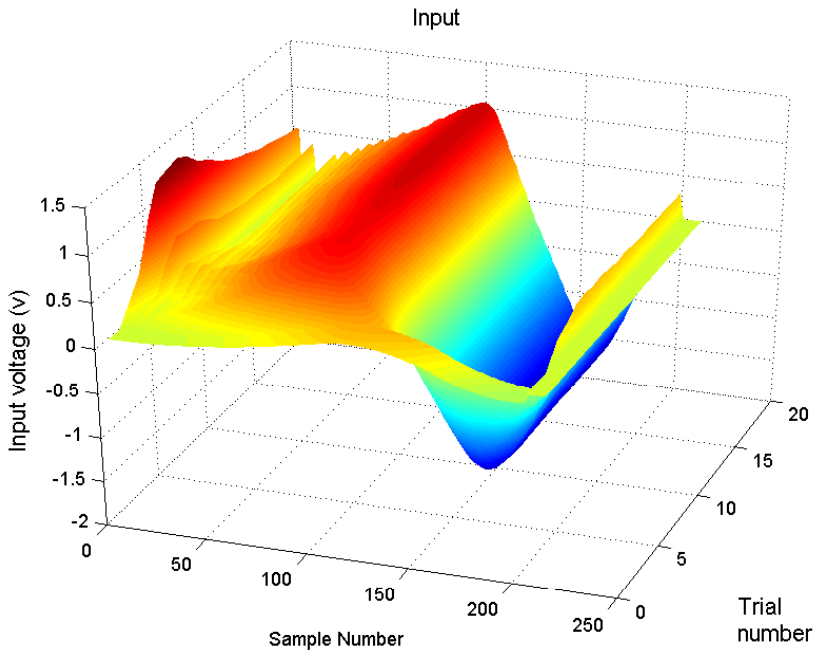

FIGURE 4.18: 3D plot for the input signal of the gantry X-axis for the first 50 trials, $D_w = 1$.

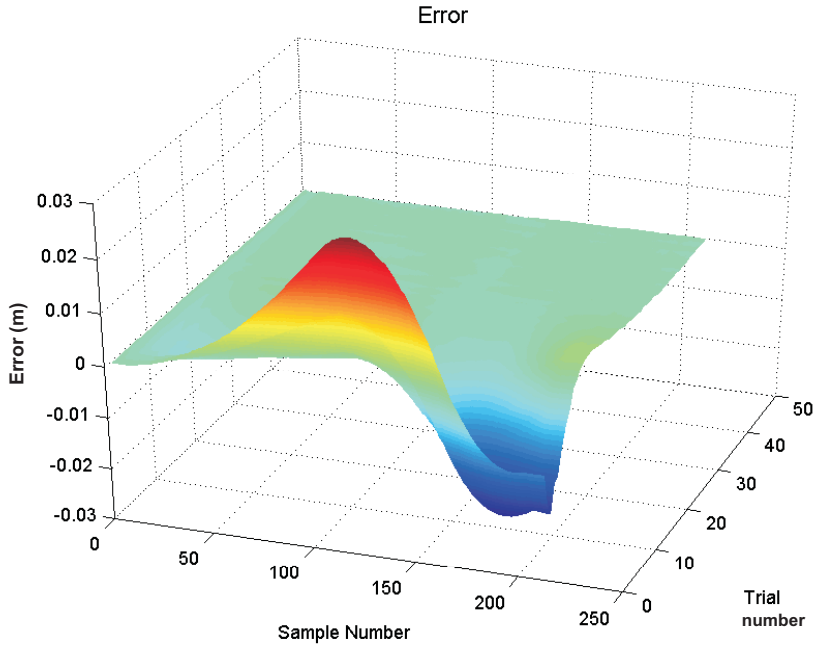

FIGURE 4.19: 3D plot for the error signal of the gantry X-axis for the first 50 trials, $D_w = 1$.

4.3.4.2 Experimental Verification for the Dual RC approach

Again, a wide range of experiments were performed with $D_w = 0$ (only past-error information is used). The control scheme shown in Figure 4.9 has been implemented using the

software described in Chapter 3. A sampling frequency of 100 Hz is again used, and, since this is the RC framework, no resetting occurs during each experimental test. The control law matrix K was designed by setting Q in (4.43) to $Q_1 \begin{bmatrix} C_r & -D_rC \end{bmatrix}^T \begin{bmatrix} C_r & -D_rC \end{bmatrix}$, and R to $R_1 I_{n_u}$. This was found through comparison across several different forms, with calculation of K performed using the Matlab `dlqr` function. The matrix L was calculated using the Matlab `kalman` function with $\hat{Q}$ equal to $\hat{Q}_1 I_{N_y+n_x}$ and $\hat{R}$ equal to $\hat{R}_1 I_{n_y}$. Table 4.3 gives sets of the 4 scalar parameters Q_1, R_1, $\hat{Q}_1$, $\hat{R}_1$ yielding the best performance in practice and Figure 4.20 shows the mean squared errors plotted against trial number.

	Designing K		Designing L	
Set	Q_1	R_1	$\hat{Q}_1$	$\hat{R}_1$
1	100	1	1	1
2	200	1	1	1
3	500	1	1	1
4	1000	1	1	1

TABLE 4.3: Parameter sets for designing K and L in new RC scheme for PE case.

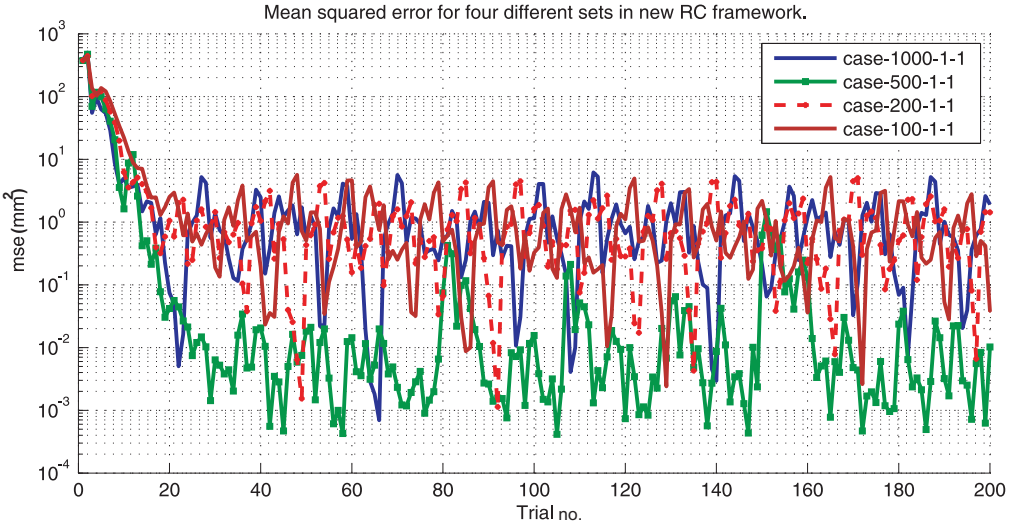

FIGURE 4.20: The mean squared error for different sets of weighting parameters for the new RC design, $D_w = 0$.

The performance achieved by set 3 is shown in Figure 4.21. It can be seen that the error goes to very low levels within few trials and reference tracking follows as a consequence of well-designed state-feedback and observer gain vectors.

Figures 4.22, 4.23, 4.24 present the results in a 3D presentation form where it is noticed that the performance obtained is of a high quality as the error decreases with trial index and the input signal has no noticeable ripples or high amplitude fluctuation over each

trial duration.

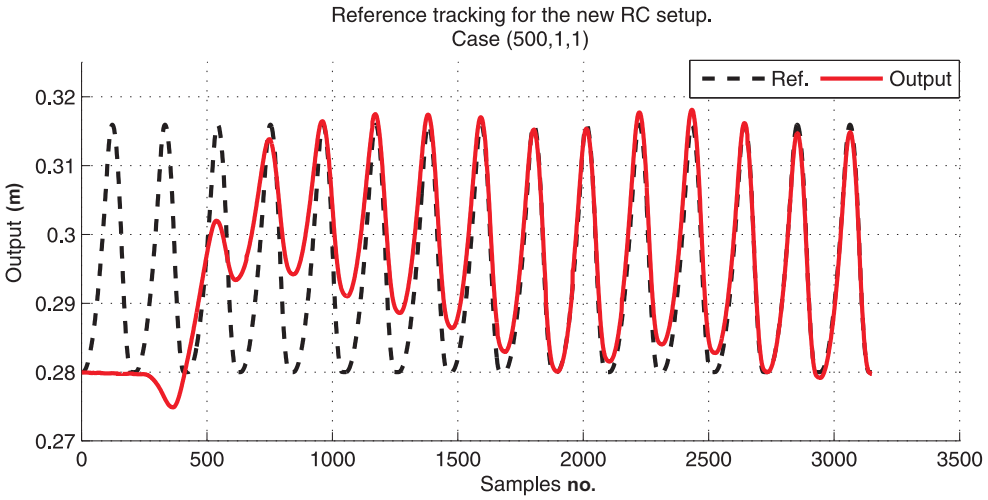

FIGURE 4.21: The output of the gantry X-axis for the first 15 trials in new RC design, $D_w = 0$.

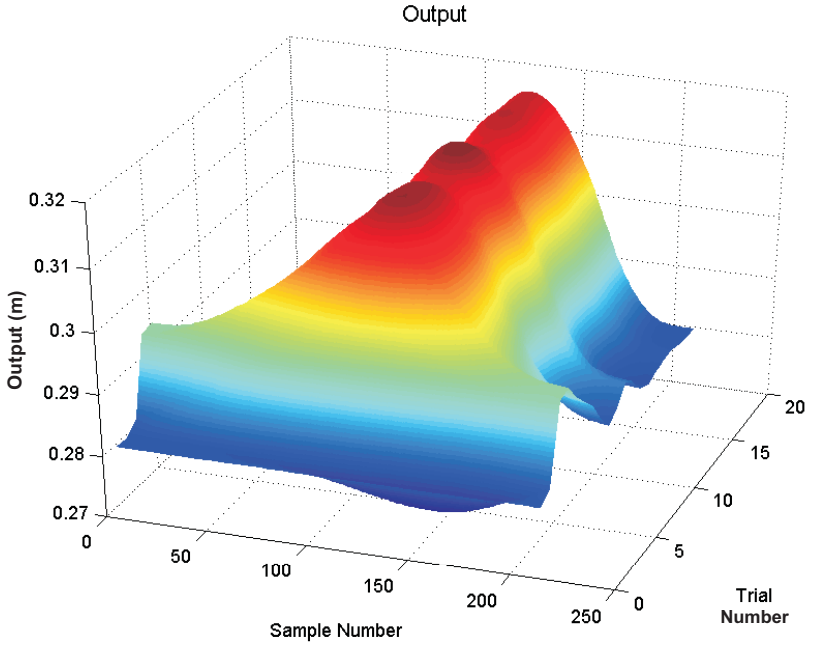

FIGURE 4.22: 3D plot of the output signal for the new RC design, $D_w = 0$.

In the case of current-error feedback design where $D_w = 1$, the control law matrix K was designed using the Matlab `dlqr` function by setting the Q matrix in (4.43) to $Q_1 \begin{bmatrix} C_r & -D_r C \end{bmatrix}^T \begin{bmatrix} C_r & -D_r C \end{bmatrix}$ and $R = R_1 I_{n_u}$. These were found through comparison of different forms. The matrix L was calculated using the Matlab `kalman` function with $\hat{Q}$ equal to $\hat{Q}_1 I_{N_y+n_x}$ and $\hat{R}$ equal to $\hat{R}_1 I_{n_y}$. The best values are shown in Table 4.4.

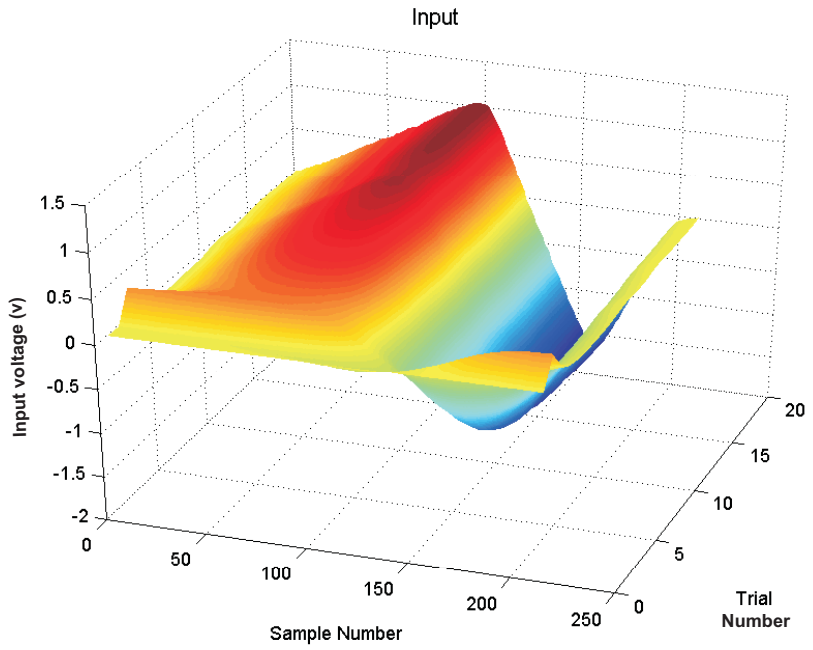

FIGURE 4.23: 3D plot of the input signal for the new RC design, $D_w = 0$.

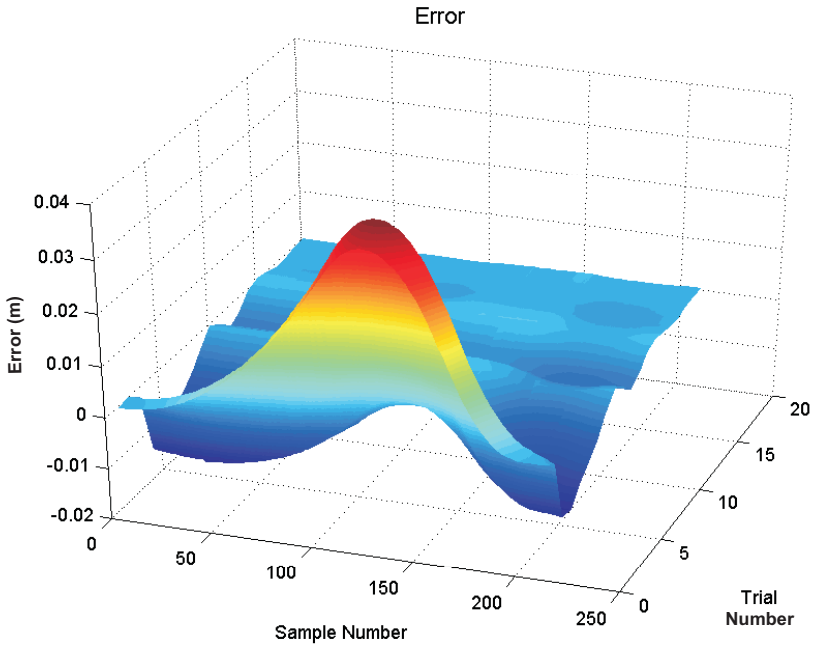

FIGURE 4.24: 3D plot of the error signal for the new RC design, $D_w = 0$.

The mean squared error figure (Figure 4.25) for all sets shows the capability of the design to track periodic references and excellent performance is obtained. This level of error reduction is achieved for a complete 200 trials.

The figures which follow show the performance of a single case within the six sets. From

	Designing K		Designing L	
Set	Q_1	R	$\hat{Q}_1$	$\hat{R}_1$
1	10	1	1	1
2	100	1	1	1
3	200	1	1	1
4	500	1	1	1
5	200	1	10	1
6	500	1	10	1

TABLE 4.4: Parameter sets for designing K and L in new RC scheme for CE case.

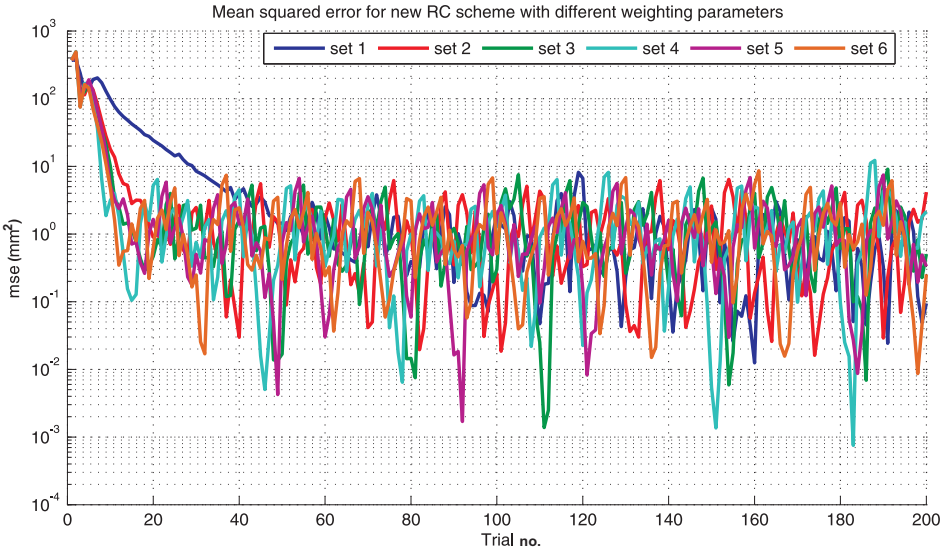

FIGURE 4.25: The mean squared error for different sets in the new RC framework in current-error case, $D_w = 1$.

Table 4.4 Set 3 is used with best results where the performance for the first 15 trials is shown in a 2D figure, see Figure 4.26, and the corresponding output, input and error are in 3D representation and shown in Figures 4.27, 4.28 and 4.29. The experimental results provide evidence for the success of the design in tracking periodic references. It was clear through experimental tests that the effect of increasing the Q weighting parameter used in the design of K is to give more effort to attaining the tracking goal and produce faster convergence. Finally, increasing the $\hat{Q}$ weighting parameter in the design of L results in a longer number of trials to achieve acceptable tracking performance.

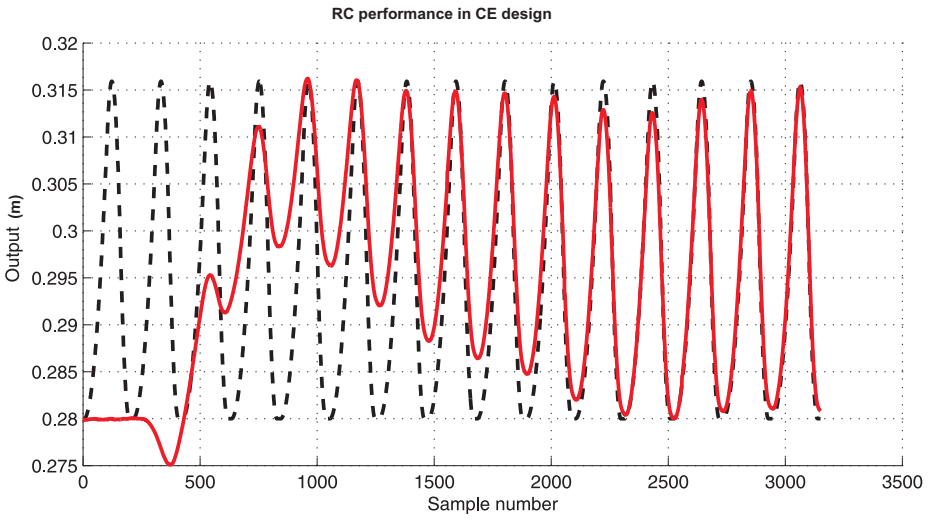

FIGURE 4.26: The output of the gantry X-axis for the first 15 trials in new RC design, $D_w = 1$.

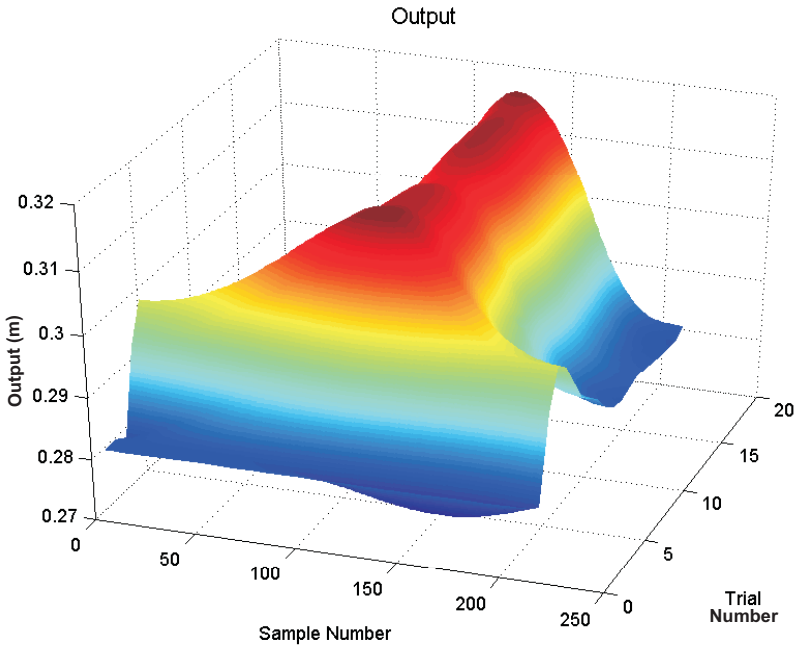

FIGURE 4.27: 3D plot of the output signal for the new RC design, $D_w = 1$.

4.4 Iterative Learning Control and Repetitive Control Duality Framework with Output Injection

A disturbance observer/compensator structure will now be developed for the ILC case in order to compare the two implementations (servomechanism controller versus disturbance observer/compensator). This differs from the implementation considered in De Roover et al. (2000) since no explicit current-error feedback is included, the stipulation of current-error feedback or previous-error feedforward is instead incorporated into the internal

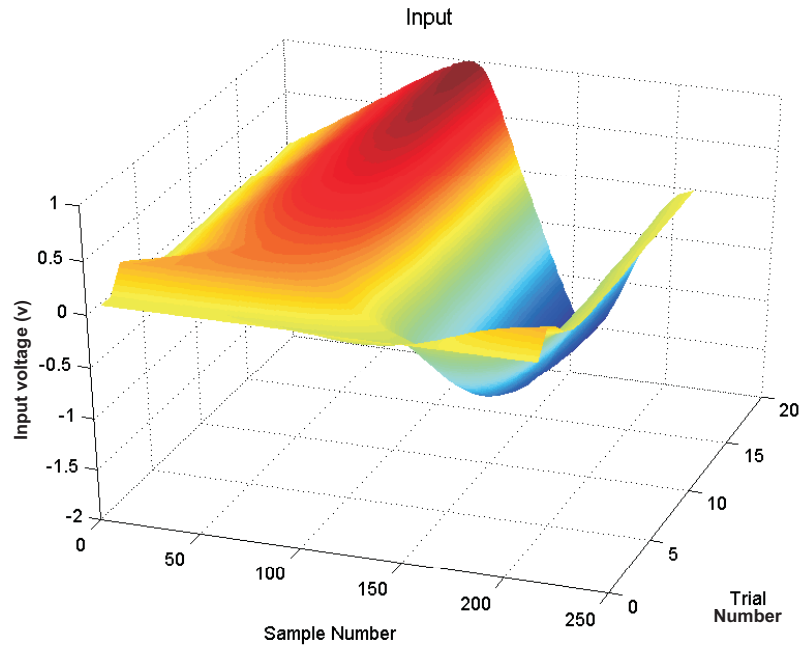

FIGURE 4.28: 3D plot of the input signal for the new RC design, $D_w = 1$.

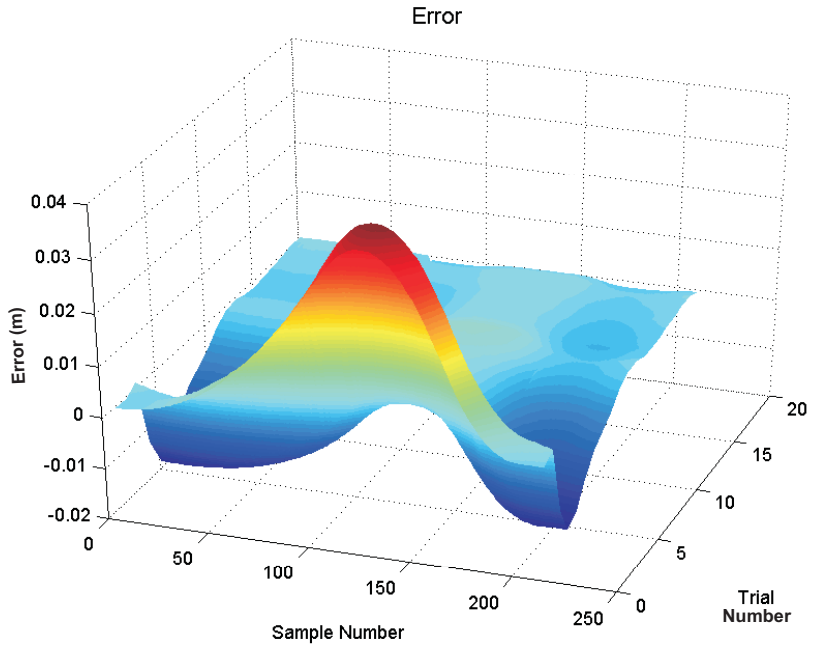

FIGURE 4.29: 3D plot of the error signal for the new RC design, $D_w = 1$.

model. This provides structural simplification as well as flexibility, but will be shown to lead to the same equivalent structure.

4.4.1 ILC Scheme with output Injection

The starting point is the series connection of plant and internal model corresponding to ILC, given by (4.29). An observer is then designed for an additive periodic disturbance assumed to exist at the plant input, and the estimator disturbance signal is then applied at the same point in order to cancel it. This differs from the observer implementations of Section 4.3 which estimate the system states. As the disturbance is removed from the system, the additive input reduces to zero, and the plant output converges to the demand trajectory. This results in the disturbance observer/compensator scheme shown in Figure 4.30.

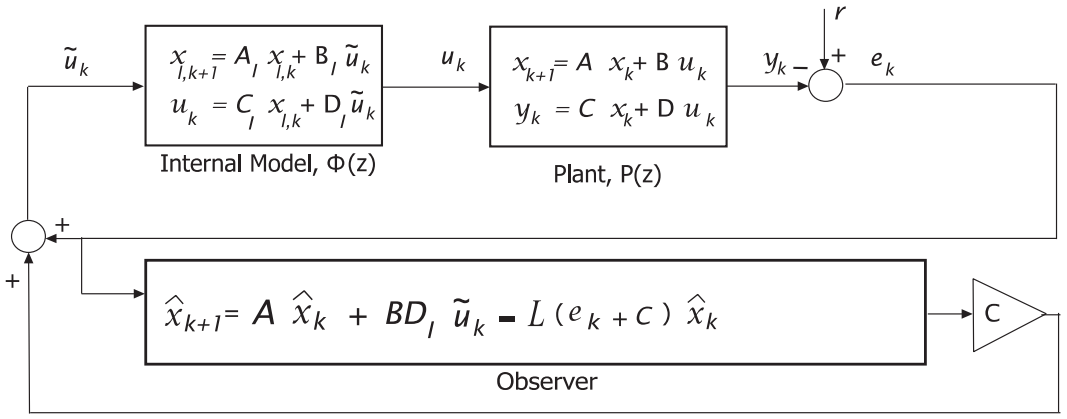

FIGURE 4.30: Synthesized iterative learning control scheme.

This results in the following coupled system

$$\begin{bmatrix} x_{l,k+1} \\ x_{k+1} \end{bmatrix} = \begin{bmatrix} A_l & 0 \\ BC_l & A \end{bmatrix} \begin{bmatrix} x_{l,k} \\ x_k \end{bmatrix} + \begin{bmatrix} B_l \\ BD_l \end{bmatrix} \tilde{u}_k \tag{4.44}$$

with an observer described by

$$\hat{x}_{k+1} = A\hat{x}_k + BD_l\tilde{u}_k - L(e_k + C\hat{x}_k) \tag{4.45}$$

This system produces the output $\hat{y}_k = C\hat{x}_k$ that is used as a correction term for the internal model. Stability analysis considers the feedback loop about $z^{-N}I_{n_u}$, which is defined between the signals `in` and `out` in Figure 4.31.

Both error cases are considered, where $L(z)$ is defined as

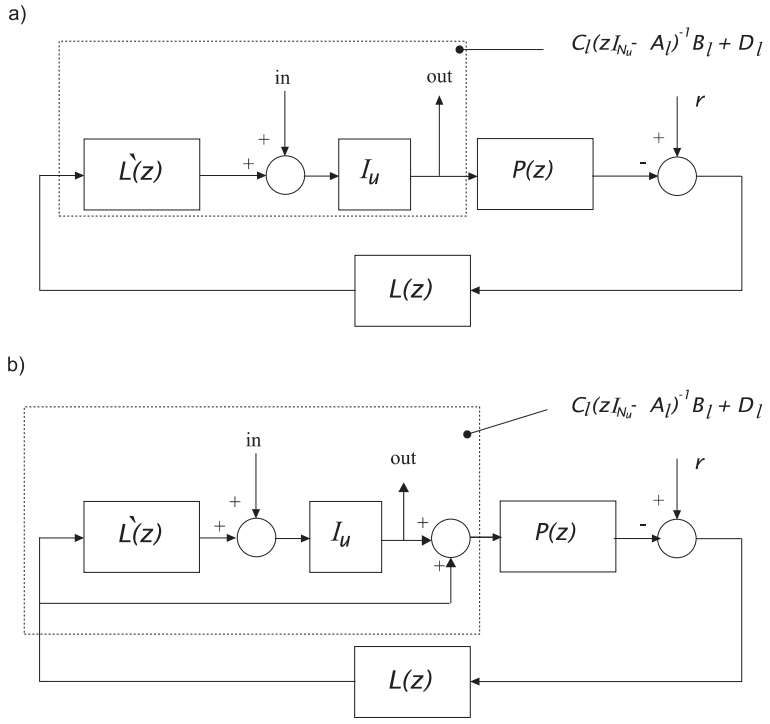

FIGURE 4.31: Internal model-based iterative learning control scheme for *a*) past-error feedforward and *b*) current-error feedback.

$$L(z) := -C\left(zI - A - BD_lC + L_lC\right)^{-1}\left(BD_l - L\right) + I_{n_u}$$

and $L'(z)$ in Figure 4.31 is such that $C_l(zI_{N_u} - A_l)^{-1}B_l + D_l = (I_{n_u} - z^{-N}I_{n_u})^{-1}L'(z)$, and hence $L'(z) = C_lB_lz^{-1} + C_lA_lB_lz^{-2} + \cdots + C_lA_l^{N-1}B_lz^{-N}$.

For the case of past-error feedforward we can write the relationship between `in` and `out` as

$$\text{out}(z) = G(z)\left(G(z) - L'(z)\right)^{-1}\text{in}(z) \tag{4.46}$$

and for current-error feedback

$$\text{out}(z) = (G(z) - I_{n_u})(G(z) - I_{n_u} - L'(z))^{-1}\text{in}(z) \tag{4.47}$$

where $G(z)$ in both cases is given by

$$G(z) = -\begin{bmatrix} DC_l & C \end{bmatrix}\left(zI - \begin{bmatrix} A_l & 0 \\ BC_l & A \end{bmatrix} + \begin{bmatrix} B_l \\ L \end{bmatrix}\begin{bmatrix} DC_l & C \end{bmatrix}\right)^{-1}\begin{bmatrix} C_l & 0 \end{bmatrix}^T + D_l$$

The stabilisation of the system then requires that the observer learning gain be designed such that $G(z)$ is stable. The feedback path dynamics are given by

$$\begin{bmatrix} \tilde{x}_{l,k+1} \\ \tilde{x}_{k+1} \end{bmatrix} = \underbrace{\begin{bmatrix} A_l & 0 \\ BC_l & A \end{bmatrix}}_{\text{system matrix}}\begin{bmatrix} \tilde{x}_{l,k} \\ \tilde{x}_k \end{bmatrix} - \underbrace{\begin{bmatrix} B_l \\ L \end{bmatrix}}_{\text{observer gain}}\overbrace{\begin{bmatrix} DC_l & C \end{bmatrix}}^{\text{output matrix}}\begin{bmatrix} \tilde{x}_{l,k} \\ \tilde{x}_k \end{bmatrix} \tag{4.48}$$

where $\tilde{x}_l = x_l$ is the internal model state and $\tilde{x} = x - \hat{x}$ is the difference between the plant and disturbance state vectors which then feeds into the internal model. The system (4.48) confirms the output injection structure, and its regulation ensures tracking of the reference. This is dual to the system in (4.35) which used output feedback.

A solution to the design of L is found by considering the dual of a general state-space model, as discussed in, for example, Kwakernaak and Sivan (1972). First consider the plant state-space model

$$\begin{aligned} x_{k+1} &= Ax_k + Bu_k \\ y_k &= Cx_k + Du_k \end{aligned} \tag{4.49}$$

and apply an exponentially stabilizing state-feedback control law $u_k = -Lx_k^*$. Taking the dual of (4.49) gives

$$\begin{aligned} x_{k+1}^* &= A^T x_k^* + C^T u_k \\ y_k &= B^T x_k^* + D^T u_k \end{aligned} \tag{4.50}$$

and hence

$$x^*_{k+1} = (A^T + C^T L)x^*_k \tag{4.51}$$

taking the dual of this last model gives

$$x_{k+1} = (A^T + C^T L)^T x_k = (A + L^T C)x_k = Ax_k + L^T C x_k \tag{4.52}$$

the regulation of which is also guaranteed since the system is exponentially stable if and only if its dual is stable (see Kwakernaak and Sivan (1972)). Therefore, the design of state-feedback for the system (4.50) provides the output feedback vector for the system in (4.52). Accordingly, comparing (4.52) with (4.48), the system (4.50) can be written as

$$\begin{bmatrix} x^*_{k+1} \\ z^*_k + 1 \end{bmatrix} = \begin{bmatrix} A_l & 0 \\ BC_l & A \end{bmatrix}^T \begin{bmatrix} x^*_k \\ z^*_k \end{bmatrix} + \begin{bmatrix} DC_l & C \end{bmatrix}^T u_k \tag{4.53}$$

$$= \begin{bmatrix} A_l^T & C_l^T B^T \\ 0 & A^T \end{bmatrix} \begin{bmatrix} x^*_k \\ z^*_k \end{bmatrix} + \begin{bmatrix} C_l^T D^T & C^T \end{bmatrix} \begin{bmatrix} B_l^T & L^T \end{bmatrix} \begin{bmatrix} x^*_k \\ z^*_k \end{bmatrix} \tag{4.54}$$

LQR will again be applied to calculate the state-feedback matrix $\begin{bmatrix} B_l^T & L^T \end{bmatrix}$, since the separation principle permits the design of both the state-feedback matrix and estimator matrix independently. In order to regulate this system, $\begin{bmatrix} B_l^T & L^T \end{bmatrix}$ can be calculated to solve

$$\begin{aligned} \min \quad & \sum_{k=1}^{\infty} \eta_k^T Q \eta_k + \mu_k^T R \mu_k \\ \eta_{k+1} \quad &= \begin{bmatrix} A_l^T & C_l^T B^T \\ 0 & A^T \end{bmatrix} \eta_k + \begin{bmatrix} C_l^T D^T \\ C^T \end{bmatrix} \mu_k \\ \mu_k \quad &= \begin{bmatrix} B_l^T & L^T \end{bmatrix} \eta_k \end{aligned}$$

which can be using the Matlab function `dlqr`. This controller has not been experimentally evaluated in this thesis, but simulations suggest that good performance is achieved using

the forms $Q = \begin{bmatrix} Q_1 I_{N_u} & 0 \\ 0 & Q_2 I_{n_x} \end{bmatrix}$, and $R = R_1 I_{n_y}$, where Q_1, Q_2 and R_1 are positive scalar weights.

4.4.2 Stability Conditions for ILC/RC with Output Injection Scheme

Necessary and sufficient conditions for existence of the output feedback realisations are now given, and are special cases of the general disturbance observer problem De Roover and Bosgra (1996).

Theorem 4.3. *Consider the ILC scheme shown in Figure 4.30 and suppose that* $[B_l^T \; L^T]$ *is chosen such that (4.48) is asymptotically stable. Then the control scheme solves the robust periodic control problem if, and only if,*

$$\operatorname{rank}\left(\begin{bmatrix} \lambda I - A & B \\ -C & D \end{bmatrix}\right) = n_x + n_u \tag{4.55}$$

for all λ *in the spectrum of the matrix* A_w *and*

$$\operatorname{rank}(B) + n_y = \operatorname{rank}\left(\begin{bmatrix} B \\ D \end{bmatrix}\right) \tag{4.56}$$

Theorem 4.4. *Consider the RC output feedback with equivalent structure*

$$\begin{bmatrix} x_{r,k+1} \\ x_{k+1} \end{bmatrix} = \begin{bmatrix} A_r & -B_r C \\ 0 & A \end{bmatrix} \begin{bmatrix} x_{r,k} \\ x_k \end{bmatrix} - \begin{bmatrix} L \end{bmatrix} \begin{bmatrix} C_r & D_r C \end{bmatrix} \begin{bmatrix} x_{r,k} \\ x_k \end{bmatrix}$$

where L is chosen such that the system is asymptotically stable. Then the stabilisation solves the robust periodic control problem if, and only if, (4.55) and (4.56) are again satisfied.

Both these output injection implementations therefore may only be applied to systems having the same number of outputs as inputs. The ILC servomechanism implementation had the restriction that $n_y \geq n_u$ (see Theorem 4.1), so that it clearly broadens the range of plants that can be controlled by the iterative learning controller.

Type	Structure	Equivalent System
ILC	Servo	$\begin{bmatrix} x_{l,k+1} \\ x_{k+1} \end{bmatrix} = \begin{bmatrix} A_l & 0 \\ BC_l & A \end{bmatrix} \begin{bmatrix} x_{l,k} \\ x_k \end{bmatrix} - \begin{bmatrix} B_l \\ BD_l \end{bmatrix} [\, K \,] \begin{bmatrix} x_{l,k} \\ x_k \end{bmatrix}$
RC	Servo	$\begin{bmatrix} x_{r,k+1} \\ x_{k+1} \end{bmatrix} = \begin{bmatrix} A_r & -B_rC \\ 0 & A \end{bmatrix} \begin{bmatrix} x_{r,k} \\ x_k \end{bmatrix} - \begin{bmatrix} B_rD \\ -B \end{bmatrix} [\, K \,] \begin{bmatrix} x_{r,k} \\ x_k \end{bmatrix}$
ILC	Disturbance	$\begin{bmatrix} x_{l,k+1} \\ x_{k+1} \end{bmatrix} = \begin{bmatrix} A_l & 0 \\ BC_l & A \end{bmatrix} \begin{bmatrix} x_{l,k} \\ x_k \end{bmatrix} - \begin{bmatrix} L_l \\ L \end{bmatrix} [\, DC_l \; C \,] \begin{bmatrix} x_{l,k} \\ x_k \end{bmatrix}$
RC	Disturbance	$\begin{bmatrix} x_{r,k+1} \\ x_{k+1} \end{bmatrix} = \begin{bmatrix} A_r & -B_rC \\ 0 & A \end{bmatrix} \begin{bmatrix} x_{r,k} \\ x_k \end{bmatrix} - \begin{bmatrix} L \end{bmatrix} [\, C_r \; D_rC \,] \begin{bmatrix} x_{r,k} \\ x_k \end{bmatrix}$

TABLE 4.5: State-feedback and output-feedback representations for the duality framework structure.

4.5 Summary of Dual Control Structure

The three controllers which have been developed in (4.31), (4.40) and the scheme in Figure 4.30) are summarized in Table 4.5, which also includes a fourth structure that results if RC is implemented in the form of a disturbance observer/compensator. The presence of this fourth controller needs further investigation and there is currently no evidence that such a structure actually exists. However, from the stability conditions derived, the controller is more restrictive than the RC servomechanism implementation that has already been developed in this thesis, and hence does not add to the range of plants which may be addressed by the framework. In principle this structure is feasible if, again, the controller includes a duplicate internal model that allows the robust servomechanism problem to be solved whilst maintaining the internal model placement corresponding to RC. Together these structures form a complete set covering RC and ILC design in either a servomechanism or a disturbance observer/compensator form.

Figure 4.32 provides a schematic comparison of plants addressed in the new RC/ILC duality framework. This figure shows how the controller structures depend on the number of inputs and outputs, and how the duality framework may be applied to a great number of plants.

Experimental results for the ILC injection scheme are left as future work since results obtained for the previously developed framework together with the results obtained in the next section already cover most of the ideas and principles discussed in this chapter.

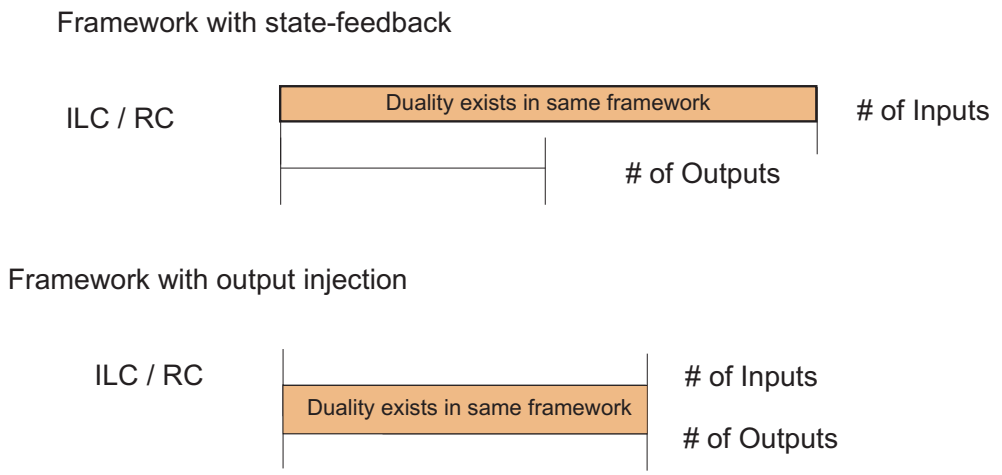

FIGURE 4.32: Comparison between the new RC/ILC designs in both state-output feedback and the growth in plants considered.

4.6 Comparing the Performance of the Duality Based ILC with Selected Optimisation based ILC Designs

The gantry robot used for experimental testing in this thesis has also been used to benchmark ILC designed using the Adjoint, Inverse and Norm Optimal algorithms. These are all model based algorithms and therefore it is relevant to compare their performance against the new duality based algorithms developed in this thesis. In all experimental results in this section the reference signal is that of Figure 3.5 since this signal was used in the previous work with the Adjoint, Inverse and Norm Optimal algorithms. The sampling frequency for all results shown is 100 Hz and no pre-stabilizing feedback control loop is applied to the robot, i.e., ILC is applied directly.

In the case of the Adjoint algorithm described in equation (2.26) with β_{k+1} being a constant gain and set to two values 1.25 and 1.5. Figure 4.33 plots the performance in the form of the mse against trial number of the adjoint algorithm Ratcliffe et al. (2006a) and selected versions of the new ILC algorithm results developed in this case for both cases (PE,CE) over 200 trials. The figure shows better performance for the new designs over the early trials, especially for the PE case, since it has a faster error convergence than the adjoint algorithm, as clearly seen starting form trial 10. The mse stays within low error levels for the new algorithm until well into the 2002 trials when divergent behaviour appears (see trial 180). Over the trial range, the adjoint algorithm gives lower error levels, without the need for zero-phase filtering which is the only currently effective answer to the long-term performance issue that after decreasing from trial-to-trial the errors may begin to build up. The performance of the new algorithm is, however, promising and could be improved by re-design of the zero-phase filter. In any practical application, only a finite number of trials will completed and if the number of these is less than the one

where divergence becomes noticeable then the new design can be used, especially if there is emphasis on 'fast' error reduction in the initial trials.

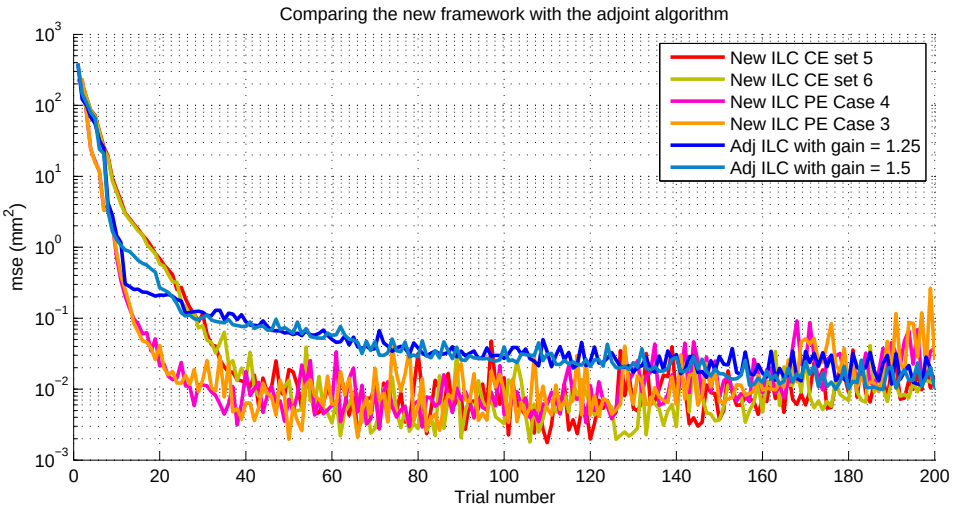

FIGURE 4.33: Comparison against the Adjoint algorithm

Figure 4.34 shows the mse against trial number over 200 trials performance for the developed ILC design in both cases (PE,CE) and the inverse algorithm Ratcliffe et al. (2006a). The equation describing the inverse algorithm is given in equation (2.25) with ϵ_{k+1} is the scalar gain and is set to 1 and 1.5. It is clear that the inverse approach has a better performance in the early trials, with a 3^{rd} order Chebychev filter with 15 Hz cutoff frequency. This is clear from trial 5 until trial 40. After trial 40 the error levels of the new ILC design are within the error levels of the inverse approach until the trial 180 where an error divergence is noticed for the new ILC design. Thus it can be said that the performance of the new ILC design has a performance similar to the inverse approach except for early trials and it is beneficial to find a better set of parameters that can bring error levels to very low values from early stages of applications and design a better filter to remedy the divergence behaviour.

Figure 4.35 shows the the mse against trial number for the new ILC design in both cases (PE,CE) and the norm-optimal ILC approach Ratcliffe et al. (2005) and also described in section 2.2.1 with $q = 1$ and 1.5 and $r = 1$ over 200 trials. A superior performance of the norm-optimal ILC, without a presence of a filter, compared to the results obtained for the new ILC design in both cases is noticed. The early trials and the performance over the 200 trials for the norm-optimal ILC is always better than the new ILC design. This is true for the results obtained in this thesis and it is not clear that tuning the new designs will remove this difference in measured performance. The new ILC design needs the application of a zero phase filter to overcome the divergence phenomena after trial 180 whilst the norm-optimal design shows no sign of error divergence.

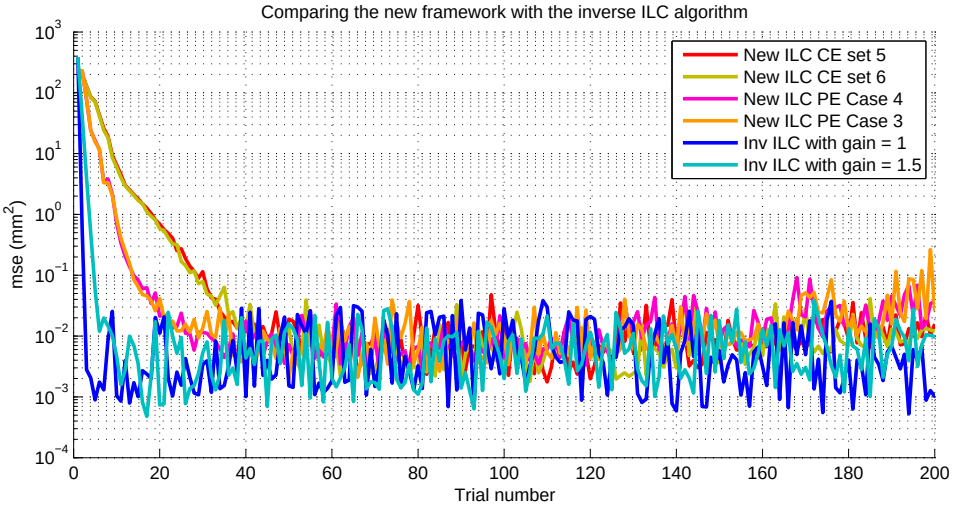

FIGURE 4.34: Comparison against the inverse algorithm

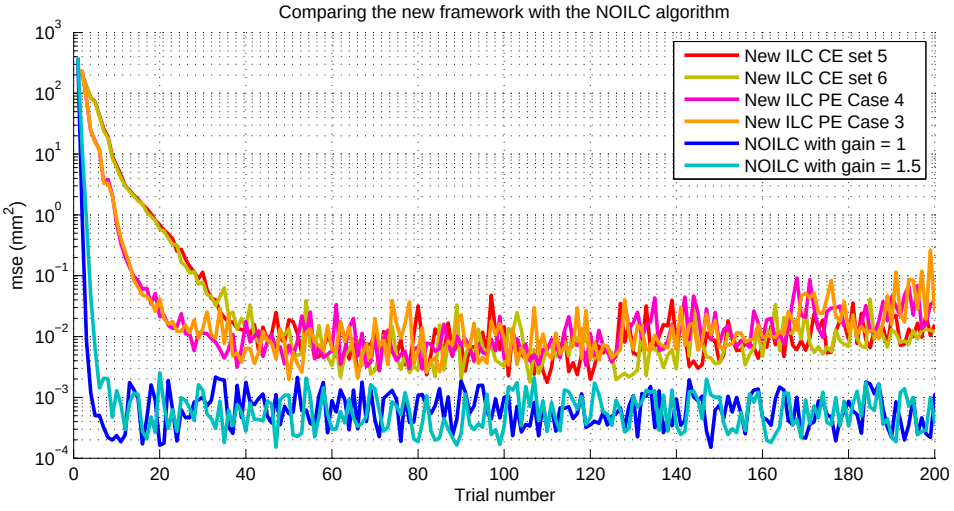

FIGURE 4.35: Comparison against norm optimal

4.7 Iterative Learning Control and Repetitive Control Duality Framework with Explicit Current-error Feedback

In the work reported in De Roover and Bosgra (1997); De Roover et al. (2000), two repetitive mode controllers were designed, and due to the position of the internal model inside the feedback loop, a dual solution exists for the two designs when state-feedback is used to regulate the disturbance system. This duality framework is designed based on explicit current-error feedback. This duality framework can be illustrated as follows, once a controller is designed under the duality framework either in RC/ILC mode, then the solution found (using state-feedback or output-feedback) can be used as a solution to

the same problem in the other mode ILC/RC. Next, the two approaches are considered and with the results given earlier can lead to a large set of admissible systems.

4.7.1 Repetitive Control Scheme with Explicit Current-error Feedback

In the work of De Roover et al. (2000) the design is based on explicitly providing a feedback loop for the current-error signal. Doing so and modifying the RC scheme of Figure 4.3 to include an explicit current-error feedback path produces the system shown in Figure 4.36.

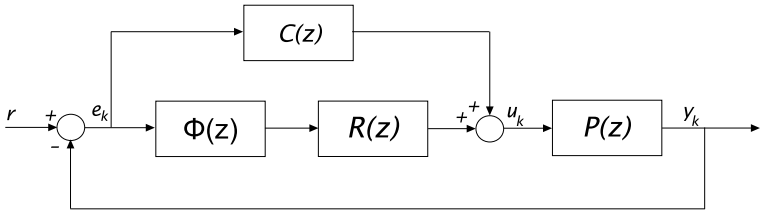

FIGURE 4.36: Repetitive control with existing feedback controller $C(z)$.

This repetitive update law is combined with a state-feedback loop around the plant to influence its pole locations. Note from the problem structure that the disturbance state at the sample i holds the sum of all errors that have occurred at sample i of the disturbance state $x_{r,k}$ over all previous repetitions (see A_r, B_r structure). Thus, regulating $x_{r,k}$ to achieve steady state error means necessarily driving the error to zero.
In De Roover et al. (2000), the current-error feedback was realised through feedback of the plant states using optimal state-feedback. Furthermore, (4.64) is used to implement the RC feedforward block. Here a simple solution is developed by including an observer and writing the equations governing the RC design as:

$$\begin{aligned} \hat{x}_{k+1} &= A\hat{x}_k + Bu_k + L\epsilon_k \\ &= (A + BK + LC + LDK)\hat{x}_k + (B + LD)K_r x_{r,k} + Le_k \end{aligned} \tag{4.57}$$

The observer is fed by the error signal and the observer output is multiplied by the estimator learning gain L

$$e_k = r_k - y_k \tag{4.58}$$

with observer error as

$$\epsilon_k = e_k + C\hat{x}_k + Du_k \tag{4.59}$$

The disturbance model is fed by the error and given as

$$x_{r,k+1} = A_r x_{r,k} + B_r e_k \tag{4.60}$$

Thus the control input comprises both the disturbance states plus the estimator states. Using optimal control through state-feedback, the input will have the following structure

$$u_k = K_r x_{r,k} + K\hat{x}_k \tag{4.61}$$

The structure is shown in Figure 4.37, where L is the plant state observer gain matrix, K_r and K are the state-feedback law matrices for the disturbance memory (internal model) and the plant respectively. In De Roover et al. (2000) it is shown that this structure corresponds to that of Figure 4.36, with $R(z) = K_r(zI_{N_y} - A_r)^{-1}B_r(I_{n_y} - z^{-N}I_{n_y})(I_{n_y} + K(zI - \overline{A})^{-1}(B + LD)), C(z) = K(zI - \overline{A})^{-1}L$, where $\overline{A} = A + BK + L(C + DK)$.

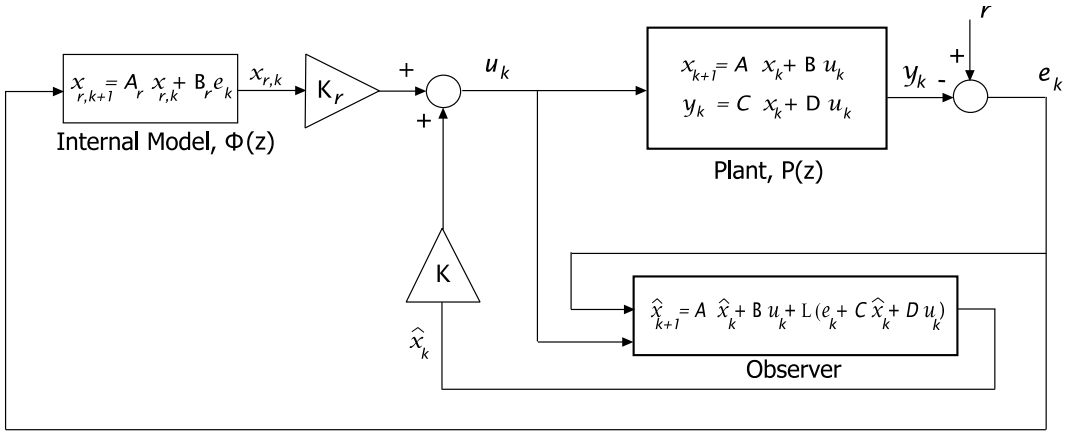

FIGURE 4.37: Repetitive control with current-error feedback.

Stability analysis considers the feedback path about $z^{-N}I_{n_y}$, which is defined between the signals `in` and `out` in Figure 4.38.

The equation that governs the structure in Figure 4.38, can be stated as in De Roover et al. (2000):

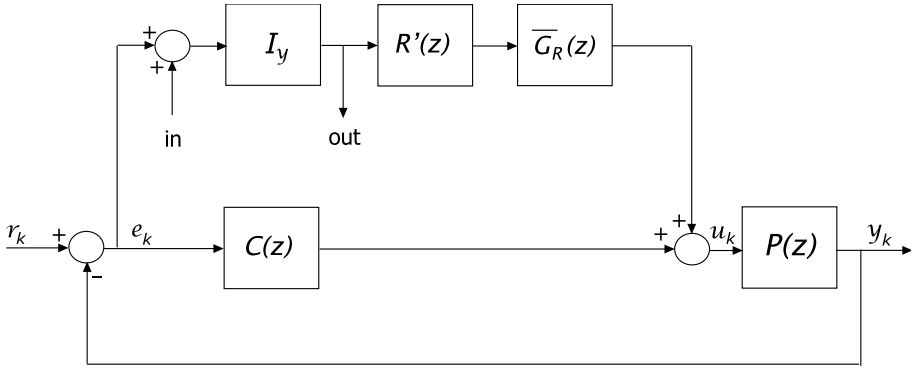

FIGURE 4.38: Internal model-based repetitive control scheme.

$$\begin{aligned} \text{out}(z) &= [I + (I + P(z)C(z))^{-1}P(z)\overline{G}_R(z)R'(z)]^{-1}\text{in}(z) \\ &= [I + \overline{G}_K R'(z)]^{-1}\text{in}(z) \end{aligned} \tag{4.62}$$

with

$$\overline{G}_K(z) = [D + (C + DK)(zI - A - BK)^{-1}B] \tag{4.63}$$

Here $K_r(zI_{N_y} - A_r)^{-1}B_r =: R'(z)(I_{n_y} - z^{-N}I_{n_y})^{-1}$ where $R'(z) = K_rB_r + K_rA_rB_r + \cdots + K_rA_r^{N-1}B_r$.

The design of the RC controller (4.61) and the observer (4.57) involves the selection of the gain matrices $\{L, K_r, K\}$, in order to assure reference tracking. From Figure 4.37 it is clear that the disturbance memory does implement the repetitive control algorithm since it has a delay in the error signal by N samples

$$u(t) = u(t - T) + Fe(t - T) \tag{4.64}$$

and F is a linear causal filter (feedback structure).

The feedback involving the memory variables was shown in De Roover et al. (2000) to have the following equivalent structure

$$\begin{bmatrix} x_{r,k+1} \\ \hat{x}_{k+1} \end{bmatrix} = \underbrace{\begin{bmatrix} A_r & -B_rC \\ 0 & A \end{bmatrix}}_{\text{system matrix}} \begin{bmatrix} x_{r,k} \\ \hat{x}_k \end{bmatrix} + \underbrace{\begin{bmatrix} -B_rD \\ B \end{bmatrix}}_{\text{input matrix}} \underbrace{\begin{bmatrix} K_r & K \end{bmatrix}}_{\text{state-feedback}} \begin{bmatrix} x_{r,k} \\ \hat{x}_k \end{bmatrix} \tag{4.65}$$

As with the ILC system designed in Section 4.3.1, state-feedback is used to provide stabilisation, and hence solve the tracking problem. Turning now to the actual design of the RC framework for given data, it can be shown De Roover et al. (2000) that the separation principle allows $[K_r\ K]$ and L to be designed independently which leads to a solution via LQR. The solution is obtained through minimisation of a cost function to regulate the states and drive the error to zero. This minimisation problem is

$$\min \quad \sum_{k=1}^{\infty} \eta_k^T Q \eta_k + \mu_k^T R \mu_k \tag{4.66}$$

$$\eta_{k+1} = \begin{bmatrix} A_r & -B_rC \\ 0 & A \end{bmatrix} \eta_k + \begin{bmatrix} -B_rD \\ B \end{bmatrix} \mu_k \tag{4.67}$$

$$\mu_k = [K_r\ \ K]\, \eta_k \tag{4.68}$$

which can be solved via the Matlab `dlqr` function. Similarly a suitable L can be calculated using the Matlab function `kalman` with the process and measurement covariance matrices $\hat{Q}$ and $\hat{R}$ respectively.

4.7.2 Iterative Learning Control Scheme with Explicit Current-error Feedback

In this section an ILC is designed in order to compensate periodic inputs/disturbances acting on a system from the input side as a dual to the repetitive controller explained earlier. It is constructed by creating a path between the observer system and the input to the internal model, and by modifying the observer structure accordingly, see Figure 4.39.

The resulting control input has the following structure

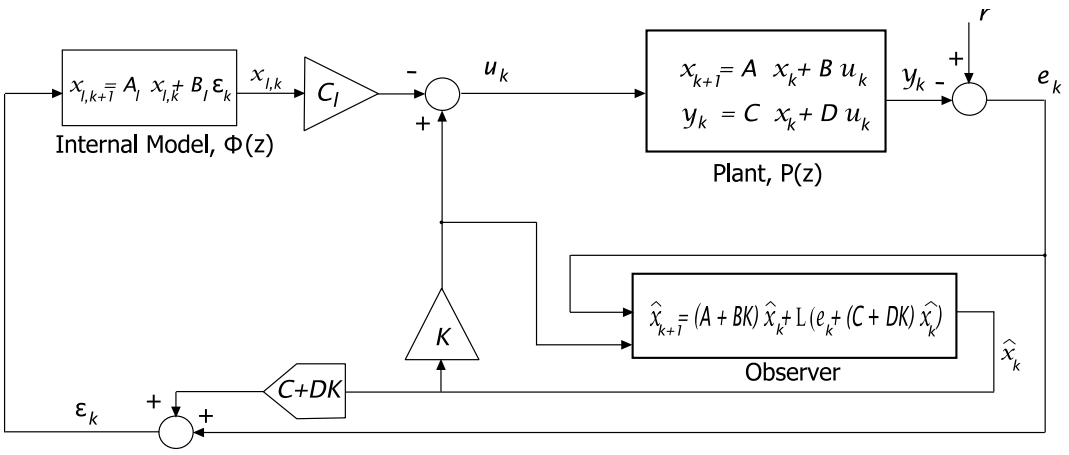

FIGURE 4.39: Iterative learning control set-up

$$u_k = K\hat{x}_k - C_l x_{l,k} - D_l \epsilon_k \tag{4.69}$$

with an observer governed by the following equation

$$\begin{aligned} \hat{x}_{k+1} &= A\hat{x}_k + B(u_k + \hat{d}_k) + L(e_k + (C + DK)\hat{x}_k) \\ &= (A + BK)\hat{x}_k + L(e_k + (C + DK)\hat{x}_k) \end{aligned} \tag{4.70}$$

with $\hat{d}_k$ denoting the internal model output

$$\begin{aligned} x_{l,k+1} &= A_l x_{l,k} + L_l \epsilon_k \\ \hat{d}_k &= C_l x_{l,k} + D_l \epsilon_k \end{aligned} \tag{4.71}$$

The dynamics in this case have a similar structure to that of Figure 4.40 with $L(z) = (I_{n_u} + C(zI - \overline{A})^{-1}L)C_l(zI_{N_u} - A_l)^{-1}L_l(I_{n_u} - z^{-N}I_{n_u})$, $C(z) = K(zI - \overline{A})^{-1}L$ and $\overline{A}$ is the same as in the developed RC case.

Stability analysis requires isolating the memory variables and considering the closed-loop path around the internal model. This is given by the relationship between the signals `in` and `out` in Figure 4.41, with $C_l(zI_{N_u} - A_l)^{-1}L_l =: (I_{n_u} - z^{-N}I_{n_u})^{-1}L'(z)$, where $L'_{j+1} := C_l A_l^j L_l, j = 0, 1, 2, \cdots, N-1$.

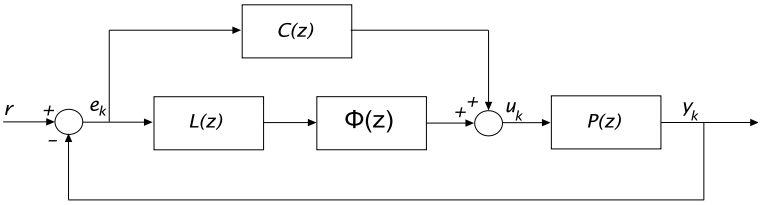

FIGURE 4.40: Iterative learning control added to existing feedback controller $C(z)$.

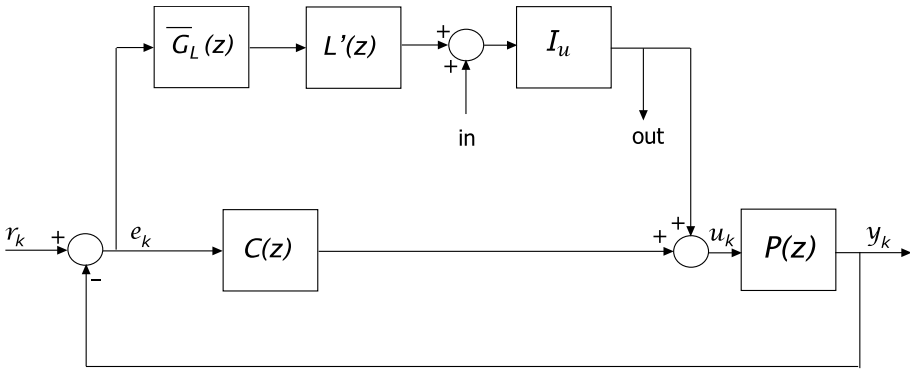

FIGURE 4.41: Internal model-based iterative learning scheme.

Notice the duality of the structure with that of Figure 4.38 where the position of the memory variables has changed from the output to the input sides. According to De Roover et al. (2000) the structure in Figure 4.39 implements an iterative learning control law of the form

$$u_{k+1} = u_k + F\epsilon_k$$

with F being a linear filter and ϵ is defined as the observer error with the following form

$$\epsilon_k = e_k + C\hat{x}_k + D(u_k + \hat{d}_k) \tag{4.72}$$

The design given in De Roover et al. (2000) is obtained using the following choices for the observer and the observer error

$$\hat{x}_{k+1} = (A + BK + LC)\hat{x}_k + Lr - LCx_k \tag{4.73}$$

and

$$\epsilon_k = r - Cx_k + C\hat{x}_k = C(\hat{x}_k - x_k) + r \tag{4.74}$$

respectively. If (4.73) is used as well as the plant description and defining $z_k = \hat{x}_k - x_k$ (the difference between the observer and plant states), gives

$$\begin{aligned} z_{k+1} &= (A + BK + LC)\hat{x}_k + Lr - LCx_k - (Ax_k + B(K\hat{x}_k - C_l x_{l,k})) \\ &= (A + LC)z_k + Lr - BC_l x_{l,k} \end{aligned} \tag{4.75}$$

and $\epsilon_k = Cz_k + r$ for zero error and disturbance output. Hence the dynamics are governed by

$$\begin{bmatrix} x_{l,k+1} \\ z_{k+1} \end{bmatrix} = \underbrace{\begin{bmatrix} A_l & 0 \\ -BC_l & A \end{bmatrix}}_{\text{system matrix}} \begin{bmatrix} x_{l,k} \\ z_k \end{bmatrix} + \underbrace{\begin{bmatrix} L_l \\ L \end{bmatrix}}_{\text{observer gains}} \underbrace{\begin{bmatrix} DC_l & C \end{bmatrix}}_{\text{output matrix}} \begin{bmatrix} x_{l,k} \\ z_k \end{bmatrix} + \begin{bmatrix} L_l \\ L \end{bmatrix} r \tag{4.76}$$

In the regulation context the reference is interpreted as a disturbance, thus $r = 0$. Doing so will lead to the design of a controller that drives the disturbance and the difference between the estimated and real states to zero which is the same system described in De Roover et al. (2000), thus it requires an output feedback scheme to solve the stabilisation problem. $\begin{bmatrix} L_l^T & L^T \end{bmatrix}$ has to be designed such that the overall system of (4.77) is stable and has favourable properties (e.g. damping ratio, loop gain, disturbance rejection). The separation principle again allows the design of the gains K and $\begin{bmatrix} L_l^T & L^T \end{bmatrix}$ separately. Following the approach of Section 4.7.1, the dual system is

$$\begin{bmatrix} x^*_{l,k+1} \\ x^*_{k+1} \end{bmatrix} = \begin{bmatrix} A_l^T & C_l^T D^T \\ 0 & A^T \end{bmatrix} \begin{bmatrix} x^*_{l,k} \\ x^*_k \end{bmatrix} + \begin{bmatrix} C_l^T DT \\ CT \end{bmatrix} \begin{bmatrix} L_l^T & L^T \end{bmatrix} \begin{bmatrix} x^*_{l,k} \\ x^*_k \end{bmatrix} \tag{4.77}$$

and $[L_l \;\; L]$ is determined by the following minimisation problem

$$\min \quad \sum_{k=1}^{\infty} \eta_k^T Q \eta_k + \mu_k^T R \mu_k \tag{4.78}$$

$$\eta_{k+1} = \begin{bmatrix} A_l^T & C_l^T B^T \\ 0 & A^T \end{bmatrix} \eta_k + \begin{bmatrix} C_l^T D^T \\ C^T \end{bmatrix} \mu_k \tag{4.79}$$

$$\mu_k = \begin{bmatrix} L_l^T & L^T \end{bmatrix} \eta_k \tag{4.80}$$

which can be calculated using the Matlab function `dlqr`. Similarly, K must be calculated such that $A + BK$ is stable, which can be achieved through solution of the problem

$$\min \quad \sum_{k=1}^{\infty} \eta_k^T \hat{Q} \eta_k + \mu_k^T \hat{R} \mu_k \tag{4.81}$$

$$\eta_{k+1} = A\eta_k + B\mu_k \tag{4.82}$$

$$\mu_k = K\eta_k \tag{4.83}$$

again using the Matlab function `dlqr`.

4.7.3 Stability Conditions for the Duality framework between RC and ILC with Explicit Current-error feedback

In order to show that the newly derived controllers augment the set of plants that can be controlled, conditions for the stability of the schemes in Sections 4.7.1 and 4.7.2 must be given.

Theorem 4.5. *Consider the RC law (4.61) and suppose that L is chosen such that $A + LC$ is asymptotically stable. Suppose also that $[K_r \;\; K]$ is chosen such that the linear system with state matrix*

$$\begin{bmatrix} A_r & -B_r C \\ 0 & A \end{bmatrix}$$

is asymptotically stable. Then (4.61) solves the problem under consideration if, and only if,

$$\operatorname{rank}\left(\begin{bmatrix} \lambda I - A & B \\ -C & D \end{bmatrix} \right) = n_x + n_y$$

for all λ in the spectrum of the matrix A_w, where n_x denotes the state vector dimension.

Theorem 4.5 requires that the plant transfer-function matrix does not have transmission zeros which are also eigenvalues of the disturbance matrix A_w. Also the transfer-function

must have at least as many inputs as outputs.

Theorem 4.6. *Consider the ILC law (4.69) and suppose that K is chosen such that $A + BK$ is asymptotically stable. Suppose also that $\begin{bmatrix} L_l^T & L^T \end{bmatrix}$ is chosen such that the linear system with state matrix*

$$\begin{bmatrix} A_l & 0 \\ BC_l & A \end{bmatrix}$$

is asymptotically stable. Then (4.69) solves the problem under consideration if, and only if,

$$\operatorname{rank}\left(\begin{bmatrix} \lambda I - A & B \\ -C & D \end{bmatrix}\right) = n_x + n_u$$

for all λ in the spectrum of the matrix A_w, where n_x denotes the state vector dimension and

$$\operatorname{rank}(B) + n_y = \operatorname{rank}\left(\begin{bmatrix} B \\ D \end{bmatrix}\right)$$

Theorem 4.6 here requires that the plant transfer-function matrix does not have transmission zeros which are also eigenvalues of the matrix A_w. Also the transfer-function must have at least as many outputs as inputs.

A routine argument also shows that the ILC will only give asymptotic tracking of the reference vector when the plant transfer-function is square and invertible due to the second condition in Theorem 4.6.

4.7.4 Experimental Verification of the Duality Framework with Explicit Current-error Feedback

Experimental results in this section are presented to verify the capability of the framework developed in De Roover et al. (2000) to provide periodic tracking accuracy and error reduction. The X-axis reference used in all the tests undertaken in this Chapter is shown in Figure 3.5, and the sample frequency is 100 Hz.

4.7.4.1 Experimental Verification for the RC Framework with Explicit Current-error Feedback

The scheme shown in Figure 4.37 has been implemented using the software described in Chapter 3. Different weighting parameters have been investigated for the calculation of

the state-feedback matrix $[K_r \;\; K]$ in the optimisation (4.66), conducted using the `dlqr` function in Matlab. The forms $Q = \begin{bmatrix} Q_1 I_{N_u} & 0 \\ 0 & Q_2 I_{n_x} \end{bmatrix}$ and $R = R_1 I_u$, where Q_1, Q_2 and R_1 are positive scalars, have been found to produce the best results, leading to high quality periodic reference tracking within a few trials. Similarly the observer matrix L has been used to implement a Kalman estimator, using the Matlab function `kalman` with the process and measurement covariance weights $\hat{Q} = \hat{Q}_1 I_{n_x}$ and $\hat{R} = \hat{R}_1 I_{n_y}$, where $\hat{Q}_1$ and $\hat{R}_1$ are positive scalars. Table 4.5 shows the weighting parameters found to perform best.

	Designing $[K_r \;\; K]$			Designing L	
Set	Q_1	Q_2	R_1	$\hat{Q}_1$	$\hat{R}_1$
1	1	0.1	1	1	1
2	10	0.1	1	1	1
3	10	1	1	1	1
4	100	1	1	1	1
5	10	1	1	10	1
6	100	1	1	10	1

TABLE 4.6: Parameter sets for designing $[K_r \;\; K]$ and L in RC scheme with explicit current-error.

Figure 4.42 shows the mean squared error for the six different parameter sets over 200 trials. The mean squared error stays at a very low level over all trials.

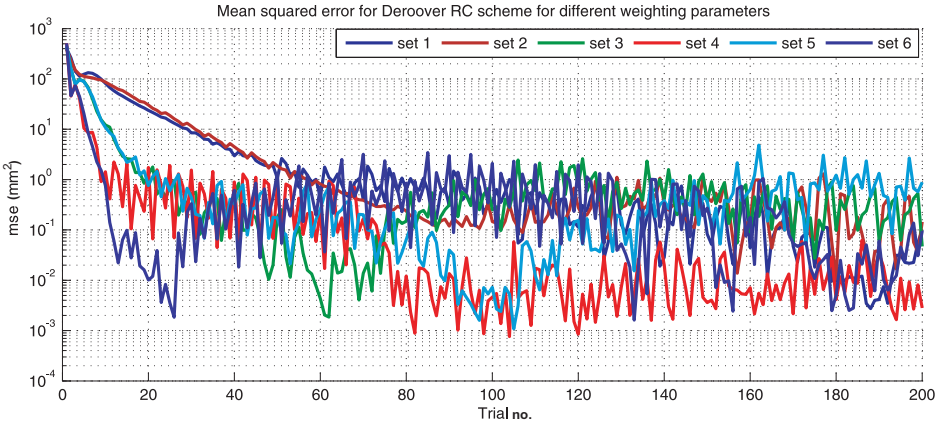

FIGURE 4.42: Mean squared error for six different sets of weighting parameters in RC framework with explicit current-error.

In Figure 4.43, set 4 is used to illustrate performance since it shows fast convergence behaviour and the mean squared error has a very low level over all trials. Excellent tracking is achieved within 10 trials as seen in Figure 4.43. The following figures show the performance of the plant using the repetitive controller in a 3D view. Figure 4.44 shows the output signal, Figure 4.45 shows the input control signal, and Figure 4.46 shows the error signal, which can be seen to reduce in norm as the number of trials increases.

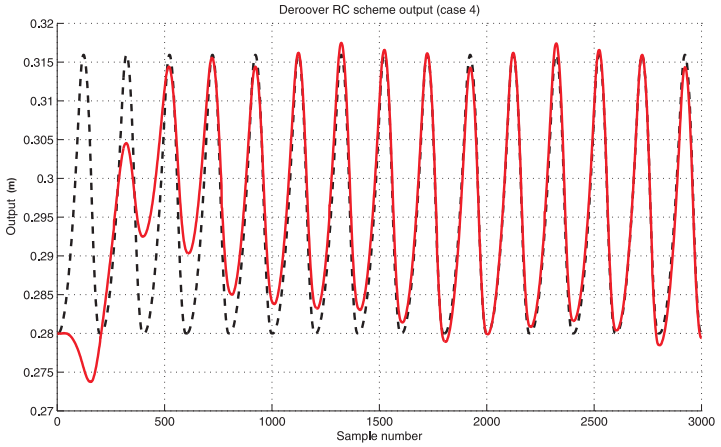

FIGURE 4.43: Reference tracking progress in the reported repetitive framework for 15 trials.

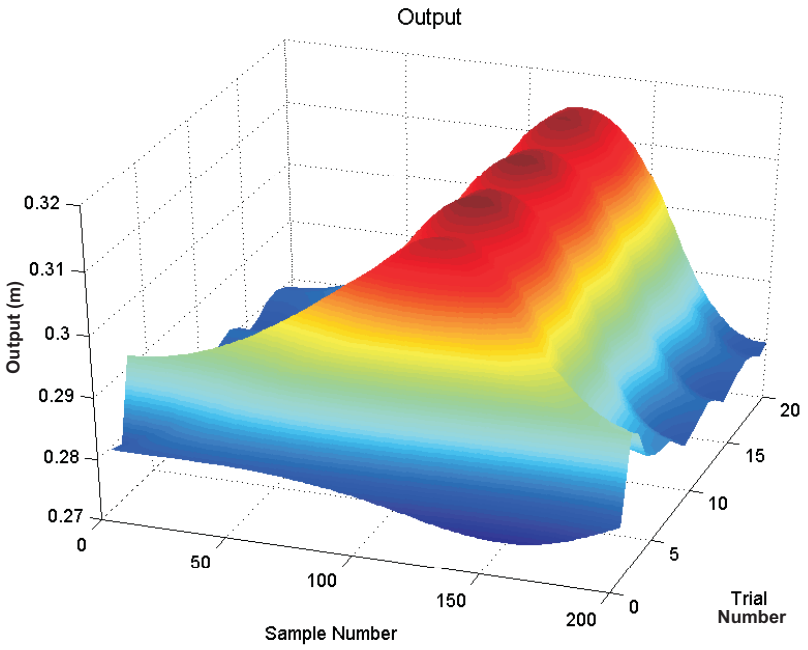

FIGURE 4.44: 3D plot for the output signal for explicit current feedback RC design for the first 20 trials.

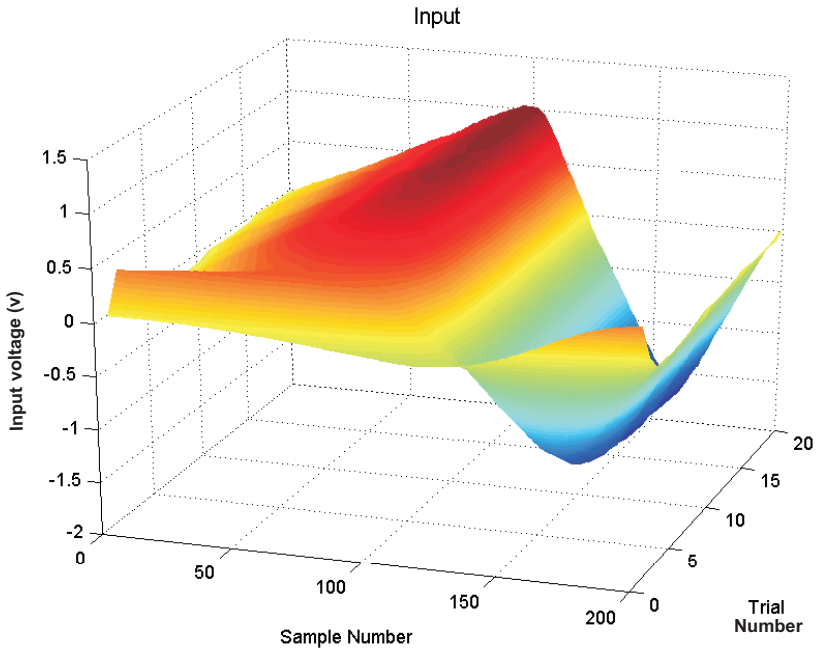

FIGURE 4.45: 3D plot for the input signal for explicit current feedback RC design for the first 20 trials.

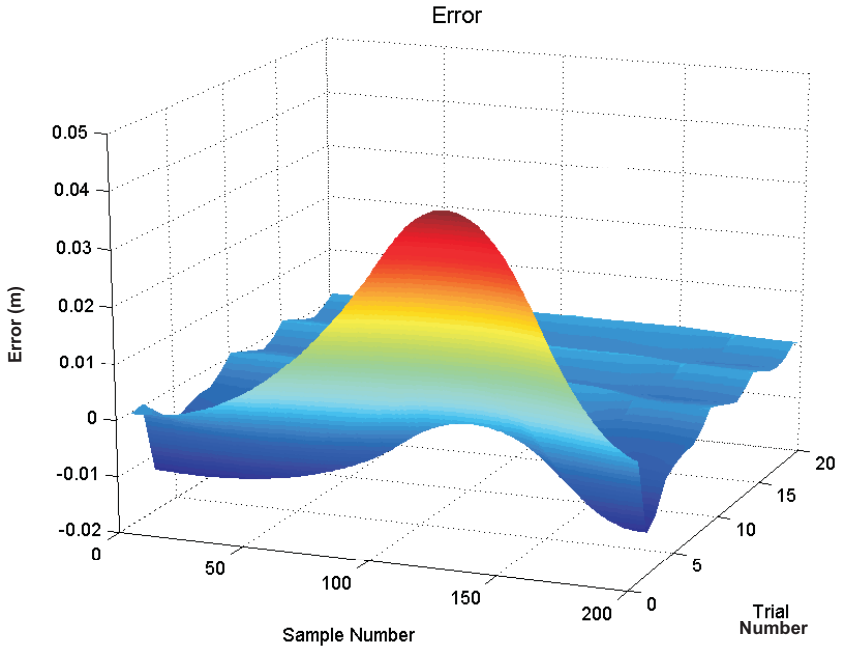

FIGURE 4.46: 3D plot for the error signal for explicit current feedback RC design for the first 20 trials.

4.7.4.2 Experimental Verification for the ILC Framework with Explicit Current-error Feedback

Experimental tests have shown a high level of success for the developed ILC, RC and RC with explicit CE feedback approaches. Here experimental verification is undertaken for the ILC design of De Roover et al. (2000). Again, the X-axis reference shown in Figure 3.5 has been used, together with a sampling frequency of 100 Hz. The ILC scheme shown in Figure 4.39 has been implemented using the software described in Chapter 3. The matrix $\begin{bmatrix} L_l^T & L^T \end{bmatrix}$ is calculated to solve the minimisation (4.78) where the forms $Q = \begin{bmatrix} Q_1 I_{N_u} & 0 \\ 0 & Q_2 I_{n_x} \end{bmatrix}$ and $R = R_1 I_y$. The matrix K has been calculated as the solution of (4.81) using the Matlab function `dlqr` with the weighting parameters $\hat{Q} = \hat{Q}_1 I_{n_x}$ and $\hat{R} = \hat{R}_1 I_{n_u}$, where $\hat{Q}_1$ and $\hat{R}_1$ are positive scalars. In the ILC framework the plant is reset between each iteration, however the state matrix $\hat{x}_k$ appearing in the observer, and $x_{l,k}$ appearing in the internal model are not reset. The system therefore starts with the final state values from the previous trial. The filter (3.6) is used in all the ILC experiments described in this Chapter, and is applied to the input signal, u_k, during the reset period between trials, in the manner described in Chapter 3. The input signal u_k equates to the state matrix of the internal model, and hence it is the states $\hat{x}_{l,k}$ which are filtered between iterations.

The best performing parameter sets are also given in Table 4.6. The mean squared error plot for six different sets of weighting parameters is given in Figure 4.47. The 4^{th} set has a higher quality performance compared to the other sets and the output, input and error plots are given in Figures 4.48, 4.49 and 4.50, respectively. The performance obtained shows near perfect reference tracking with very low error over all trials.

	Designing K		Designing $\begin{bmatrix} L_l^T & L^T \end{bmatrix}$		
Set	$\hat{Q}_1$	$\hat{R}_1$	Q_1	Q_2	R_1
1	1	1	10	1	1
2	1	1	100	1	1
3	1	1	200	1	1
4	1	1	500	1	1
5	10	1	100	1	1
6	100	1	100	10	1

TABLE 4.7: Parameter sets for designing K and $\begin{bmatrix} L_l^T & L^T \end{bmatrix}$ in ILC scheme with explicit current-error.

4.8 Conclusions

In this chapter, optimal control techniques are used to develop new solutions for the framework that links ILC and RC under duality. The new framework uses either state-

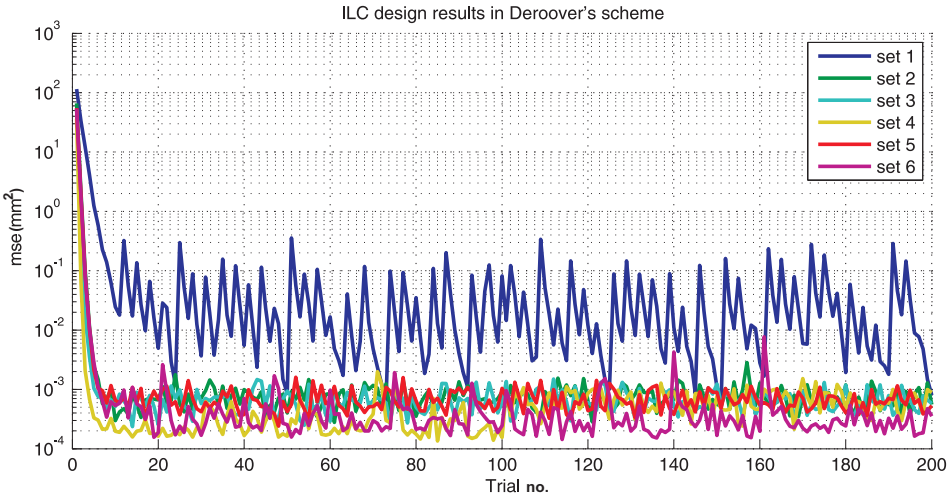

FIGURE 4.47: Mean squared error for different weighting parameter sets with explicit current feedback ILC design for 200 trials.

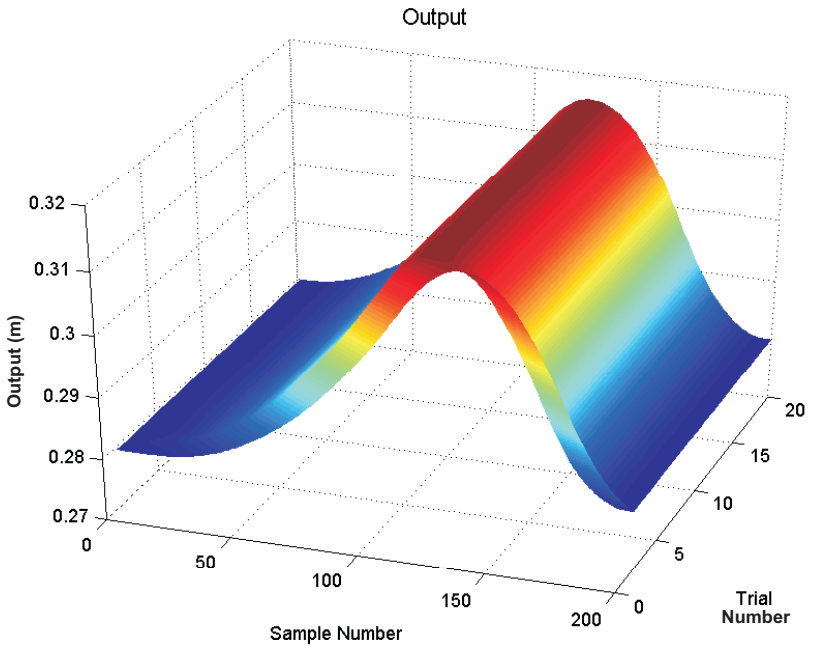

FIGURE 4.48: 3D plot for the output signal for explicit current feedback ILC design.

feedback for ILC and RC controllers or output-feedback for ILC, and expands the set of plants that can be tackled within the duality framework. In addition, experimental verification results have been obtained which confirm that high quality performance is possible using this approach. Such work is increasingly important in ILC/RC given the low number of actual implementations reported in the literature.

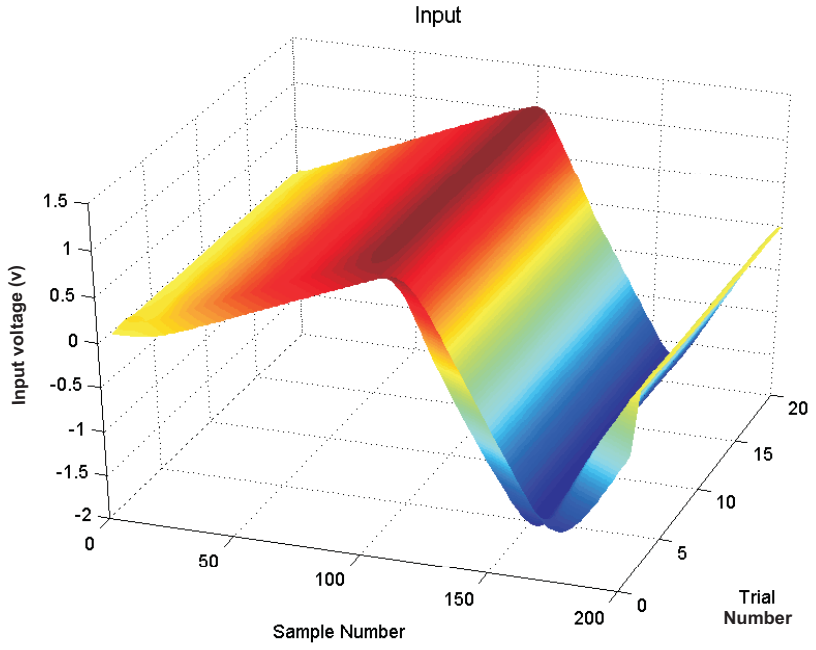

FIGURE 4.49: 3D plot for the input signal for explicit current feedback ILC design.

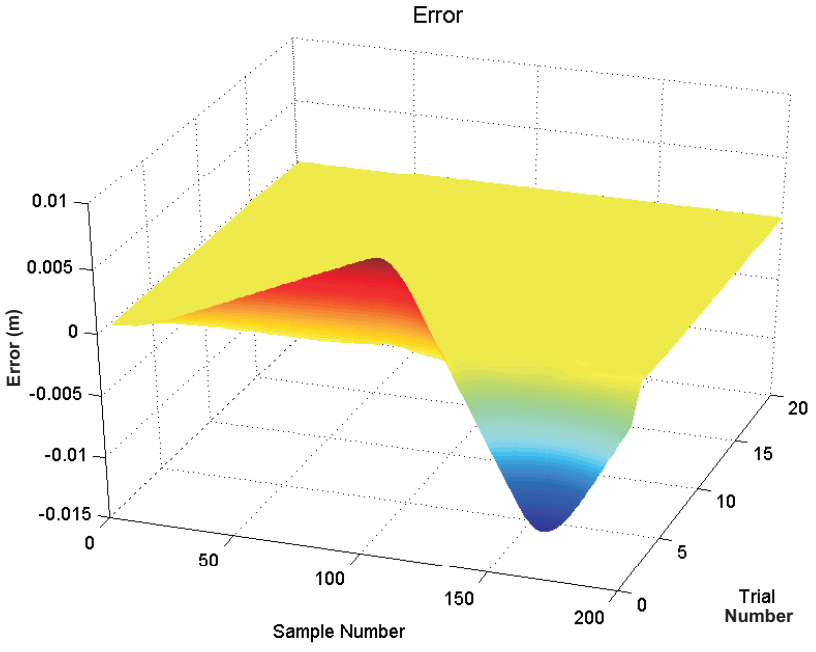

FIGURE 4.50: 3D plot for the error signal for explicit current feedback ILC design.

Chapter 5

Model and Experience-Based Initial Input Construction for Iterative Learning Control

5.1 Introduction to Initial Input Construction Idea

Current research directions in iterative learning control can be broadly categorized into two groups: first is the path where control design is undertaken using a plant model and the second is where no prior knowledge is assumed. In the majority of publications the initial choice of input is either not addressed, or assumed to be equal to zero. This, in turn, leads to the use of $e = r - y_0 = r$ in subsequent trial updates. Whilst this choice of initial input is logical, if a better choice can be found, the system will converge to the required trajectory faster.

In operation, the performance achieved using ILC depends on the choice of input employed on the initial trial. This dictates the initial error, and, in conjunction with the ILC scheme used, the error incurred over future trials. Careful selection of an initial input is especially important for applications which cannot tolerate a large error, such as robots with physical movement constraints. It is also of great importance for applications in which the maximum number of trials that can be performed is limited. One example exists within stroke rehabilitation where ILC has been used to produce accurate movement control of patient's arms via electrical stimulation. During clinical treatment sessions, only six trials were performed with any given reference trajectory in accordance with clinical need, and accurate tracking was vital to promote effectiveness of treatment Freeman et al. (2009a); Hughes et al. (2009).

The issue of how the initial input may be selected to best effect is addressed in this chapter, and it is assumed that previous experimental input and output data is available from which to construct an input for an arbitrary new trajectory. This differs from the case in which experimental data of a specific type is gathered for the explicit purpose of being used in the generation of a new input. One such example is considered in Hoelzle et al. (2009) where the reference is known to consist of a sequence of basis tasks. Here ILC is used to track each basis task individually and the resulting experimental data collected is used in constructing joined segments to form the new control input including different reference lengths.

When an arbitrary reference is used, the unsuitability or lack of previous data can lead to an inaccurate initial input estimate. The approaches considered in Arif et al. (2001, 2002) use a k-nearest neighbour search to extract from a set of previously applied data those query points which are most closely associated with a new reference. Using the corresponding previously applied inputs, these points are then used to generate a polynomial representation of the initial input required to track the new reference. This approach requires full state information, may lead to significant error if insufficient previous data is available, and provides no method in which to accurately predict the error in advance.

To provide close control over the initial error that will be attained, the approach developed here splits the construction of an initial input into two components: one that is generated using previous data, and the other which is derived through application of an assumed model of the plant. Firstly, previous data alone is used to generate an initial input, allowing an accurate prediction of the resulting error to be made. The second component compensates for a lack of previous data, applying the model to minimise the predicted error. This is achieved using a robust model-based approach which allows multiplicative plant uncertainty to be incorporated and addressed in a straightforward and transparent manner.

Each case is addressed by constructing an optimisation problem to yield the most suitable choice of initial input. It is shown that minimisation of the error using appropriate data design techniques provides a robust solution to the selection of an initial input. Solutions are verified experimentally and the predicted initial input is shown to represent a successful starting point for any ILC update technique to speed up the learning process. The next sections give a detailed explanation for the selection of the initial input for different cases.

Figure 5.1 shows a schematic summary of the two paths; the first using assumed plant model and the second using previous converged input and output data.

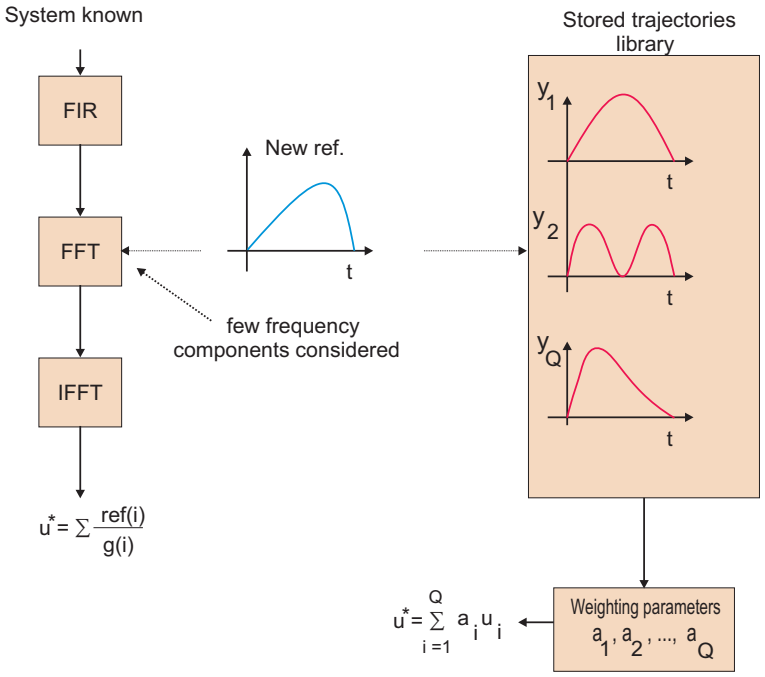

FIGURE 5.1: Two separate paths for the initial input construction idea.

5.1.1 Discrete Fourier Transform

The Discrete Fourier Transform (DFT) is used extensively in this chapter and is now summarised. Let $u = \begin{bmatrix} u(0) & u(1) & \cdots & u(N-1) \end{bmatrix}^T \in \mathbb{R}^N$ be a sequence of N elements, then (under the necessary assumption relating to existence) the DFT of this sequence, denoted by $\widehat{u}$, is defined as

$$\hat{u}_i = \sum_{n=0}^{N-1} u_n e^{-j2\pi ni/N} \tag{5.1}$$

where $\hat{u} \in \mathbb{C}^N$ and $i = \{0, 1, \cdots, N-1\}$. Typically in ILC the length of the reference signal, T, has a fixed time duration, and for a given $N \in 2^M, M \in \mathbb{Z}$, the sampling frequency must be chosen as $f_s = \frac{N}{T}$. The Inverse Discrete Fourier Transform (IDFT) is given by

$$u_n = \frac{1}{N} \sum_{i=0}^{N-1} \hat{u}_i e^{j2\pi ni/N} \tag{5.2}$$

If g is the impulse response of a linear time time-invariant (LTI) system, then convolution between g and u produces the output sequence

$$y(q) = \sum_{i=0}^{q} g(q-i)u(i) = \sum_{i=0}^{q} g(i)u(q-i), \qquad q = 0, 1, \cdots, N-1 \tag{5.3}$$

The DFT of y (the convolution output) can then be calculated using

$$\hat{y} = \hat{g} \odot \hat{u} \tag{5.4}$$

where $\odot$ denotes component-wise multiplication.

The frequency-domain allows analysis and design to tackle the effect of model uncertainty and exogenous noise in a straight forward manner. This is the key point for choosing FFT which will be used in the analysis of the next section, where an initial input is constructed based on an assumed model description, and the initial input is found using an optimisation formulation.

5.2 Model-based Initial Input Construction

Let the reference trajectory vector be given by y_d, and the goal is to select an initial input vector u_0^* which speeds up learning when used with a suitable ILC algorithm. The following SISO discrete linear time-invariant system state-space model is considered

$$\begin{aligned} x(t+1) &= Ax(t) + Bu(t), \quad 0 \leq t < N \\ y(t) &= Cx(t) + Du(t), \quad x(0) = 0 \end{aligned} \tag{5.5}$$

where again N is the number of samples, $x(t)$ is the $n \times 1$ state vector, $y(t)$ is the output and $u(t)$ is the input. This model is assumed to be linear or identified using many techniques available Ljung (1987). Also since N is finite ($N < \infty$ samples), introduce the supervectors

$$y_k = \begin{bmatrix} y(0) \\ y(1) \\ \vdots \\ y(N-1) \end{bmatrix}, \quad u_k = \begin{bmatrix} u(0) \\ u(1) \\ \vdots \\ u(N-1) \end{bmatrix} \tag{5.6}$$

Then, using the transition matrix solution for $y(q)$ of (5.5), the process dynamics on trial k can be described by the matrix equation

$$y_k = Gu_k \tag{5.7}$$

where the $N \times N$ matrix G is given by

$$G = \begin{bmatrix} D & 0 & 0 & \dots & 0 \\ CB & D & 0 & \dots & 0 \\ CAB & CB & D & \dots & 0 \\ \vdots & \vdots & \vdots & \ddots & \vdots \\ CA^{N-2}B & CA^{N-3}B & CA^{N-4}B & \dots & D \end{bmatrix} \tag{5.8}$$

The ILC law considered in this chapter is of the form

$$u_{k+1} = u_k + Le_k \tag{5.9}$$

where L is a possibly non-causal LTI filter, and the error on trial k is

$$e_k = [y_d(0) - y_k(0),\ y_d(1) - y_k(1),\ \cdots,\ y_d(N-1) - y_k(N-1)]^T \tag{5.10}$$

where y_d denotes the reference signal. Using the system representation (5.7), the error evolution equation can be written as

$$e_{k+1} = (I - GL)e_k \tag{5.11}$$

Taking the DFT of (5.9) now gives (with obvious notation)

$$\hat{u}_{k+1} = \hat{u}_k + \hat{l} \odot \hat{e}_k \tag{5.12}$$

and also

$$\hat{e}_{k+1} = (\hat{I} - \hat{g} \odot \hat{l}) \odot \hat{e}_k \tag{5.13}$$

where $\hat{I} \in \mathbb{R}^N$ and has each entry equal to unity. Also

$$\hat{e}_{k+1} = (\hat{I} - \hat{g} \odot \hat{l})^k \odot \hat{e}_0 \tag{5.14}$$

where the power operation is applied in component-wise fashion.

Consider the error progression starting from an arbitrary initial input, u_0,

$$\begin{aligned}\|e_{k+1}\|^2 &= \sum_{i=0}^{N-1} |\hat{e}_{k+1,i}|^2 = \sum_{i=0}^{N-1} |(1-\hat{g}_i\hat{l}_i)^k \hat{e}_{0,i}|^2 \\ &= \sum_{i=0}^{N-1} |1-\hat{g}_i\hat{l}_i|^{2k} |\hat{e}_{0,i}|^2 \\ &= \sum_{i=0}^{N-1} |1-\hat{g}_i\hat{l}_i|^{2k} |\hat{y}_{d,i} - \hat{g}_i\hat{u}_{0,i}|^2 \end{aligned} \tag{5.15}$$

where $\|\cdot\|$ denotes the l_2 norm. This shows how components of the initial error, e_0, contribute to the error norm produced over subsequent trials and this error is minimized with respect to the initial input by setting $\hat{u}_0$ equal to

$$\hat{u}^*_{0,i} = \frac{\hat{y}_{d,i}}{\hat{g}_i}, \qquad i = 0, 1, \cdots, N-1 \tag{5.16}$$

This effectively generates a steady-state inverse over the trial duration.

Theorem 5.1. *The tracking error vector, e, generated through application of input (5.16) to the plant (5.5) satisfies*

$$\tilde{e} = \tilde{u}^*_0 * \tilde{g} \tag{5.17}$$

where $*$ denotes convolution, and $\tilde{x}$ denotes a time reversed vector x of length N such that $\tilde{x}(i) = x(N-1-i)$, for $i = 0, 1, \ldots, N-1$.

Proof. The initial input (5.16) corresponds to the time-domain input

$$u^*_0 = \frac{1}{N} \sum_{i=0}^{N-1} \left(\frac{\hat{y}_{d,i}}{\hat{g}_i} \right) e^{j2\pi ni/N} \qquad n = 0, 1, \ldots, N-1 \tag{5.18}$$

applied over the trial length duration $t \in [0, T]$. Using (5.3), this results in the plant output

$$y(q) = \sum_{i=0}^{q} \left(\frac{1}{N} \sum_{p=0}^{N-1} \hat{g}_p e^{j2\pi pi/N} \right) \left(\frac{1}{N} \sum_{m=0}^{N-1} \left(\frac{\hat{y}_{d,m}}{\hat{g}_m} e^{2j\pi m(q-i)/N} \right) \right) \tag{5.19}$$

Note that, if $g(q) = 0$ for $q = 0, 1, \ldots, n$, then $y(q) = 0$ for $q = 0, 1, \ldots, n$. To find the

error between the output and the reference signal, first express the reference signal as

$$y_d(q) = \frac{1}{N}\sum_{m=0}^{N-1}\hat{y}_{d,m}e^{j2\pi qm/N} \tag{5.20}$$

$$= \frac{1}{N}\sum_{m=0}^{N-1}\sum_{p=0}^{N-1}\hat{y}_{d,m}\delta_{p,m}e^{j2\pi mq/N} \tag{5.21}$$

$$= \frac{1}{N}\sum_{m=0}^{N-1}\sum_{p=0}^{N-1}\left(\frac{\hat{y}_{d,m}}{\hat{g}_m}\right)\hat{g}_p\delta_{p,m}e^{j2\pi mq/N} \tag{5.22}$$

where $\delta_{p,m}$ is the Kronecker delta function which equals 1 when $p = m$, and 0 at all other time instance. Over the required interval, this function can equivalently be expressed as

$$\delta_{p,m} = \frac{1}{N}\sum_{i=0}^{N-1}e^{j2\pi i(p-m)/N} \tag{5.23}$$

and hence (5.22) becomes

$$y_d(q) = \frac{1}{N}\sum_{m=0}^{N-1}\sum_{p=0}^{N-1}\left(\frac{\hat{y}_{d,m}}{\hat{g}_m}\right)\hat{g}_p\left(\frac{1}{N}\sum_{i=0}^{N-1}e^{j2\pi i(p-m)/N}\right)e^{j2\pi mq/N} \tag{5.24}$$

$$= \sum_{i=0}^{N-1}\left(\frac{1}{N}\sum_{p=0}^{N-1}\hat{g}_p e^{j2\pi pi/N}\right)\left(\frac{1}{N}\sum_{m=0}^{N-1}\left(\frac{\hat{y}_{d,m}}{\hat{g}_m}\right)e^{j2\pi m(q-i)/N}\right) \tag{5.25}$$

$$= \sum_{i=0}^{N-1}u_0^*(q-i)g(i) \tag{5.26}$$

This resembles the 'standard' convolution expression (5.3) which operates over samples $q = 0, 1, \ldots, N-1$ and assumes zero initial conditions, but now the convolution sum is expanded to include the previous $N-1$ samples (the input 'looped' such that $u(-i) = u(N-1-i)$ for $i = 0, 1, \ldots N-1$). The error resulting from applying u_0^* is then

$$e(q) = \sum_{i=0}^{N-1}u_0^*(q-i)g(i) - \sum_{i=0}^{q}u_0^*(q-i)g(i) \tag{5.27}$$

$$= \sum_{i=q+1}^{N-1}u_0^*(q-i)g(i) \qquad q = 0, 1, \ldots N-1 \tag{5.28}$$

which can also be written as

$$e(q) = \sum_{i=0}^{N-q-2}u_0^*(-i-1)g(i+q+1) = \sum_{i=0}^{N-q-2}u_0^*(N-i-1)g(i+q+1) \tag{5.29}$$

$$= \sum_{i=0}^{N-q-2}u_0^*(i+q+1)g(N-i-1) \tag{5.30}$$

Comparison with (5.3) shows that this is a standard convolution sum but here the direction of time is reversed — the error at sample q depends on the elements of u_o^* ahead of this point, and components of g are taken from the end rather than the beginning. If $\tilde{x}$ is now used to denote a time reversed vector x of length N, such that $\tilde{x}(i) = x(N-1-i)$ for $i = 0, 1, \ldots, N-1$, then (5.30) can be expressed as

$$\tilde{e}(q) = \sum_{i=0}^{q-1} u_0^*(i+N-q)g(N-i-1) \tag{5.31}$$

$$= \sum_{i=0}^{q-1} \tilde{u}_0^*(q-i)\tilde{g}(i) \tag{5.32}$$

and hence $\tilde{e}$ is generated through standard convolution of $\tilde{u}_0^*$ with $\tilde{g}$.
This completes the proof and leads to the following remark.

Remark 5.1. *Providing that g has settled to an arbitrarily small level over time T, the reversed error will start from approximately zero, but may build up gradually. The extent of its increase will depend on the combined effect of*

- *the length of plant transient response, as dictated by the number of samples by which $g(\cdot)$ is greater than an arbitrarily small value, and*
- *the magnitude of u_0^* at the end of the trial*

Reducing these guarantees that $\tilde{e}$ does not increase significantly, thus ensuring that e is small over initial samples.

The robustness of the proposed initial input will now be considered, and, as in all such analysis, is based on an assumption concerning the structure of the uncertainty. In particular, assume that only a DFT, $\hat{g}_0$, of a nominal model impulse response, g_0, is available and that the DFT, $\hat{g}$, of the true model impulse response, g, is related to it through a multiplicative uncertainty, $\hat{m}$, expressed as

$$\hat{g} = \hat{g}_0 \odot \hat{m} \tag{5.33}$$

To address this uncertainty, modify the update (5.16) to

$$\hat{u}_{0,i}^* = \hat{\zeta}_i \frac{\hat{y}_{d,i}}{\hat{g}_{0,i}} \tag{5.34}$$

where $\hat{\zeta}_i \in \mathbb{C}$. Applying this to the error norm expression (5.15) produces

$$\|e_{k+1}\|^2 = \sum_{i=0}^{N-1} \left|1 - \hat{g}_{0,i}\hat{m}_i\hat{l}_i\right|^{2k} \left|\hat{y}_{d,i} - \hat{\zeta}_i\hat{m}_i\hat{y}_{d,i}\right|^2 \tag{5.35}$$

$$= \sum_{i=0}^{N-1} \left|1 - \hat{g}_{0,i}\hat{m}_i\hat{l}_i\right|^{2k} \left|1 - \hat{\zeta}_i\hat{m}_i\right|^2 |\hat{y}_{d,i}|^2 \tag{5.36}$$

and an optimal first input is now associated with computing, over i,

$$\min_{\hat{\zeta}_i} \left|1 - \hat{\zeta}_i\hat{m}_i\right| \tag{5.37}$$

This minimisation is conducted over the region of uncertainty space containing all possible $\hat{m}_i$.

Remark 5.2. *From (5.35), the design of the learning filter $\hat{l}$ is associated with computing, over i,*

$$\min_{\hat{l}_i} \left|1 - \hat{g}_{0,i}\hat{m}_i\hat{l}_i\right| \tag{5.38}$$

and, in particular, it can be shown that if $\hat{l}_i$ satisfies

$$\left|1 - \hat{g}_{0,i}\hat{m}_i\hat{l}_i\right| < 1 \tag{5.39}$$

over i, this is a sufficient condition for monotonic error convergence Longman (2000). The frequency-domain design of the learning filter $\hat{l}$ has received considerable attention in the literature (see, for example Freeman et al. (2009b); Norrlof and Gunnarsson (2002b); Gunnarsson and Norrlof (1999); Norrlof (2000); Longman (2000)). These approaches typically lead to the design of $\hat{l}_i \approx 1/\hat{g}_{0,i}$ over low frequencies (when $\hat{m}_i$ is small), and $\hat{l}_i \approx 0$ over higher frequencies (when $\hat{m}_i$ is large).

If the learning filter, l, has already been designed by any method which suitably reduces $\left|1 - \hat{g}_{0,i}\hat{m}_i\hat{l}_i\right|$ (e.g. through use of an uncertainty weighting approach Freeman et al. (2009b)), then this knowledge may be utilised in the construction of a robust first input by setting

$$\hat{\zeta}_i = \hat{g}_{0,i}\hat{l}_i \tag{5.40}$$

and thereby unifying (5.37) and (5.38). The selection of $\hat{\zeta}_i$ to produce the initial input, however, is not as critical as that of the learning filter since it does not directly influence the convergence rate. Motivated by comments made about the design of $\hat{l}$, the simpler

criterion of selecting either $\hat{\zeta}_i = 1$ or $\hat{\zeta}_i = 0$ will be considered.

With these values the solution to (5.37) is

$$\hat{\zeta}_i = \begin{cases} 1 & \text{if } |1-(1)\hat{m}_i| < |1-(0)\hat{m}_i| = 1 \\ 0 & \text{otherwise} \end{cases} \tag{5.41}$$

When applied in (5.34), this yields

$$\hat{u}^*_{0,i} = \begin{cases} \hat{y}_{d,i}/\hat{g}_{0,i} & \text{if } |1-\hat{m}_i| < 1 \\ 0 & \text{otherwise} \end{cases} \tag{5.42}$$

Suppose now that $|1-\hat{m}_i| < 1$ for the first M frequencies so that (5.42) is replaced by

$$\hat{u}^*_{0,i} = \begin{cases} \hat{y}_{d,i}/\hat{g}_{0,i} & i = 0, 1, \ldots M-1 \\ 0 & i = M, M+1, \ldots N-1 \end{cases} \tag{5.43}$$

This assumption of reduced plant uncertainty at lower frequencies is realistic in practice, and simplifies the design process when full uncertainty information is not available. The error progression associated with using (5.43) is given by

$$\|e^*_{k+1}\|^2 = \sum_{i=0}^{M-1} \left|1-\hat{g}_{0,i}\hat{m}_i\hat{l}_i\right|^{2k} |\hat{y}_{d,i}|^2 |1-\hat{m}_i|^2 + \sum_{i=M}^{N-1} \left|1-\hat{g}_{0,i}\hat{m}_i\hat{l}_i\right|^{2k} |\hat{y}_{d,i}|^2 \tag{5.44}$$

Over the first M frequencies, the smaller region containing $\hat{m}_i$ means that good design practice yields a filter $\hat{l}_i$ providing rapid convergence as the trial number increases. The left-hand term in (5.44) therefore converges rapidly, leaving the slower right-hand term which is associated with greater plant uncertainty.

Remark 5.3. *Commonly in the literature the initial input, u_0, is chosen as either the zero vector, or the reference y_d. The error improvement resulting from using (5.43) in place of the zero vector is*

$$\|e_{k+1}\|^2 - \|e^*_{k+1}\|^2 = \sum_{i=0}^{M-1} \left|1-\hat{g}_{0,i}\hat{m}_i\hat{l}_i\right|^{2k} |\hat{y}_{d,i}|^2 \left(1-|1-\hat{m}_i|^2\right) > 0 \tag{5.45}$$

The error improvement compared with using the reference as the initial input is

$$\begin{aligned}\|e_{k+1}\|^2 - \|e^*_{k+1}\|^2 &= \sum_{i=0}^{M-1} \left|1 - \hat{g}_{0,i}\hat{m}_i\hat{l}_i\right|^{2k} |\hat{y}_{d,i}|^2 \left(|1 - \hat{g}_{0,i}\hat{m}_i|^2 - |1 - \hat{m}_i|^2\right) \\ &\quad + \sum_{i=M}^{N-1} \left|1 - \hat{g}_{0,i}\hat{m}_i\hat{l}_i\right|^{2k} |\hat{y}_{d,i}|^2 \left(|1 - \hat{g}_{0,i}\hat{m}_i|^2 - 1\right) \end{aligned} \tag{5.46}$$

Remark 5.4. *Restricting u^*_0 to the first M frequencies via (5.43), also affects the error on the first trial (as given by (5.30) or, alternatively, (5.32)). The difference in error is equal to the plant response to the input*

$$\Delta u^*_0(n) = \frac{1}{N}\sum_{i=M}^{N-1} \left(\frac{\hat{y}_{d,i}}{\hat{g}_i}\right) e^{j2\pi ni/N} \qquad n = 0, 1, \ldots N-1 \tag{5.47}$$

whose magnitude is determined by the size of the frequency components of y_d greater than M, and length of the transient response of the plant.

5.2.1 Experimental Verification for Model-Based Initial Input Construction in ILC

The model-based input construction (5.43) technique has been simultaneously applied to all axes of the gantry robot using values of $M = 3$ and $M = 8$ which dictate the number of frequencies used in the initial input. In general, the number selected depends on the frequency content of the reference, the frequency-response of the plant, and the accuracy of the identified model. On each axis the standard gradient algorithm described in Chapter 2 has been applied, given by

$$u_{k+1} = u_k + \beta G^* e_k \tag{5.48}$$

where G^* is the adjoint operator. This update is described in, for example, Hatonen et al. (2009). Due to their similarity in structure, X-axis results alone are given, and the corresponding reference trajectory is shown in Figure 5.2 b). As stated in Chapter 3, all experimental results in this thesis have been conducted using a sampling frequency of $100Hz$. In Chapter 4, the ILC and RC approaches developed were applied directly to the gantry robot, with no feedback controller, other than that comprising part of the RC/ILC design. This was to aid experimental benchmarking with previous approaches. In this Chapter ILC is applied in combination with a feedback controller, using the

series configuration shown in Figure 3.7. This configuration has been chosen since it represents a typical situation that may be encountered in industry, where the ILC update is 'plugged-in' in to an existing feedback controller. It hence is intended to increase the generality of the initial input construction validation tests described in this chapter. The filter (3.6) is used in all the experiments described in this Chapter, and applied to the input signal, u_k, during the reset period between trials, in the manner described in Chapter 3. The PID controller is given in continuous time by

$$C(s) = K_p + \frac{K_i}{s} + K_d s \tag{5.49}$$

with gains $K_p = 6$, $K_i = 3$, and $K_d = 0.2$. This is discretised prior to implementation using the software described in Chapter 3.

For comparison, results are also shown with the zero vector taken as the initial input (which corresponds to $M = 0$). Using these initial inputs, the results in Figures 5.2 a), b) and c) show the input, output and error respectively on the second trial of gradient-based ILC with $\beta = 0.5$ in (5.48) which is used in all the results presented in this chapter. Figures 5.2 a), b) and c) show the advantage gained form applying an initial input to the gantry since the error is clearly reduced over the second trial compared to zero initial input start (part c)) and the input signal is still within acceptable values. This is reflected in Figure 5.3 which shows the evolution of the mean squared error in each case, and the benefit, especially over initial trials, of the proposed initial input selection can be seen. With only 3 frequency components, the norm of the error for the first trial is approximately equal to the norm of trial 6 with zero initial input. With 8 frequency components the first trial error norm is approximately equal to error norm at the trial 8 with zero initial input. It is clear that the tracking error reduces as the number of additional frequencies incorporated in the initial input increases.

5.3 Time-domain Experience-based Input Construction

The presence of plant uncertainty inherently degrades the performance of model-based approaches to constructing the initial input. However, the need for an explicit plant representation can be avoided by instead using stored experimental data, as developed next where the method resulting. Here it is assumed that a set of previous references have been applied to the plant, and a suitable ILC law has yielded a set of corresponding converged inputs. These will be used to build an initial input for a new reference. The availability of such data is realistic in, for example, industrial applications, where references are changed regularly in line with modifications in the process or product line being manufactured. Furthermore, within the stroke rehabilitation implementation discussed previously, six different references were typically used within each treatment session of 1

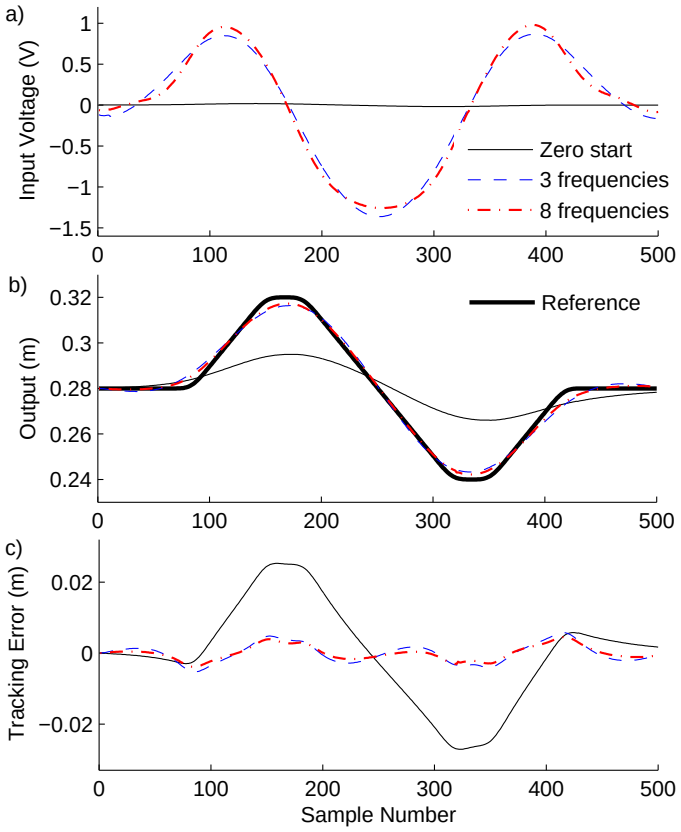

FIGURE 5.2: Effect of model-based initial input selection on X-axis a) input, b) output, and c) error during second trial.

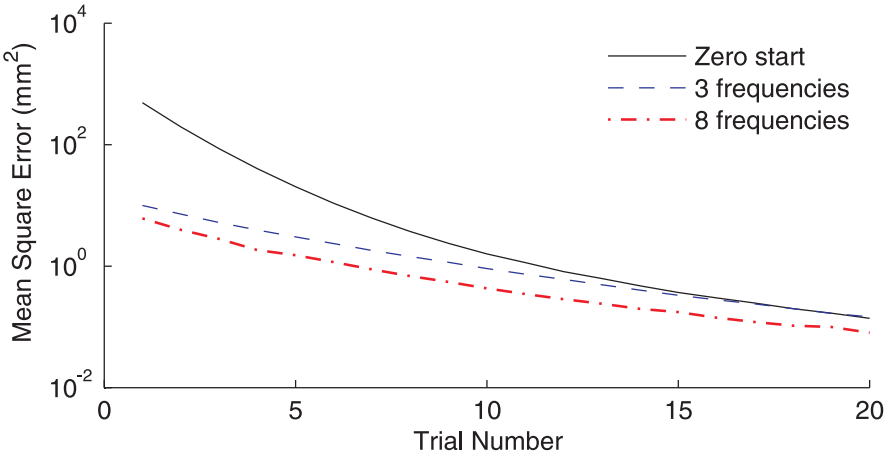

FIGURE 5.3: X-axis error evolution using model-based initial input selection.

hour duration Hughes et al. (2009).

In this section the analysis, which yields an optimal input selection, is conducted in the

time-domain. Let a previous set of Q reference trajectories be given by

$$\begin{aligned} y_{d1} &= [y_{d1}(0), y_{d1}(1) \dots y_{d1}(N-1)]^T \\ y_{d2} &= [y_{d2}(0), y_{d2}(1) \dots y_{d2}(N-1)]^T \\ &\vdots \\ y_{dQ} &= [y_{dQ}(0), y_{dQ}(1) \dots y_{dQ}(N-1)]^T \end{aligned} \tag{5.50}$$

with corresponding converged inputs

$$\begin{aligned} u_1^* &= [u_1^*(0), u_1^*(1) \dots u_1^*(N-1)]^T \\ u_2^* &= [u *_2 (0), u_2^*(1) \dots u_2^*(N-1)]^T \\ &\vdots \\ u_Q^* &= \left[u_Q^*(0), u_Q^*(1) \dots u_Q^*(N-1)\right]^T \end{aligned} \tag{5.51}$$

These are assumed to be of the same length as the new reference, although suitable techniques may be applied if this is not the case and are described in Section 5.4. To find the linear combination of previous references that most closely represents the new reference, y_d, the parameter vector

$$a = [a_1, a_2, \dots a_m]^T \tag{5.52}$$

is required to solve the following minimisation problem

$$\min_a \|e_0\|_i^2 = \min_a \|y_d - a_1 y_{d1} - a_2 y_{d2} \cdots - a_Q y_{dQ}\|^2 \tag{5.53}$$

with l_i being suitable vector norm, e.g. l_2 norm. Here the linear combination of recorded references is sought which closely approximates the new reference.

Define the set of previously recorded reference trajectories

$$Y_d = [y_{d1}, y_{d2} \dots y_{dQ}] \tag{5.54}$$

Then (5.53) is equivalent to

$$\min_a \|\hat{y_d} - Y_d a\|^2 \tag{5.55}$$

and this last problem has the Least Squares (LS) solution

$$a = \left(Y_d^T Y_d\right)^{-1} Y_d^T y_d \tag{5.56}$$

Superposition now ensures that the corresponding linear combination of inputs provides a suitable initial input

$$u_0^* = U^* a \tag{5.57}$$

with

$$U^* = \left[u_1^*, u_2^* \dots u_Q^*\right] \tag{5.58}$$

The solution can be written in a more direct form to directly optimise the final output to which the set of previous references converge, instead of the references. This is achieved by replacing (5.56) with

$$a = \left(Y^{*T} Y^*\right)^{-1} Y^{*T} y_d \tag{5.59}$$

where

$$Y^* = \left[y_1^*, y_2^* \dots y_Q^*\right] \tag{5.60}$$

and y_i^* is the output vector associated with u_i^* for $i = 1, 2, \cdots Q$. This technique leads to error improvement compared to zero initial input, as demonstrated in Section 5.3.2.

5.3.1 Shifted Previous Reference Trajectories

To maximise the use of information provided by previous trajectories, shifted copies of the whole set is considered to provide a wider range of data with which to predict the initial input. Let q be the matrix row shift operator such that

$$q^C Y_d = \begin{bmatrix} 0 & 0 & \dots & 0 \\ \vdots & \vdots & \vdots & \vdots \\ 0 & 0 & \cdots & 0 \\ y_{d1}(0) & y_{d2}(0) & \dots & y_{dQ}(0) \\ \vdots & \vdots & \vdots & \vdots \\ & & & \\ y_{d1}(N-1-C) & y_{d2}(N-1-C) & \dots & y_{dQ}(N-1-C) \end{bmatrix}^T \tag{5.61}$$

Then Y_d in (5.56) is replaced with a version containing shifted copies at C sample intervals with dimension $N \times (Q \times \lfloor N/C \rfloor)$, where $\lfloor . \rfloor$ denotes the floor function, given by

$$\overline{Y_d} = \left[Y_d, q^C Y_d, q^{2C} Y_d, \cdots q^{C \times \lfloor N/C \rfloor} Y_d\right]^T \tag{5.62}$$

Using the previously implemented references, (5.60) becomes

$$\overline{Y}^* = \left[Y^*, q^C Y^*, q^{2C} Y^*, \cdots q^{C\times\lfloor N/C\rfloor} Y^*\right]^T \tag{5.63}$$

To yield a combination of output data which most accurately fits the new reference, define the shifted combination of the converged inputs

$$\overline{U}^* = \left[U^*, q^C U^*, q^{2C} U^*, \cdots q^{C\times\lfloor N/C\rfloor} U^*\right]^T \tag{5.64}$$

Then, the optimisation problem is given by

$$\min_a \|e_0\|^2 = \min_a \|y_d - \bar{Y}^* a\|^2 \tag{5.65}$$

with

$$a = \left[a_1, a_2, \cdots a_{Q\times\lfloor N/C\rfloor}\right]^T \tag{5.66}$$

and superposition ensures that the corresponding linear combination of inputs provides a suitable initial input

$$u_0^* = \overline{U}^* a = \overline{U}^* (\overline{Y}^{*T} \overline{Y}^*)^{-1} \overline{Y}^{*T} y_d \tag{5.67}$$

with

$$\overline{U}^* = \left[U^*, q^C U^*, q^{2C} U^*, \cdots q^{C\times\lfloor N/C\rfloor} U^*\right]^T \tag{5.68}$$

Since the error norm resulting from applying (5.68) is precisely the minimised quantity in (5.65), the performance gained through use of a given set of stored trajectories can be accurately predicted prior to its application.

Remark 5.5. *To consider the robustness associated with applying u_0^* in the ILC algorithm (5.9), note first that the error norm for the r^{th} previously applied reference is*

$$\|e_{k+1}\|^2 \;=\; \sum_{i=0}^{N-1} \left|1 - \hat{g}_{0,i}\hat{m}_i\hat{l}_i\right|^{2k} \left|\hat{y}_{dr,i} - \hat{u}^*_{r,i}\hat{g}_{0,i}\hat{m}_i\right|^2 \quad , r = 1, 2, \ldots, Q \tag{5.69}$$

and the assumption that the ILC law has converged implies that either $\left|1 - \hat{g}_{0,i}\hat{m}_i\hat{l}_i\right| \leq 1$ (case 1), and/or $\left|\hat{y}_{dr,i} - \hat{u}^*_{r,i}\hat{g}_{0,i}\hat{m}_i\right|^2 = 0$ (case 2), over all frequencies i. If reference y_{dr} contains the set of frequency components Γ_r, this implies that case 2 is not true for $i \in \Gamma_r$ (due to the presence of plant uncertainty), which in turn means that case 1 must be true for $i \in \Gamma_r$. It follows that convergence of the new reference, y_d, is only guaranteed over frequencies in $\Gamma := \{\Gamma_1, \Gamma_2, \ldots, \Gamma_Q\}$. If satisfying case 1 is a result of an ILC

learning cut-off after M frequencies, then Γ may be expanded to $\Gamma \cup \Omega$ where Ω contains the frequency components $M, M+1, \ldots, N-1$, and $\cup$ denotes the union of sets. For frequencies contained within $\Phi \backslash (\Gamma \cup \Omega)$, where Φ is the set of frequency components of y_d, the ILC algorithm may not provide robust convergence, and its progress must be carefully monitored. Since noise may also be present on the plant input, the additional frequencies injected means it is necessary in practice to choose M to filter out all frequencies over which case 1 cannot be guaranteed.

5.3.2 Experimental Verification for the Time domain Initial Input Construction Approach

Experimental verification for the time-domain initial input construction based on the use of the stored references is given in this section. To yield the stored data, thirty trials of the gradient ILC update (5.48) with $\beta = 0.5$ have been applied using the three reference trajectories given in Figure 5.4. Test conditions are exactly the same as in Section 5.2.1, with identical PID values used in the series configuration of PID and ILC shown in Figure 3.7. To evaluate the initial input, the gradient update of (5.48) is again used with a value of $\beta = 0.5$. As before, reference duration is 5 seconds and a sampling frequency of 100 Hz has been used. As in all ILC tests conducted in this thesis, the filter (3.6) has been applied to the control input u_k in between trials, using the procedure described in Chapter 3.

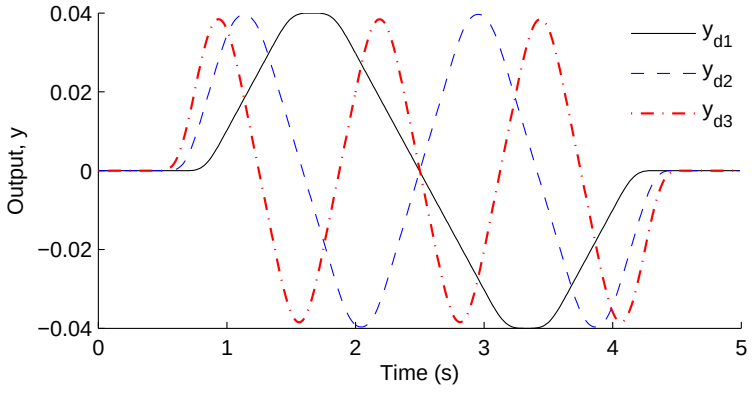

FIGURE 5.4: Set of three stored references for experience-based input selection.

The stored references, together with their associated converged inputs, are used to generate an initial input to the tracking of a new reference (shown in Figure. 5.5 b) using (5.56) and (5.57). To show the improvement due to using a greater number of stored references, the optimisation has been performed using $Q = 1$ and $Q = 3$ sets of previous data within U^*. Figures 5.5 a), b) and c) show the input, output and error respectively

on the second trial of gradient-based ILC, using these values.

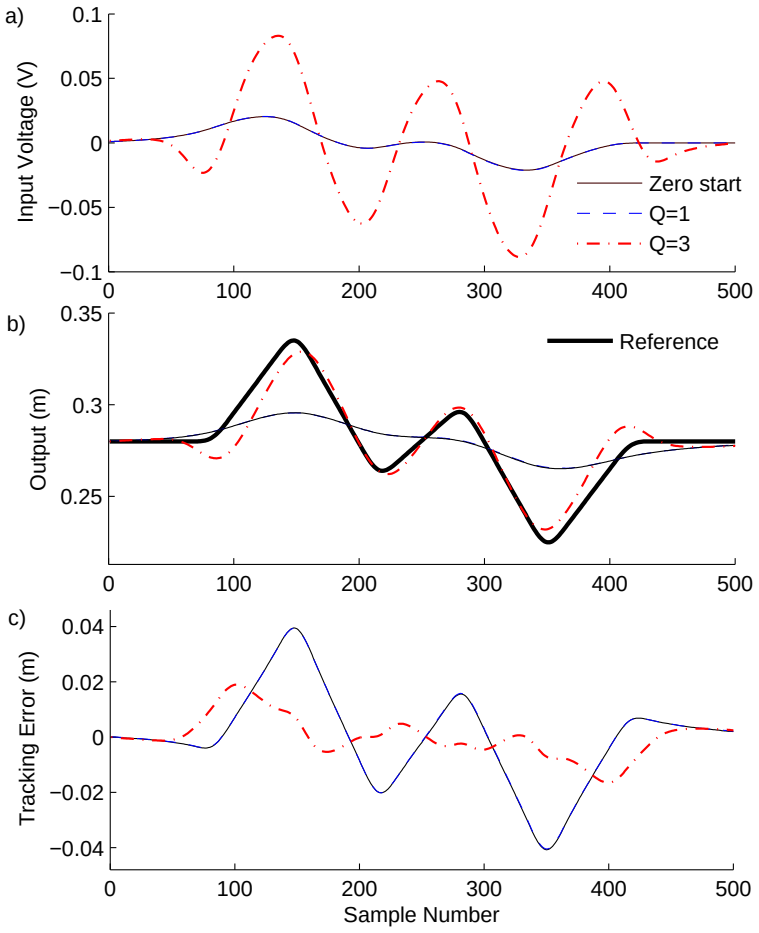

FIGURE 5.5: Effect of experience-based initial input selection on X-axis a) input, b) output, and c) error during second trial.

Using $Q = 1$, there is virtually no distinguishable difference between these signals compared with using the zero vector, since y_{d1} does not alone comprise a significant component of the new reference. However, when all three stored references are used ($Q = 3$), their linear combination can far better approximate the reference, and leads to a lower mean squared error (and optimal solution $\|e_0\|^2$), as shown in Figure 5.6.

5.3.2.1 Experimental Verification for the Time-Domain Shifted Previous Reference Trajectories Initial Input Construction

To enhance the use of shifted data, the same reference set is again used together with shifted samples of $C = 20$ which gives a shift of $20/100 = 0.02s$ using a sampling frequency of $100Hz$. The initial input is constructed using (5.67) and (5.68) with the

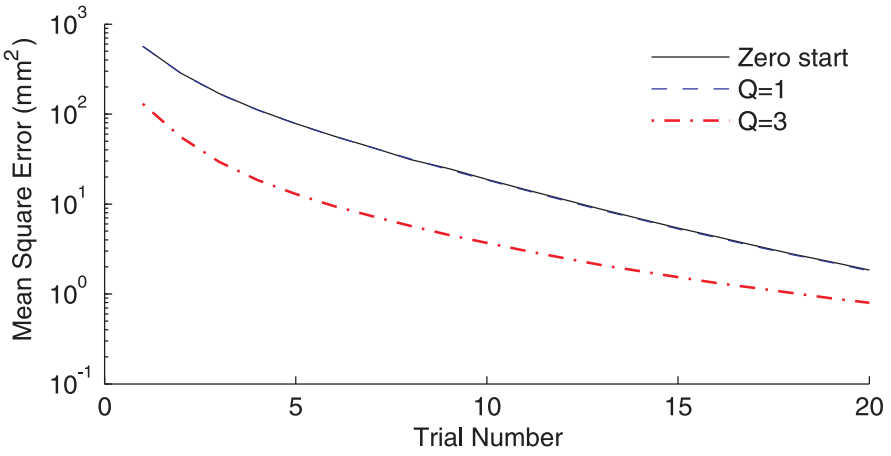

FIGURE 5.6: X-axis error evolution using experience-based initial input selection.

previous stored data contained in the matrix U^* given by (5.58). Test conditions are exactly the same as previously, with identical PID values used in the series configuration of PID and ILC shown in Figure 3.7. The gradient update of (5.48) is again used with a value of $\beta = 0.5$. As previously, the filter (3.6) has been applied to the control input u_k in between trials, in the manner described in Chapter 3.

Figure 5.7 shows the results obtained from applying the shifting technique compared to non-shifted approach as well as the locally weighted learning approach described in Arif et al. (2001) which requires a plant model. The k-nearest neighbour value of $k = 3$ applied to the data obtained in previous experiments produces the best results, together with the use of a Gaussian kernel weighting function. However, it is clear from the results here that the performance is inferior to the shifted references method developed in this chapter. The locally weighted learning input also contains high frequency components which adversely affect the convergence rate in later trials.

Figures 5.8 a), b) and c) show the input, output and error respectively on the second trial of gradient-based ILC (adjoint algorithm). Results using $Q = 1$ have been obtained, but there is virtually no distinguishable difference between these signals compared with using the zero vector, since y_{d1} does not alone comprise a significant component of the new reference. As can be seen from the results, when all three stored references are used ($Q = 3$), their linear combination is a much better approximation of the reference, and leads to a lower mean squared error (and optimal solution $\|e_0\|^2$).

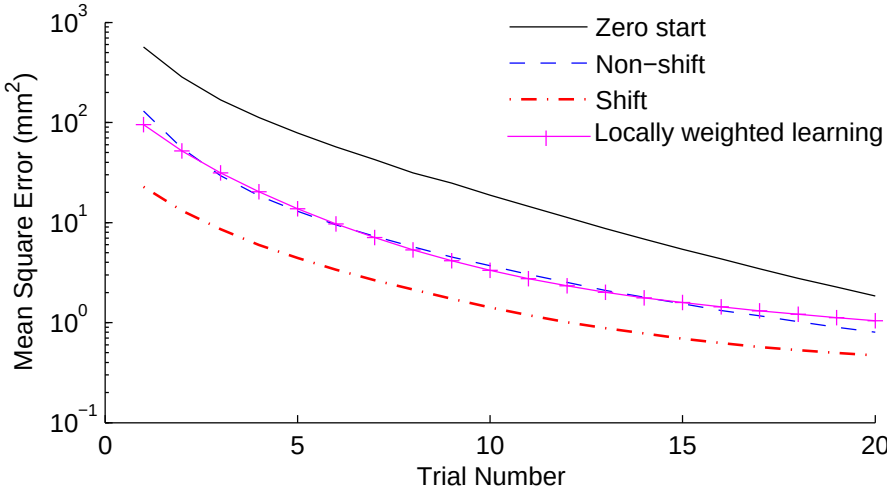

FIGURE 5.7: X-axis error evolution using shifted previous references (shift = 20/100 = 0.02s).

5.4 Hybrid Model and Experience-based Approach

The use of previous data in many cases leads to superior results compared to the model-based approach of Section 5.2 since it depends on the linearity of a plant and not on an assumed plant model. Unfortunately this approach is inherently limited by the available set of previous trajectories. In this section, a model-based approach will be applied to solve this problem, whilst maximising the use of the previous data that is available.

Remark 5.6. *As previously, it is assumed that the previous data set is at least as long as the new reference. If this is not the case, a choice of methods can be applied to extend their length. These include the following.*

- *The end values of the reference, output and input may be held to provide the necessary length extension, or zeros may be inserted at the beginning.*
- *The end value of the reference may be held, and the steady-state inverse technique applied to generate a suitable input vector. This input then provides the missing data needed to extend the converged inputs. Note that this effectively requires that the reference store is of sufficient length for the transient response to decay to a negligible value.*
- *Insert additional copies of the reference, input and output at the end of each vector or pad the beginning of each with zeros.*

Note that these approaches require the response of the plant to settle at the termination

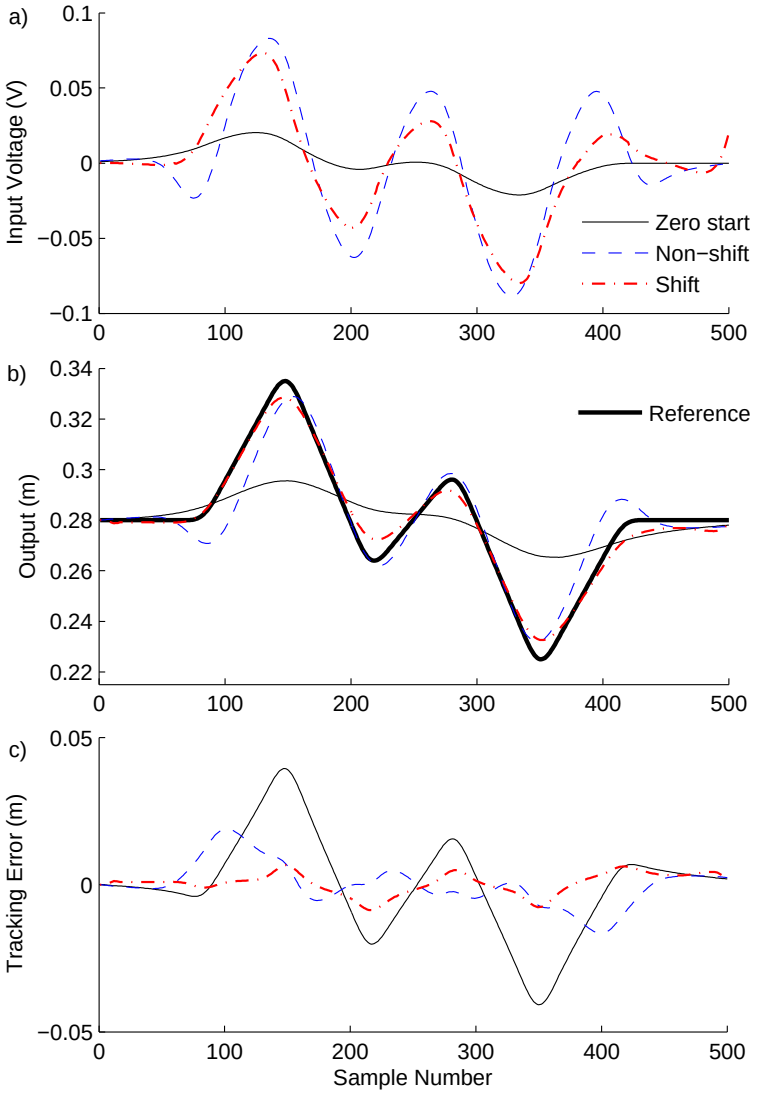

FIGURE 5.8: Effect of shifted experience-based initial input selection on X-axis a) input, b) output, and c) error during second trial.

of the reference.

Having produced a set of previous data of the requisite length, the model-based approach is then applied in order to provide a and u_0^* (using (5.56), (5.57) or alternatively (5.66), (5.67)). The approach now is to then find an additional input, $\overline{u}$, to compensate for any lack of useful experimental data. To achieve this, the methodology of experience-based input construction is repeated, now using data which includes the effects of previous

experience. Proceeding accordingly, (5.55) becomes

$$\begin{aligned}\min_{\overline{u}} \|e_0\|^2 &= \min_{\overline{u}} \|y_d - \overline{Y}^* a - G\overline{u}\|^2 \\ &= \min_{\overline{u}} \sum_{i=0}^{N-1} |\hat{y}_{d,i} - \hat{\overline{Y}}_i^* a - \hat{g}_{0,i}\hat{m}_i\hat{\overline{u}}_i|^2 \end{aligned} \tag{5.70}$$

Here $\hat{\overline{Y}}^*$ contains the column-wise DFT of $\overline{Y}^*$ and hence

$$\hat{\overline{Y}}^* = \begin{bmatrix} \hat{\overline{Y}}_0^* \\ \hat{\overline{Y}}_1^* \\ \vdots \\ \hat{\overline{Y}}_{N-1}^* \end{bmatrix} = \begin{bmatrix} \hat{\overline{Y}}_{1,0}^* & \hat{\overline{Y}}_{2,0}^* & \cdots & \hat{\overline{Y}}_{P,0}^* \\ \hat{\overline{Y}}_{1,1}^* & \hat{\overline{Y}}_{2,1}^* & \cdots & \hat{\overline{Y}}_{P,1}^* \\ \vdots & \vdots & \vdots & \vdots \\ \hat{\overline{Y}}_{1,N-1}^* & \hat{\overline{Y}}_{2,N-1}^* & \cdots & \hat{\overline{Y}}_{P,N-1}^* \end{bmatrix} \tag{5.71}$$

where $P = Q \times \lfloor N/C \rfloor$. Therefore, following the approach taken in model-based input construction, only the first M frequencies will be updated, using

$$\hat{\overline{u}}_i = \begin{cases} \frac{\hat{y}_{d,i} - \hat{\overline{Y}}_i^* a}{\hat{g}_{0,i}} & i = 0, 1, \cdots, M-1 \\ 0 & i = M, M+1, \cdots, N-1 \end{cases} \tag{5.72}$$

The resulting solution obtained through application of IFFT, is added to the initial input generated using previous data.

$$\overline{u}_0^* = u_0^* + \overline{u} \tag{5.73}$$

The addition of the model-based input provides a reduction in error since the resulting difference in error norm is given by

$$\begin{aligned}\|y_d - \overline{Y}^* a - G\overline{u}\|^2 \;-\; \|\hat{y}_d - \overline{Y}^* a\|^2 &= \sum_{i=0}^{M-1} |(\hat{y}_{d,i} - \hat{\overline{Y}}_i^* a)(1 - \hat{m}_i)|^2 \\ &+ \sum_{i=M}^{N-1} |\hat{y}_{d,i} - \hat{\overline{Y}}_i^* a|^2 \\ &= \sum_{i=0}^{M-1} |\hat{y}_{d,i} - \hat{\overline{Y}}_i^* a|^2 (|1 - \hat{m}_i|^2 - 1) < 0 \end{aligned} \tag{5.74}$$

5.4.1 Experimental Verification for the Hybrid Model Experienced-Based Approach

The same previous trajectory set as in Section 5.3 is used, together with the initial input (5.73). Here the model-based input component has been calculated using (5.72) with frequency cut-offs of $M = 1, 2, 3$. The stored trajectory component u_0^* is calculated as in Section 5.3, using (5.56) and (5.57). Test conditions are exactly the same as previously, with identical PID values used in the series configuration of PID and ILC shown in Figure 3.7. The gradient update of (5.48) is again used with a value of $\beta = 0.5$. As previously, the filter (3.6) has been applied to the control input u_k in between trials, in the manner described in Chapter 3.

Results are shown for the model experienced-based combined approach in Figure 5.9. The advantage of using a higher frequency cut-off is clear, as is the improvement gained from a greater number of stored previous reference trajectories.

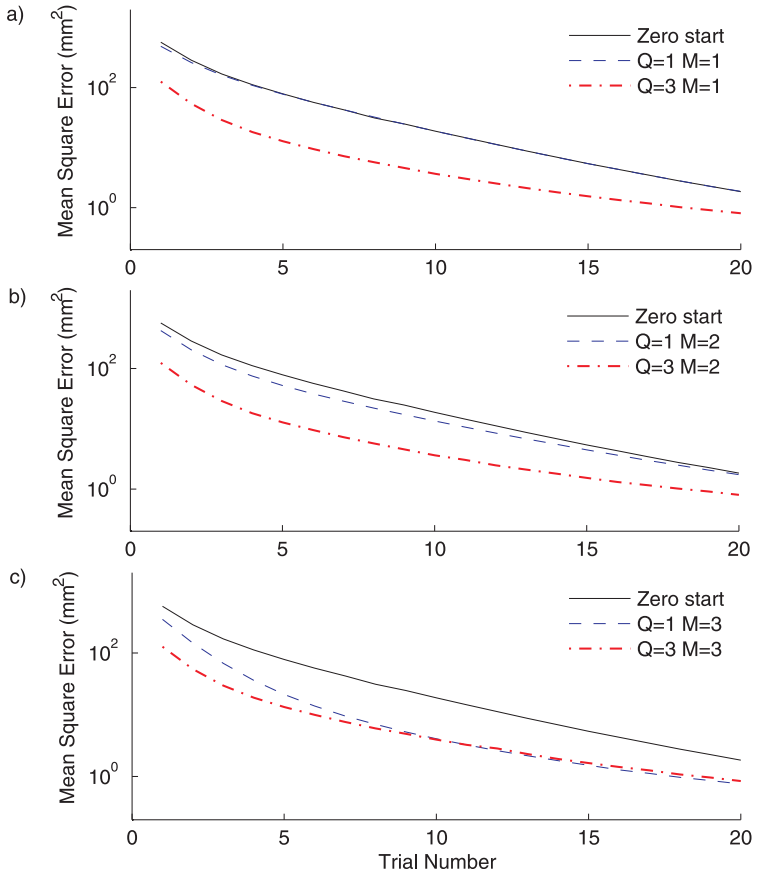

FIGURE 5.9: Hybrid approach mean squared error with $Q = 1, 3$ for a) $M = 1$, b) $M = 2$, and c) $M = 3$.

5.5 Frequency-domain Experience-based Input Construction

The experience-based input generated in Section 5.3 relies only on the assumption of system linearity. However it is likely that some plants include non-linearities which will decrease the subsequent performance. To address this issue, this section develops a method which allows the optimal selection of previous experimental data to be weighted in the frequency-domain. This can therefore be used to focus on those frequencies which most closely satisfy the property of linearity.

The optimisation of (5.55) (or alternatively (5.65) in the shifted case) is now conducted in the frequency-domain to produce

$$\min_a \|e_0\|^2 = \min_a \|y_d - \overline{Y}^* a\|^2 = \min_a \sum_{i=0}^{N-1} \left|\hat{y}_{d,i} - \hat{\overline{Y}}_i^* a\right|^2 \tag{5.75}$$

Unlike the case treated in Section 5.2, this cannot be solved in a component-wise fashion, but, by separating real and imaginary components, can be rewritten as

$$\begin{aligned}\min_a \sum_{i=0}^{N-1} \hat{w}_i \Big(&\Big(\mathrm{Re}\{\hat{y}_{d,i}\} - a_1 \mathrm{Re}\{\hat{\overline{Y}}_{1,i}^*\} - a_2 \mathrm{Re}\{\hat{\overline{Y}}_{2,i}^*\} \cdots - a_P \mathrm{Re}\{\hat{\overline{Y}}_{P,i}^*\}\Big)^2 \\ &+ \Big(\mathrm{Im}\{\hat{y}_{d,i}\} - a_1 \mathrm{Im}\{\hat{\overline{Y}}_{1,i}^*\} - a_2 \mathrm{Im}\{\hat{\overline{Y}}_{2,i}^*\} \cdots - a_P \mathrm{Im}\{\hat{\overline{Y}}_{P,i}^*\}\Big)^2 \Big)\end{aligned} \tag{5.76}$$

Here the real-valued weighting $\hat{w}_i \geq 0$ has been introduced to place emphasis on different frequencies. This expression can then be written as

$$\min_a \left(\left\| \hat{W} \left(\mathrm{Re}\{\hat{\mathrm{y}}_\mathrm{d}\} - \mathrm{Re}\{\hat{\overline{\mathrm{Y}}}^*\}\mathrm{a} \right) \right\|^2 + \left\| \hat{W} \left(\mathrm{Im}\{\hat{\mathrm{y}}_\mathrm{d}\} - \mathrm{Im}\{\hat{\overline{\mathrm{Y}}}^*\}\mathrm{a} \right) \right\|^2 \right) \tag{5.77}$$

where $\hat{W} = \mathrm{diag}\left\{\sqrt{\hat{w}_0}, \sqrt{\hat{w}_1}, \ldots \sqrt{\hat{w}_{N-1}}\right\}$. The LMS solution to (5.77) is

$$\begin{aligned}a = &\left(\mathrm{Re}\{\hat{\overline{\mathrm{Y}}}^*\}_\mathrm{W}^\mathrm{T} \mathrm{Re}\{\hat{\overline{\mathrm{Y}}}^*\}_\mathrm{W} + \mathrm{Im}\{\hat{\overline{\mathrm{Y}}}^*\}_\mathrm{W}^\mathrm{T} \mathrm{Im}\{\hat{\overline{\mathrm{Y}}}^*\}_\mathrm{W}\right)^{-1} \\ &\left(\mathrm{Re}\{\hat{\overline{\mathrm{Y}}}^*\}_\mathrm{W}^\mathrm{T} \mathrm{Re}\{\hat{\mathrm{y}}_\mathrm{d}\}_\mathrm{W} + \mathrm{Im}\{\hat{\overline{\mathrm{Y}}}^*\}_\mathrm{W}^\mathrm{T} \mathrm{Im}\{\hat{\mathrm{y}}_\mathrm{d}\}_\mathrm{W}\right)\end{aligned} \tag{5.78}$$

where

$$\begin{aligned}\mathrm{Re}\{\hat{\overline{\mathrm{Y}}}^*\}_\mathrm{W} &= \hat{\mathrm{W}}\mathrm{Re}\{\hat{\overline{\mathrm{Y}}}^*\}, \qquad &\mathrm{Im}\{\hat{\overline{\mathrm{Y}}}^*\}_\mathrm{W} &= \hat{\mathrm{W}}\mathrm{Im}\{\hat{\overline{\mathrm{Y}}}^*\} \\ \mathrm{Re}\{\hat{\mathrm{y}}_\mathrm{d}\}_\mathrm{W} &= \hat{\mathrm{W}}\mathrm{Re}\{\hat{\mathrm{y}}_\mathrm{d}\}, \qquad &\mathrm{Im}\{\hat{\mathrm{y}}_\mathrm{d}\}_\mathrm{W} &= \hat{\mathrm{W}}\mathrm{Im}\{\hat{\mathrm{y}}_\mathrm{d}\}\end{aligned} \tag{5.79}$$

which is then used to produce the initial input via (5.67). Results are now provided in which the frequency-wise weight is chosen to be an ideal cliff filter with cut-off M, and

hence

$$\hat{w}_i = \begin{cases} 1 & i = 0, 1, \ldots M-1 \\ 0 & i = M, M+1, \ldots N-1 \end{cases} \tag{5.80}$$

This choice of weighting combines with the learning filter that is recommended in the discussion within Section 5.3, to maximise the amount of useful experience contained in the initial input (i.e. components which are not then subsequently removed by an ILC filter with cut-off M).

5.5.1 Experimental Verification for the Frequency-Domain Experience-Based Input Construction

Figure 5.10 shows the performance of the frequency-based technique using the stored reference set used in Section 5.3. Two values of cut-off frequency have been used ($M = 3$, $M = 5$) to illustrate how this approach enables control to be exerted over the frequency content of the previous trajectory data. These are applied in the weight (5.80) which is used in (5.78) to produce the matrix a, which yields the initial input u_0^* via (5.57). Here the matrix U^* contains the previous stored data. Test conditions are exactly the same as previously, with identical PID values used in the series configuration of PID and ILC shown in Figure 3.7. The gradient update of (5.48) is again used with a value of $\beta = 0.5$. As previously, the filter (3.6) has been applied to the control input u_k in between trials, in the manner described in Chapter 3.

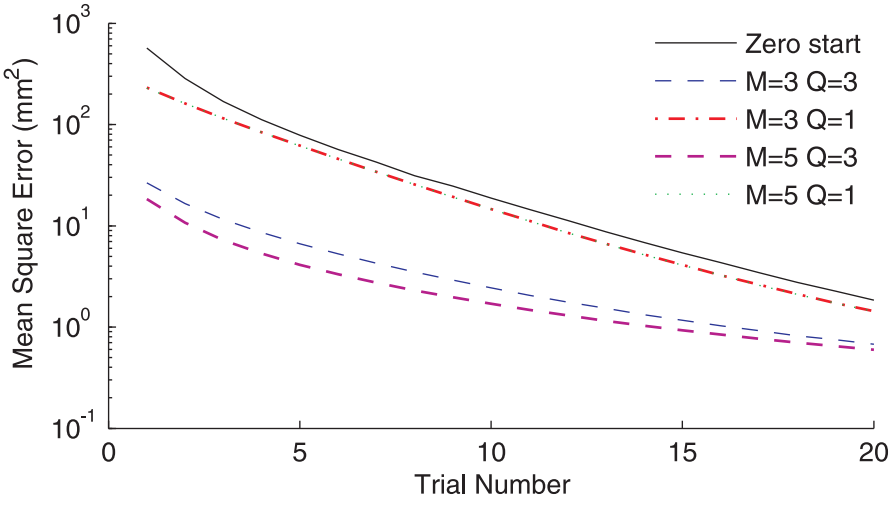

FIGURE 5.10: Composite frequency-domain approach with $Q = 1, 2, 3$ and $M = 3, 5$.

The corresponding input, output and error signals for the second trial of the gradient-based ILC algorithm described in Chapter 2, are shown in Figure 5.11. It is clear that a high frequency cut-off succeeds in reducing the initial tracking error, although this must be balanced against additional wear on the plant actuators.

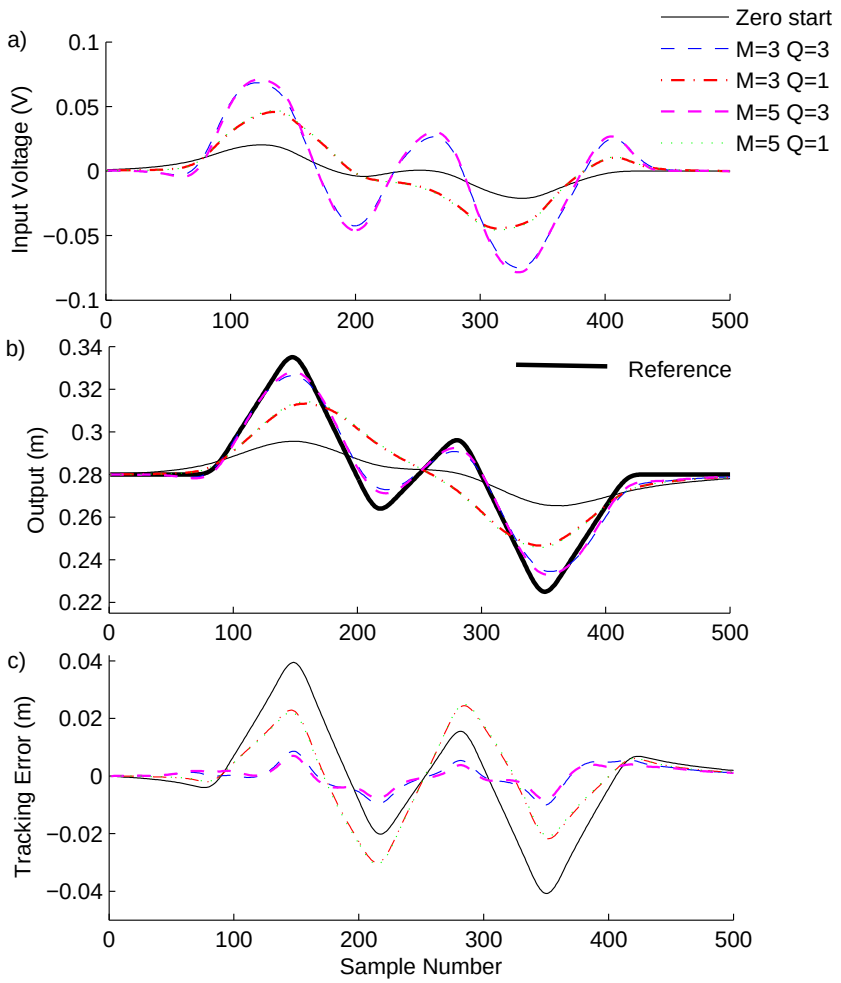

FIGURE 5.11: Composite frequency-domain approach with $Q = 1, 2, 3$ and $M = 3, 5$.

Note that a lack of experimental sets is still a limiting factor as it was in Section 5.3. Therefore it is also advisable to employ the composite approach of Section 5.4 with the method introduced in this section. This involves simply using the resulting a in the optimisation given by (5.70).

In conclusion, application of optimisation techniques to initial input problem both in frequency-domain and time-domain have led to solutions that generate an initial input that reduces the error in the early trials compared to zero start. Performance enhancement had been confirmed through practical evaluation on the gantry robot.

5.6 Summary of Chapter

The error signal in ILC is highly dependent on the initial input. Optimal techniques have been explicitly used in this chapter to build up an initial control demand based on two different aspects. The first uses the presence of the model description to construct the control input demand, while the second relies on previous available data and the linearity of system and not on a plant description. In each case, the construction issue is investigated through the generation of an optimal cost function that minimizes the initial error signal in ILC. The former approach is conducted in the frequency-domain and the latter in the time-domain.

The initial input constructed in each case is compared to a zero initial input start. The error improvement is very clear in the results obtained from applying the developed initial input construction techniques on the gantry robot X-axis. The results obtained show significantly improved reference tracking in less trials than the start with zero initial input for each case. The error reduces faster in fewer trials as the number of frequency components considered increases in the model-based approach, and the number of stored references increases in the stored trajectory approach.
A hybrid approach between the frequency-domain and time-domain approaches is developed to maximize the use of previous information whilst minimising the initial error signal in ILC.

Chapter 6

Conclusions and Future Work

This thesis has made substantial novel contributions to ILC and RC in two major areas, which are the duality between these two control design methods and the choice of the initial input. In both cases the analysis is supported by experimental verification on a gantry robot which has been extensively used to benchmark many ILC and RC algorithms. The contributions are summarised in turn next.

Due to the internal model principle, ILC and RC duplicate a model of the disturbance in the feedback loop, and previous work has shown that RC and ILC differ in the location of the internal model. In particular, in RC the internal model is located at the system output and in ILC it is located at the system input. The ability to treat RC and ILC in the same framework is highly appealing since controllers found to operate well in one area can, in principle, be synthesized for application to the other. In previous work, this structure was used to derive dual ILC and RC schemes which incorporate separate past-error and current-error feedback control loops. In this thesis, the necessity for current-error feedback is removed, and dual ILC and RC servomechanism controllers are formulated in which state-feedback is used to solve the stabilization, and hence tracking, problem. To provide a comparison between feedback architectures, an output injection implementation was then developed for ILC. Stability conditions are given and the new controllers are shown to extend the set of underlying plants which may be controlled in the duality framework.

In operation, the performance achieved using ILC depends on the choice of input employed over the initial trial. This dictates the initial error, and, in conjunction with the ILC scheme used, the error incurred over future trials. Careful selection of an initial input is especially important for applications which cannot tolerate a large error, such as robots with physical movement constraints. It is also of great importance for applications in which the maximum number of trials that can be performed is limited. One

example exists within stroke rehabilitation where ILC has been used to produce accurate movement control of patients' arms via electrical stimulation. During clinical treatment sessions, only six trials were performed with any given reference trajectory in accordance with clinical need, and accurate tracking was vital to promote effectiveness of treatment.

The issue of how the initial input may be selected to best effect is addressed in this thesis, and it is assumed that previous experimental input and output data is available from which to construct an input for an arbitrary new trajectory. New methods for generating the initial input signal for ILC have been developed and experimentally evaluated using a gantry robot facility. These combine both experience and model-based components in order to maximise tracking accuracy over subsequent trials, whilst maintaining close control over possible performance deterioration due to uncertainty in the plant model or the presence of additive noise on the input. Substantial improvements are shown to exist compared with the use of more arbitrarily chosen initial inputs. The error associated with the model-based component of the initial input depends on the time taken for the plant impulse response to approximately equal zero.

Future Work

For the duality approach and the prediction algorithm formulation there are several directions for future work:

For the duality framework:

- Investigate the effect of cost function weighting parameters on error convergence for the duality framework, since no such information is currently available.
- Allowing the feedback state, $\hat{x}_k$, to be omitted so that a simple structure ILC law of the form $u_{k+1} = u_k + Le_k$ is effectively designed (attempt to set $K = 0$ and find a solution to this case; partial state-feedback).
- Experimental verification for the MIMO case, where no results currently exist.

For the prediction algorithm, the following areas should be developed:

- Modifications for slow and non-minimum phase plants should be developed to allow the input to be applied a significant time before the start of the trajectory in order to avoid an initial impulsive action. This will involve using a reference shift method (such as that described in (Cai et al. (2008b))), and the extension of the region in which the model-based steady-state inverse technique is applied.

- Investigating the number of required frequency components needed to construct the initial input without adding large spikes in the steady-state inverse case.
- Developing a new ILC technique for dealing with ill-conditioned systems based on Singular Value Decomposition (SVD).

References

H-S. Ahn, Y. Q. Chen, and K. L. Moore. Iterative learning control: Brief survey and categorization. *Systems, Man, and Cybernetics, Part C: Applications and Reviews, IEEE Transactions on*, 37(6):1099–1121, 2007.

H. Akagi. New trends in active filters for power conditioning. *IEEE Transactions on Industry Applications*, 32(6):1312–1322, 2002.

J. D. Álvarez, R. Costa-Castelló, M. Berenguel, and L. J. Yebra. A repetitive control scheme for distributed solar collector field. *International Journal of Control*, 83(5): 970–982, 2010.

J. D. Alvarez, L. J. Yebra, and M. Berenguel. Repetitive control of tubular heat exchangers. *Journal of Process Control*, 17(9):689–701, 2007.

N. Amann, D. H. Owens, and E. Rogers. Iterative learning control for discrete-time systems with exponential rate of convergence. *IEE Proceedings of Control Theory and Applications*, 143(2):217–224, 1996a.

N. Amann, D. H. Owens, and E. Rogers. Iterative learning control using optimal feedback and feedforward actions. *International Journal of Control*, 65(2):277–293, 1996b.

N. Amann, D.H. Owens, and E. Rogers. Predictive optimal iterative learning control. *International Journal of Control*, 69(2):203–226, 1998.

M. Arif, T. Ishihara, and H. Inooka. Incorporation of experience in iterative learning controllers using locally weighted learning. *Automatica*, 37(6):881 – 888, 2001.

M. Arif, T. Ishihara, and H. Inooka. Experience-based iterative learning controllers for robotic systems. *Journal of Intelligent and Robotics Systems.*, 35(4):381–396, 2002.

S. Arimoto, S. Kawamura, and F. Miyazaki. Bettering operation of dynamic systems by learning: A new control theory for servomechanism or mechatronics systems. *23rd IEEE Conference on Decision and Control, Las Vegas, Nevada, USA*, 23:1064–1069, December 1984a.

S. Arimoto, S. Kawamura, and F. Miyazaki. Bettering operation of robots by learning. *Journal of Robotic Systems*, 1:123–140, 1984b.

K. Barton, J. Van de Wijdeven, A. Alleyne, O. Bosgra, and M. Steinbuch. Norm optimal cross-coupled iterative learning control. In *47th IEEE Conference on Decision and Control, Cancun, Mexico.*, pages 3020–3025. IEEE, 2008.

K. L. Barton and A. G. Alleyne. A cross-coupled iterative learning control design for precision motion control. *IEEE Transactions on Control Systems Technology*, 16(6): 1218–1231, 2008.

K. L. Barton, D. J. Hoelzle, A. G. Alleyne, and A. J. W. Johnson. Cross-coupled iterative learning control of systems with dissimilar dynamics: design and implementation. *International Journal of Control*, 1:11, 2010.

M. Berenguel and E. F. Camacho. Frequency-based adaptive control of systems with antiresonance modes. *Control Engineering Practice*, 4(5):677–684, 1996.

C. A. Bode, B. S. Ko, and T. F. Edgar. Run-to-run control and performance monitoring of overlay in semiconductor manufacturing. *Control Engineering Practice*, 12(7):893–900, 2004.

D. A. Bristow, M. Tharayil, and A. G. Alleyne. A survey of iterative learning control. *Control Systems Magazine, IEEE*, 26(3):96–114, June 2006.

S. Buso, L. Malesani, and P. Mattavelli. Comparison of current control techniques for active filter applications. *IEEE Transactions on Industrial Electronics*, 45(5):722–729, 2002.

Z. Cai. *Iterative learning control: Algorithm development and experimental benchmarking.* PhD thesis, School of Electronics and Computer Science, University of Southampton, 2009.

Z. Cai, C. Freeman, P. Lewin, and E. Rogers. Experimental comparison of stochastic iterative learning control algorithms. In *American Control Conference, Seattle, Washington, USA*, pages 4548–4553, June 2008a.

Z. Cai, C. T. Freeman, P. L. Lewin, and E. Rogers. Iterative learning control for a non-minimum phase plant based on a reference shift algorithm. *Control Engineering Practice*, 16(6):633–643, 2008b.

E. F. Camacho, M. Berenguel, and F. R. Rubio. *Advanced control of solar plants.* Springer Berlin, 1997.

E. F. Camacho, F. R. Rubio, M. Berenguel, and L. Valenzuela. A survey on control schemes for distributed solar collector fields. part I: Modeling and basic control approaches. *Solar Energy*, 81(10):1240–1251, 2007a.

E. F. Camacho, F. R. Rubio, M. Berenguel, and L. Valenzuela. A survey on control schemes for distributed solar collector fields. Part II: Advanced control approaches. *Solar Energy*, 81(10):1252–1272, 2007b.

Z. Cao and G. F. Ledwich. Adaptive repetitive control to track variable periodic signals with fixed sampling rate. *IEEE/ASME Transactions on Mechatronics*, 7(3):378–384, 2002.

H. I. Cha, S. S. Kim, M. G. Kang, and Y. H. Chung. Real-time digital control of PWM inverter with PI compensator UPS. In *Proceedings of the IEEE Industry Applications Society Annual Meeting*, pages 1124–1128, 1990.

Y. Q. Chen and C. Wen. Iterative Learning Control: Convergence, Robustness and Applications, vol. LNCIS-248 of. *Lecture Notes series on Control and Information Science*, 1999.

Y-Q. Chen, J-X. Xu, and T. H. Lee. Current iteration tracking error assisted iterative learning control of uncertain nonlinear discrete-time systems. In *35th IEEE Conference on Decision and Control, Kobe, Japan.*, 1996.

K. K. Chew and M. Tomizuka. Digital control of repetitive errors in disk drive systems. *IEEE Control Systems Magazine*, 10(1):16 –20, January 1990.

C. J. Chien and A. Tayebi. Further results on adaptive iterative learning control of robot manipulators. *Automatica*, 44(3):830–837, 2008.

B. Chu, Z. Cai, D. Owens, E. Rogers, C. Freeman, and P. Lewin. Experimental verification of accelerated norm-optimal iterative learning control. In *UKACC International Conference on Control, Coventry, UK.*, 2010 (CD ROM).

W. C. Cohen and E. F. Johnson. Dynamic characteristics of double-pipe heat exchangers. *Industrial & Engineering Chemistry*, 48(6):1031–1034, 1956.

D. De Roover and O. H. Bosgra. Dualization of the internal model principle in compensator and observer theory. *Selected Topincs in Identification, Modelling and Control*, 9:79–88, 1996.

D. De Roover and O. H. Bosgra. Dualization of the internal model principle in compensator and observer theory with application to repetitive and learning control. In *Proceedings of the American Control Conference, Albuquerque, New Mexico, USA*, volume 6, pages 3902 – 3906, 1997.

D. De Roover, O. H. Bosgra, and M. Steinbuch. Internal model-based design of repetitive and iterative learning controllers for linear multivariable systems. *International Journal of Control*, 73(10):914–929, 2000.

C. A. Deoser and M. Vidyasagar. *Feedback Systems:Input-Output Properties.* Acadimic Press, New York, 1975.

B. G. Dijkstra and O. H. Bosgra. Extrapolation of optimal lifted system ILC solution, with application to a waferstage. In *Proceedings of the American Control Conference, Anchorage, Alaska, USA*, volume 4, pages 2595–2600. IEEE, 2002.

H. Elci, R. W. Longman, M. Q. Phan, J. N. Juang, and R. Ugoletti. Simple learning control made practical by zero-phase filtering: Applications to robotics. *IEEE Transactions on Circuits and Systems I: Fundamental Theory and Applications*, 49(6): 753–767, 2002.

E. Fornasini and G. Marchesini. Doubly-indexed dynamical systems: State-space models and structural properties. *Theory of Computing Systems*, 12(1):pp 59–72, 1978.

B. A. Francis and W. M. Wonham. The internal model principle for linear multivariable regulators. *Applied Mathematics and Optimization*, 2:170–194, 1975.

B. A. Francis and W. M. Wonham. The internal model principle of control theory. *Automatica*, 12(5):457–465, 1976.

C. Freeman, A-M Hughes, J. Burridge, P. Chappell, P. Lewin, and E. Rogers. Iterative learning control of FES applied to the upper extremity for rehabilitation. *Control Engineering Practice*, 17(3):368–381, 2009a.

C. Freeman, P. Lewin, E. Rogers, D. Owens, and J. Hatonen. Discrete fourier transform based iterative learning control design for linear lants with experimental verification. *ASME Journal of Dynamic Systems, Measurement and Control*, 2009b.

C. Freeman, P. Lewin, E. Rogers, and J. Ratcliffe. Iterative learning control for synchronisation of multi-axis automation processes. In *23rd IAR Workshop on Advanced Control and Diagnosis, Coventry University, UK*, pages 309–314, November 2008a.

C. T. Freeman, A. M. Hughes, J. H. Burridge, P. H. Chappell, P. L. Lewin, and E. Rogers. A robotic workstation for stroke rehabilitation of the upper extremity using FES. *Medical Engineering & Physics*, 31(3):364–373, 2009c.

C. T. Freeman, P. L. Lewin, E. Rogers, D. H. Owens, and J. Hatonen. An optimality-based repetitive control algorithm for discrete-time ssystems. *IEEE Transactions on Circuits and Systems I: Regular Papers*, 55(1):412–423, February 2008b.

C. T. Freeman, P. L. Lewin, E. Rogers, D. H. Owens, and J. J. Hatonen. An optimality based repetitive control algorithm for discrete-time systems. *IEEE Transactions on Circuits and Systems I: Fundamental Theory and Applications*, 55(1):412–423, February 2008c.

C.T. Freeman, A. M. Hughes, J. H. Burridge, P. H. Chappell, P. L. Lewin, and E. Rogers. A model of the upper extremity using FES for stroke rehabilitation. *Journal of Biomechanical Engineering*, 131:031011, 2009d.

M. French and E. Rogers. Non-linear iterative learning by an adaptive Lyapunov technique. *International Journal of Control*, 73(10):840–850, 2000.

J. A. Frueh and M. Q. Phan. Linear quadratic optimal learning control (LQL). *International Journal of Control*, 73(10):832–839, 2000.

S. Fukuda and R. Imamura. Application of a sinusoidal internal model to current control of three phase utility-interface-converters. *IEEE Transactions on Industrial Electronics*, 52:420–426, 2005.

K. Furuta and M. Yamakita. The design of a learning control system for multivariable systems. In *Proceedings of the IEEE International Symposium on Intelligent Control, Philadelphia, Pennsylvania, USA*, pages 371–376, 1987.

T. C. C. George and M. Tomizuka. Contouring control of machine tool feed drive systems: A task coordinate frame approach. *IEEE Transactions on Control Systems Technology*, 9(1):130–139, 2001.

R. Griñó, R. Cardoner, R. Costa-Castelló, and E. Fossas. Digital repetitive control of a three-phase four-wire shunt active filter. *IEEE Transactions on Industrial Electronics*, 54(3):1495–1503, 2007.

R. Grino, R. Costa-Castelló, and E. Fossas. Digital control of a single-phase shunt active filter. In *IEEE 34th Annual Power Electronics Specialist Conference, Acapuloco, Mexico*, volume 3, pages 1038–1042. IEEE, 2003.

S. Gunnarsson and M. Norrlof. A frequency domain analysis of a second order iterative learning control algorithm. In *Proceedings of the Conference on Decision and Control, Phoenix, Arizona, USA*, pages 1587–1592, 1999.

S. Gunnarsson, M. Norrlof, E. Rahic, and M. Ozbek. On the use of accelerometers in iterative learning control of a flexible robot arm. *International Journal of Control*, 80 (3):363–373, 2007.

K. Hamamoto and T. Sugie. Iterative learning control for robot manipulators using the finite dimensional input subspace. *IEEE Transactions on Robotics and Automation*, 18(4):632–635, 2002.

T. Haneyoshi, A. Kawamura, and R. G. Hoft. Waveform compensation of PWM inverter with cyclic fluctuating loads. In *Annual IEEE Industrial application Society Conference, PESC'86 Record.*, volume 24, pages 744–751. IEEE, 1986.

S. Hara, Y. Yamamoto, T. Omata, and M. Nakano. Repetitive control system: A new type servo system for periodic exogenous signals. *IEEE Transactions on Automatic Control*, 33(7):659–668, July 1988.

T. J. Harte, J. Hatonen, and D. H. Owens. Discrete-time inverse model-based iterative learning control: Stability, monotonicity and robustness. *International Journal of Control*, 78(8):577–586, 2005.

J. J. Hatonen, S. Daley, and D. H. Owens. Robust monotone gradient-based discrete-time iterative learning control. *International Journal of Robust Nonlinear Control*, 19: 634–661, 2009.

J. J. Hatonen, C. T. Freeman, D. H. Owens, P. L. Lewin, and E. Rogers. Robustness analysis of a gradient-based repetitive control algorithm. In *IEEE Conference on Decision and Control, The Bahamas*, pages 1301–1306. IEEE, December 2004.

J. J. Hatonen, T. J. Harte, D. H. Owens, J. D. Ratcliffe, P. L. Lewin, and E. Rogers. A new robust iterative learning control algorithm for application on a gantry robot. In *Proceedings of the IEEE Conference on Emerging Technologies and Factory Automation, Lisbon, Portugal*, volume 2, pages 305–312, September 2003.

S. Hattori, M. Ishida, and T. Hori. Suppression control method for torque vibration of brushless dc motor utilizing repetitive control with fourier transform. In *Proceedings of the 6th International Workshop on Advanced Motion Control, Nagoya, Japan*, pages 427 –432, April 2000.

M. F. Heertjes and René M.J.G. Van de Molengraft. Set-point variation in learning schemes with applications to wafer scanners. *Control Engineering Practice*, 17(3):345 – 356, 2009.

G. Hillerstrom. Adaptive suppression of vibrations-a repetitive control approach. *IEEE Transactions on Control Systems Technology*, 4(1):72–78, 1996.

G. Hillerstrom and J. Sternby. Application of repetitive control to a peristaltic pump. In *American Control Conference, San Francisco, California, USA*, pages 136–141. IEEE, 1993.

L. Hladowski, Z. Cai, K. Galkowski, E. Rogers, C. Freeman, P. Lewin, and W. Paszke. Repetitive process based iterative learning control designed by LMIs and experimentally verified on a gantry robot. In *American Control Conference, St. Louis, Missouri, USA*, pages 949–954, June 2009.

L. Hladowski, K. Galkowski, Z. Cai, E. Rogers, C. T. Freeman, and P. L. Lewin. Experimentally supported 2D systems based iterative learning control law design for error convergence and performance. *Control Engineering Practice*, 18(4):339–348, 2010.

D. J. Hoelzle, A. G. Alleyne, and A. J. W Johnson. Iterative learning control using a basis signal library. In *Proceedings of the American Control Conference, St. Louis, Missouri, USA*, pages 925–930. IEEE Press, 2009.

H. Holm, H. Bach, M. V. Hansen, and D. Franke. Planning of finite element modelled welding control variable trajectories by PI-controllers and by iterative learning. In *Proceedings of the 6th International Conference on Trends in Welding Research, Pine Mountain, Georgia, USA*, 2002.

G. L. Hsu, W. S. Yao, and M. C. Tsai. Implementation of Plug-in Type Repetitive Controller for Position-based Periodic Control Systems. In *The 17th IFAC world Congress, Seoul, Korea.*, 2008.

C. Hua and R.G. Hoft. High performance deadbeat controlled PWM inverter using a current source compensator and nonlinear loads. In *Annual IEEE Power Electronics Specialists Conference. PESC'92 Record*, pages 443–450. IEEE, 1992.

Y. C. Huang, M. Chan, Y. P. Hsin, and C. C. Ko. Use of iterative learning control on improving intra-oral hydraulic loading system of dental implants. In *Proceedings of the IEEE International Symposium on Intelligent Control, Houston, Texas, USA*, pages 63–68, Oct. 2003a.

Y. C. Huang, M. Chan, Y. P. Hsin, and C. C. Ko. Use of PID and iterative learning controls on improving intra-oral hydraulic loading system of dental implants. *JSME International Journal Series C*, 46(4):1449–1455, 2003b.

A-M. Hughes, C. Freeman, J. Burridge, P. Chappell, P. Lewin, and E. Rogers. Feasibility of iterative learning control mediated by functional electrical stimulation for reaching after stroke. *Journal of Neurorehabilitation and Neural Repair*, 23(6):559–568, July 2009.

A. M. Hughes, C. T. Freeman, J. Burridge, P. Chappell, P. Lewin, and E. Rogers. Shoulder and elbow muscle activity during fully supported trajectory tracking in people who have had a stroke. *Journal of Electromyography and Kinesiology*, 20(3):465–476, 2010.

T. Inoue, M. Nakano, T. Kubo, S. Matsumoto, and H. Baba. High accuracy control of a proton synchrotron magnet power supply. In *Proceedings of the 8th IFAC World Congress, Kyoto, Japan*, 1981.

P. Jintakosonwit, H. Fujita, and H. Akagi. Control and performance of a fully-digital-controlled shunt active filter for installation on a power distribution system. *IEEE Transactions on Power Electronics*, 17(1):132–140, 2002.

T.A. Johansen, K.J. Hunt, and I. Petersen. Gain-scheduled control of a solar power plant. *Control Engineering Practice*, 8(9):1011–1022, 2000.

K. Kaneko and R. Horowitz. Repetitive and adaptive control of robot manipulators with velocity estimation. *IEEE Transactions on Robotics and Automation*, 13(2):204–217, 1997.

A. Kawamura and R. Hoft. Instantaneous feedback controlled pwm inverter with adaptive hysteresis. *IEEE Transactions on Industry Applications*, IA-20(4):769 –775, 1984.

D. H. Kim and T. C. Tsao. Robust Performance Control of Electrohydraulic Actuators for Cam Motion Generation. *IEEE Transactions on Control Systems Technology*, 8 (2):220–227, 2000.

K. Kinosita, T. Sogo, and N. Adachi. Iterative learning control using adjoint systems and stable inversion. *Asian Journal of Control*, 4(1):60–67, 2002.

Y. Koren. Cross-coupled biaxial computer control for manufacturing systems. *Journal of Dynamic Systems, Measurement, and Control*, 102:265, 1980.

H. Kwakernaak and R. Sivan. *Linear optimal control systems*. John Wiley and Sons, Inc. New York, 1972.

F. Le, I. Markovsky, C. T. Freeman, and E. Rogers. Identification of electrically stimulated muscle models of stroke patients. *Control Engineering Practice*, 18(4):396–407, 2010.

J. H. Lee, K. S. Lee, and W. C. Kim. Model-based iterative learning control with a quadratic criterion for time-varying linear systems. *AUTOMATICA-OXFORD-*, 36: 641–657, 2000.

K. S. Lee, S. H. Bang, and K. S. Chang. Feedback-assisted iterative learning control based on an inverse process model. *Journal of Process Control*, 4(2):77–89, 1994.

W. Li, P. Maisser, and H. Enge. Self-learning control applied to vibration control of a rotating spindle by piezopusher bearings. *Proceedings of the Institution of Mechanical Engineers, Part I: Journal of Systems and Control Engineering*, 218(3):185–196, 2004.

T. Lin, D. H. Owens, and J. H
"at
"onen. Newton method based iterative learning control for discrete non-linear systems. *International Journal of Control*, 79(10):1263–1276, 2006.

L. Ljung. *System identification : Theory for the user*. Prentice Hall PTR, 1987.

R. W. Longman. Iterative learning control and repetitive control for engineering practice. *International Journal of Control*, 73(10):930–954, 2000.

A. Meaburn and F. M. Hughes. Resonance characteristics of distributed solar collector fields. *Solar Energy*, 51(3):215–221, 1993.

J. H. Moon, M. N. Lee, and M. J. Chung. Repetitive control for the track-following servo system of an optical disk drive. *IEEE Transactions on Control Systems Technology*, 6 (5):663–670, 2002.

K. L. Moore and Y Chen. A seperative high-order framework for monotonic cenvergent iterative learning controller design. In *The American Control Conference. Denver, Colorado USA*, 2003.

K. L. Moore, Y. Q. Chen, and V. Bahl. Monotonically convergent iterative learning control for linear discrete-time systems. *Automatica*, 41(9):1529–1537, 2005.

K. L. Moore and YangQuan. Chen. On monotonic convergence of high-order iterative learning update laws. In *The 15-th IFAC Congress, Barcelona, Spain*, 2002.

K. L. Moore, M. Johnson, and M. J. Grimble. *Iterative learning control for deterministic systems*. Springer-Verlag New York, Inc. Secaucus, NJ, USA, 1993.

M. Norrlof. Comparative study on first and second order ILC - frequency domain analysis and experiments. In *Proceedings of the 39th Conference on Decision and Control, Sydney, Australia.*, pages 3415 – 3420, 2000.

M. Norrlof. An adaptive iterative learning control algorithm with experiments on an industrial robot. *IEEE Transactions on Robotics and Automation*, 18(2):245–251, April 2002.

M. Norrlof. Disturbance rejection using an ILC algorithm with iteration varying filters. *Asian Journal of Control*, 6(3):432–438, 2004.

M. Norrlof and S. Gunnarsson. Experimental comparison of some classical iterative learning control algorithms. *IEEE Transactions on Robotics and Automation*, page 636641, 2002a.

M. Norrlof and S. Gunnarsson. Time and frequency domain convergence properties in iterative learning control. *International Journal of Control*, 75:1114–1126(13), 2002b.

Y. Onuki and H. Ishioka. Compensation for repeatable tracking errors in hard drives using discrete-time repetitive controllers. *IEEE/ASME Transactions on Mechatronics*, 6(2):132–136, 2001.

D. H. Owens, L. M. Li, and S. P. Banks. MIMO multi-periodic repetitive control system: stability analysis. *Proceedings of European Control Cconference, Porto, Portugal*, pages 3393–3397, 2001.

D. H. Owens and E. Rogers. Robust iterative learning control: theory and experimental verification. *International Journal of Robust and Nonlinear Control*, 18(10):999–1000, 2008.

D. H. Owens, M. Tomas-Rodriguez, J. J. Hatonen, and L. M. Li. Discrete time linear optimal multi-periodic repetitive control: A benchmark tracking solution. *International Journal of Control*, 79(9):991–1001, 2006.

H. D. Owens. Iterative learning control - convergence using high gain feedback. In *Proceedings of the IEEE Conference on Decision and Control. Tuscan, Arizona, USA*, 1992.

J. Ratcliffe, L. van Duinkerken, P. Lewin, E. Rogers, J. Hatonen, T. Harte, and D. Owens. Fast norm-optimal iterative learning control for industrial applications. *Proceedings of the American Control Conference, Portland, Oregon, USA*, 3:1951–1956, June 2005.

J. D. Ratcliffe. *Iterative learning control implemented on a multi-axis system.* PhD thesis, School of Electronics and Computer Science, University of Southampton, 2005.

J. D. Ratcliffe, T. J. Harte, J. J. Hatonen, P. L. Lewin, E. Rogers, and D. H. Owens. Practical implementation of a model inverse optimal iterative learning controller on a gantry robot. In *IFAC Workshop on Adaptation and Learning in Control and Signal Processing (ALCOSP 04) and IFAC Workshop on Periodic Control Systems (PSYCO 04), Yokohama, Japan*, pages 687–692, 2004.

J. D. Ratcliffe, J. J. Hatonen, P. L Lewin, E. Rogers, and D. H. Owens. Repetitive control of synchronized operations for process applications. *International Journal of Adaptive Control and Signal Processing*, 21(4):300–325, May 2007.

J. D. Ratcliffe, P. L. Lewin, and E Rogers. Comparing the performance of two iterative learning controllers with optimal feedback control. In *International Symposium on Intelligent Control, Munich, Germany*, pages 838–843, 2006a.

J. D. Ratcliffe, P. L. Lewin, E. Rogers, J. J. Hatonen, and D. H. Owens. Norm-optimal iterative learning control applied to gantry robots for automation applications. *IEEE Transactions on Robotics*, 22(6):1303–1307, December 2006b.

R. Roesser. A discrete state-space model for linear image processing. *IEEE Transactions on Automatic Control*, 20(1):1 – 10, February 1975.

E. Rogers. Robustness of iterative learning control schemes — algorithms with experimental benchmarking. *Bulletin of the Polish Academy of Sciences (Technical Sciences)*, 56(3):205–215, 2008.

E. Rogers, K. Galkowski, and D. Owens. *Control system theory and applications for linear repetitive processes.* Springer, 2007.

I. Rotariu, B. G. Dijkstra, and M. Steinbuch. Comparison of standard and lifted ILC on motion system. In *Proceedings of the 3rd IFAC symposium on mechatronic system, Sydney, Australia*, 2004.

I. Rotariu, R. Ellenbroek, and M. Steinbuch. Time-frequency analysis of a motion system with learning control. In *Proceedings of the American Control Conference, Maui, Hawaii, USA*, volume 4, pages 3650–3654. IEEE, 2003.

S. S. Saab. A discrete-time stochastic learning control algorithm. *IEEE Transactions on Automatic Control*, 46(6):877–887, 2002.

S. K. Sahoo, S. K. Panda, and J. X. Xu. Iterative learning-based high-performance current controller for switched reluctance motors. *IEEE Transactions on Energy Conversion*, 19(3):491–498, 2004.

N. Sakagami, M. Inoue, and S. Kawamura. Theoretical and experimental studies on iterative learning control for underwater robots. *International Journal of Offshore and Polar Engineering*, 13(2):120–127, 2003.

N. Sakagami and S. Kawamura. Time optimal control for underwater robot manipulators based on iterative learning control and time-scale transformation. In *Proceedings of OCEANS*, volume 3, pages 1180–1186. IEEE, 2004.

A. Schollig and R. D'Andrea. Optimization-based iterative learning control for trajectory tracking. In *Proceedings of the European Control Conference, Budapest, Hungary*, pages 1505–1510, 2009.

Z. K. Shi. Real-time learning control method and its application to AC-servomotor control. In *Proceedings of the International Conference on Machine Learning and Cybernetics, Beijing, China*, volume 2, pages 900–905. IEEE, 2002.

D. M. Shin, J. Y. Choi, and J. S. Lee. A P-type Iterative Learning Controller for Uncertain Robotic Systems with Exponentially Decaying Error Bounds. *Journal of Robotic Systems*, 20(2):79–91, 2003.

N. Singer, W. Singhose, and W. Seering. Comparison of filtering methods for reducing residual vibration. *European Journal of Control*, 5(2):208–218, 1999.

B. Singh, K. Al-Haddad, and A. Chandra. A new control approach to three-phase active filter for harmonics and reactive power compensation. *IEEE Transactions on Power Systems*, 13(1):133–138, 2002.

T. Singh and W. Singhose. Tutorial on input shaping/time delay control of maneuvering flexible structures. In *Proceedings of the American Control Conference, Las Vegas, Nevada, USA*, volume 3, pages 1717–1731, 2002.

D. Sun and JK Mills. Adaptive learning control of robotic systems with model uncertainties. In *Proceedings of the IEEE International Conference on Robotics and Automation, Leuven, Belgium*, volume 2, pages 1847–1852. IEEE, 1998.

M. Sun, S. S. Ge, and I. M. Y. Mareels. Adaptive repetitive learning control of robotic manipulators without the requirement for initial repositioning. *IEEE Transactions on Robotics*, 22(3):563–568, 2006.

K. K. Tan, S. N. Huang, and S. Zhao. A novel predictive and iterative learning control algorithm. *Control and Intelligent Systems*, 31(1):1–9, 2003.

A. Tayebi. Adaptive iterative learning control for robot manipulators. *Automatica*, 40 (7):1195–1203, 2004.

A. Tayebi and J. X. Xu. Observer-based iterative learning control for a class of time-varying nonlinear systems. *IEEE Transactions on Circuits and Systems I: Fundamental Theory and Applications*, 50(3):452–455, 2003.

C. H. Tsai and C. J. Chen. Application of iterative path revision technique for laser cutting with controlled fracture. *Optics and Lasers in Engineering*, 41(1):189–204, 2004.

Y. Y. Tzou, S. L. Jung, and H. C. Yeh. Adaptive repetitive control of PWM inverters for very low THD AC-voltage regulation with unknown loads. *IEEE Transactions on Power Electronics*, 14(5):973–981, 2002a.

Y. Y. Tzou, R. S. Ou, S. L. Jung, and M. Y. Chang. High-performance programmable AC power source with low harmonic distortion using DSP-based repetitive control technique. *IEEE Transactions on Power Electronics*, 12(4):715–725, 2002b.

M. Uchiyama. Formulation of high-speed motion pattern of a mechanical arm by trial. *Transactions of the Society for Instrumentation and Control Engineers*, 14(6):706–712, 1978.

M. Van de Wal, G. van Baars, F. Sperling, and O. Bosgra. Multivariable feedback control design for high-precision wafer stage motion. *Control Engineering Practice*, 10 (7):739–755, 2002.

J. Wallen, S. Gunnarsson, R. Henriksson, S. Moberg, and M. Norrlof. ILC applied to a flexible two-link robot model using sensor-fusion-based estimates. In *Proceedings of the IEEE Conference on Decision and Control, Shanghai, China.*, pages 458–463. IEEE, 2009.

J. Wallen, M. Norrlof, and S. Gunnarsson. Arm-side evaluation of ILC applied to a six-degrees-of-freedom industrial robot. In *Proceedings of 17th IFAC World Congress, Seoul, Korea*, pages 450–13, 2008.

J. Wang and T. C. Tsao. Repetitive control of linear time varying systems with application to electronic cam motion control. In *Proceedings of the American Control Conference, Boston, Massachusetts, USA*, volume 4, pages 3794–3799. IEEE, 2004.

C. Wood, S. Rich, M. Frandsen, M. Davidson, R. Maxfield, J. Keller, B. Day, M. Mecham, and K. Moore. Mechatronic design and integration for a novel omni-directional robotic vehicle. In *Proceedings of the 3rd Mechatronics Forum International Conference, Atlanta, Georgia, USA*, 2000.

H. Wu, Z. Zhou, S. Xiong, and W. Zhang. Adaptive iteration learning control and its applications for FNS multi-joint motion. In *Proceedings of the 17th IEEE Instrumentation and Measurement Technology Conference, Baltimore, Maryland, USA*, volume 2, pages 983–987. IEEE, 2000.

J. X. Xu, Y. Chen, T. H. Lee, and S. Yamamoto. Terminal iterative learning control with an application to RTPCVD thickness control. *Automatica*, 35(9):1535–1542, 1999.

J. X. Xu, S. K. Panda, and T. H. Lee. *Real-time Iterative Learning Control: Design and Applications*. Springer Verlag, 2008.

Y. Yamamoto. 7. Learning Control and Related Problems in Infinite-Dimensional Systems. *Essays on control: Perspectives in the Theory and its Applications*, page 191, 1993a.

Y. Yamamoto. Essays on control: Perspectives in the theory and its applications. *Learning Control and Related Problems in Infinite-Dimensional Systems*, pages 191–222, 1993b.

Z. Yao, H. Wang, and C. Yang. A sort of iterative learning control algorithm for tracking of robot trajectory. *Acta Armamentarii*, 3, 2004.

K. Yasuhide, K. Tetsuya, and Y. Shigeo. Robust speed control of ultrasonic motor based on H-infinity control with repetitive compensator. *JSME International Journal, Series C*, 42(4):884–890, 1999.

Y. Ye and D. Wang. Learning more frequency components using P-type ILC with negative learning gain. *IEEE Transactions on Industrial Electronics*, 53(2):712–716, 2006.

C. Zhenwei and G. Ledwich. Tracking variable periodic signals with fixed sampling rate. In *Proceedings of the 40th IEEE Conference on Decision and Control, Orlando, Florida, USA*, volume 5, pages 4885–4890, 2001.

K. Zhou and D. Wang. Digital repetitive learning controller for three-phase CVCF PWM inverter. *IEEE Transactions on Industrial Electronics*, 48(4):820–830, 2002.

K. Zhou and D. Wang. Digital repetitive controlled three-phase PWM rectifier. *IEEE Transactions on Power Electronics*, 18(1):309–316, 2003.